TAMPEREEN TEKNILLINEN YLIOPISTO
TAMPERE UNIVERSITY OF TECHNOLOGY

Mikko Heikkilä

Energy Efficient Boom Actuation Using a Digital Hydraulic Power Management System

Julkaisu 1388 • Publication 1388

Tampere 2016

Tampereen teknillinen yliopisto. Julkaisu 1388
Tampere University of Technology. Publication 1388

Mikko Heikkilä

Energy Efficient Boom Actuation Using a Digital Hydraulic Power Management System

Thesis for the degree of Doctor of Science in Technology to be presented with due permission for public examination and criticism in Konetalo Building, Auditorium K1702, at Tampere University of Technology, on the 17th of June 2016, at 12 noon.

Tampereen teknillinen yliopisto - Tampere University of Technology
Tampere 2016

ISBN 978-952-15-3758-5 (printed)
ISBN 978-952-15-3763-9 (PDF)
ISSN 1459-2045

Abstract

Hydraulic systems are widely used in mobile machines such as construction machinery and forest machinery. Modern hydraulics relies on Load Sensing (LS) systems. The solution is based on adjusting the flow and pressure according to the requirements of actuators. And further, the actuators are controlled by proportional valves by throttling the flow. A problem of LS systems is poor energy efficiency, especially when the load is overrunning. Moreover, in multi-actuator systems, the supply pressure is set according to the highest demand, whereas the actuator flows are controlled independently; thus, the pressure matching losses can become extremely high in a case where actuators with high flow demand operate at pressure levels significantly below that of the maximum pressure. A solution to tackle these problems could be a Digital Hydraulic Power Management System (DHPMS). Based on digital pump/motor technology, the DHPMS has the potential for high energy efficiency. Moreover, multiple independent outlets enable new innovative system layouts.

In this thesis a novel approach for hydraulic systems is considered. A piston-type DHPMS with displacement controlled actuators could theoretically compose a lossless hydraulic drive. The research investigates the possibility of putting the direct control approach into practice. In addition, a control method for a Digital Hydraulic Hybrid (DHH) with displacement controlled actuators is proposed. The hybrid system utilizes a hydraulic accumulator as an energy source/sink; the prime mover can be assisted during high power demand and the recoverable energy can be temporarily stored for reuse. Simulations and experimental test are used to validate the system.

The results imply that the DHH with displacement controlled actuators is a feasible approach; a model based controller provides good position tracking without position feedback, and the power of an electric motor can be stabilized by utilizing the accumulator. Moreover, the full capacity of the energy storing device can be utilized because the DHPMS can act as a hydraulic transformer. The measurements show that for the studied trajectory, the direct cylinder control decreases the system losses by about 50% in comparison with an Electrical Load Sensing (ELS) system with a proportional controlled cylinder. Hydraulic losses in the supply lines are instead reduced by about 89%. Thus, the energy saving potential of the new approach is substantial, but the structure of the DHPMS has to be well considered; the efficiency of the system mainly depends on the efficiency of the multi-outlet digital pump/motor unit. In addition, pumping pistons with small geometrical displacement are needed to accomplish sophisticated control performance.

Preface

This study was carried out at the Department of Intelligent Hydraulics and Automation (IHA) at Tampere University of Technology (TUT). The study was partly funded by the Doctoral Program in Concurrent Mechanical Engineering (DPCME) and the Academy of Finland (Grant No. 139540).

I would like to express my deepest gratitude to my supervisor Adj. Prof. Matti Linjama for his support, guidance and advice during this thesis process. I would also like to thank Prof. Seppo Tikkanen for his valuable comments and our productive discussions, and the Head of IHA, Prof. Kalevi Huhtala for providing excellent facilities for the research.

I wish to thank the preliminary examiners Prof. Hubertus Murrenhoff and Prof. Torben Andersen for their comments and criticism. In addition, the suggestions by Prof. Jouko Halttunen are greatly appreciated. I also wish to thank John Shepherd for checking the language of the thesis.

I am grateful to the whole personnel of IHA, especially to the laboratory staff for their assistance with experimental installations. Special thanks are also due to the digital hydraulics research group for good working atmosphere, and to my colleagues of the "Kavitaatio" room for many creative scientific discussions over the years.

Finally, I wish to thank my family for their support and encouragement throughout the years.

Tampere, 2016

Mikko Heikkilä

Contents

Acronyms

BDC	Bottom Dead Center
BR	Bosch Rexroth
DFCU	Digital Flow Control Unit
DHH	Digital Hydraulic Hybrid
DHPMS	Digital Hydraulic Power Management System
DHT	Digital Hydraulic Transformer
DPCME	Doctoral Program in Concurrent Mechanical Engineering
DVS	Digital Valve System
ELS	Electrical Load Sensing
GMA	Geometric Moving Average
HPV	High Pressure Valve
IHA	Department of Intelligent Hydraulics and Automation
LPV	Low Pressure Valve
LS	Load Sensing
MPC	Model Predictive Control
MPG	Miles Per Gallon
PCM	Pulse Code Modulation
PNM	Pulse Number Modulation
PWM	Pulse Width Modulation
RMSE	Root Mean Square Error
TDC	Top Dead Center
TUT	Tampere University of Technology

Nomenclature

α	Angular acceleration	[rad/s^2]
Δp	Pressure difference over the DHPMS	[Pa]
Δp_{comp}	Absolute value of the pressure difference in pre-/decompression	[Pa]
Δt_{pulses}	Time between the sequential gear ring pulses	[s]
ΔV_{comp}	Volume loss due to pre-/decompression	[m^3]
η_{mh}	Hydromechanical efficiency of the DHPMS	
η_{tot}	Total efficiency of the DHPMS	
η_{vol}	Volumetric efficiency of the DHPMS	
γ	Forgetting factor in GMA recursion	
κ	Heat capacity ratio	
ω	Angular velocity	[rad/s]
θ_{off}	DHPMS piston angle at which the valve is commanded off	[°]
θ_{on}	DHPMS piston angle at which the valve is commanded on	[°]
θ_{valve}	Valve opening/closing delay in degrees	[°]
$\theta_{\Delta\text{p}}$	Pre-/decompression time in degrees	[°]
ζ	Damping factor of the off-line low-pass signal filter	
A_{disp}	Area of the pumping piston	[m^2]
A_{A}	Cylinder effective area for the piston side	[m^2]
A_{B}	Cylinder effective area for the rod side	[m^2]
A_{cyl}	Effective area A or B of the cylinder	[m/s]
B_{oil}	Bulk modulus of the fluid	[Pa]
B_{eff}	Effective bulk modulus	[Pa]
C_{h}	Hydraulic capacitance	[m^3/Pa]
C_{leak}	DHPMS valve leak coefficient	[m^3/(s Pa)]

CF	Correction factor in valve timing and fluid volume control	
d_{valve}	Valve opening/closing delay in seconds	[s]
f_{CutOff}	Cut-off frequency of the off-line low-pass signal filter	
F_{Cylinder}	Cylinder force, $F_{\text{Cylinder}} = p_{\text{A}} \cdot A_{\text{A}} - p_{\text{B}} \cdot A_{\text{B}}$	[N]
I	Moment of inertia	[kgm^2]
K_{v}	Orifice flow factor	[m^3/(s $\sqrt{\text{Pa}}$)]
L	Length	[m]
m	Mass	[kg]
M_{idx}	Mode index of the DHPMS	
M_{M}	Motoring mode of the DHPMS	
M_{P}	Pumping mode of the DHPMS	
n	Rotational speed	[r/s]
n_{filt}	Filtered rotational speed of the DHPMS	[°/s]
N_{pistons}	Number of pistons of the DHPMS	
N_{pulses}	Number of teeth of the gear ring	
n_{pulses}	Measured rotational speed of the DHPMS	[°/s]
n_{s}	Synchronous speed of the electric motor	[r/s]
P	Power	[W]
p	Pressure	[Pa]
P_{Accu}	Hydraulic power of the accumulator, $P_{\text{Accu}} = Q_{\text{Accu}} \cdot p_{\text{Accu}}$	[W]
p_{Accu}	Accumulator pressure	[Pa]
p_{A}	Cylinder piston side pressure	[Pa]
p_{back}	Back-pressure (non-load pressure) of the cylinder	[Pa]
p_{B}	Cylinder rod side pressure	[Pa]
P_{Cylinder}	Cylinder output power, $P_{\text{Cylinder}} = F_{\text{Cylinder}} \cdot v$	[W]
P_{DHPMS}	Hydraulic power of the DHPMS, $P_{\text{DHPMS}} = Q_{\text{A}} \cdot p_{\text{A}} + Q_{\text{B}} \cdot p_{\text{B}}$	[W]
P_{EMotor}	Power of the electric motor, $P_{\text{EMotor}} = T_{\text{EMotor}} \cdot \omega$	[W]
P_{i}	Power of the i:th DHPMS piston	[W]
p_{i}	Pressure at the i:th DHPMS piston chamber	[Pa]
p_{S}	Supply pressure (ELS pressure control)	[Pa]
p_{tr}	Orifice transition pressure	[Pa]

p_{T}	Inlet pressure of the DHPMS	[Pa]
Q	Flow	[m^3/s]
Q_{i}	Flow at the DHPMS outlet i	[m^3/s]
$Q_{\max}$	Theoretical maximum flow of the DHPMS	[m^3/s]
Q_{T}	Flow at the DHPMS inlet	[m^3/s]
R	Utilization rate of the DHPMS outlet per revolution	
s	Piston stroke of the DHPMS	[m]
s_{N}	Nominal slip of the electric motor	[r/s]
T	Shaft torque	[Nm]
T_{DHPMS}	Torque of the DHPMS	[Nm]
T_{EMotor}	Torque of the electric motor	[Nm]
T_{N}	Nominal torque of the electric motor	[Nm]
V	Volume	[m^3]
v	Velocity	[m/s]
V_{tot}	Total compression volume of the DHPMS pumping cylinder	[m^3]
V_0	Dead volume of the DHPMS pumping cylinder	[m^3]
V_{cyl}	Estimated fluid volume of the cylinder chamber	[m^3]
V_{disp}	Geometrical piston displacement of the DHPMS	[m^3]
V_{err}	Fluid volume error of the cylinder chamber	[m^3]
V_{g}	DHPMS geometrical displacement per revolution	[m^3]
v_{i}	Velocity of the i:th DHPMS piston chamber	[Pa]
V_{ref}	Fluid volume reference for the cylinder chamber	[m^3]
v_{ref}	Cylinder velocity reference	[m/s]
W	Energy, $W = \int P \, dt$	[J]
x	DHPMS piston position	[m]
y	Cylinder piston position	[m]
y_{ref}	Cylinder position reference	[m]
$\mathbf{M}$	Mode vector of the DHPMS $[M_{\mathrm{P}}, M_{\mathrm{M}}]$	
$\mathbf{u}_{\mathrm{A}}$	Control signal vector for the DHPMS supply A valves	
$\mathbf{u}_{\mathrm{B}}$	Control signal vector for the DHPMS supply B valves	
$\mathbf{u}_{\mathrm{T}}$	Control signal vector for the DHPMS tank valves	

1 Introduction

1.1 Motivation for the study

Hydraulic systems are widely used in applications where high forces are needed to be generated. A typical example is mobile working machines which benefit from the high power to weight ratio that hydraulic systems can provide. In addition, hydraulics enable flexible system layouts, which are important in boom systems, for example. However, a disadvantage of hydraulic systems has been poor overall efficiency despite the reasonable efficiency of single components. Liang and Virvalo have studied the energy utilization of a hydraulic crane in [1]; according to their calculations, the system efficiency is under 0.36 even when modern Load Sensing (LS) hydraulics are used. The authors list fundamental problems of the hydraulic system as follows:

- ⋆ Pressure losses over the proportional control valves
- ⋆ Large energy losses for an overrunning load
- ⋆ Pressure matching losses in a multi-actuator system

There have also been several proposals for improving conventional LS and proportional controlled systems. For example, Electrical Load Sensing (ELS) control is studied in [2, 3], while an ELS system with dual circuit architecture is presented in [4]. A negative load sensing system based on velocity control by utilizing an outflow control notch is proposed in [5]. Additionally, solutions based on independent metering are presented in [6–8]. However, less conventional solutions are needed in order to increase the efficiency of hydraulic systems to an appropriate level.

1.2 Review of energy efficient hydraulics

1.2.1 Digital hydraulics

Digital hydraulics is an alternative for traditional hydraulics. The digitalization of hydraulic systems is based on the use of actively controlled on/off valves. For example, an analog proportional control valve can be replaced with an on/off switching valve or parallel connected on/off valves. Other applications are digital (multi-chamber) cylinders, linear transformers and digital pump/motors. A benefit of digital hydraulic systems is the deterministic operation of the simple components and their programmability. In addition, digital solutions can significantly improve the energy efficiency of the systems in comparison with traditional hydraulics.

Hydraulic switching control techniques have been studied by Scheidl et al. in [9]. The basic idea is to use Pulse Width Modulation (PWM) for implementing different mean flow rates with an on/off valve. According to the authors, it is beneficial to utilize simple switching valves instead of proportional valves due to their good repeatability and small hysteresis. Moreover, energy saving converter principles can provide good efficiency and fast dynamics. Figure 1.1 shows a diagram of a simple hydraulic buck converter; the principle of operation is based on inertia of the fluid column inside the inductance pipe. The utilization of two independent pressure sources enables energy recuperation. The accumulator is needed to decrease the pressure ripple but large capacitance reduces the system stiffness, which is undesirable feature in the dynamic system. Therefore, an approach of multiple hydraulic buck converters in parallel is considered; the phase shifted operation reduces pressure pulsations and makes the accumulator unnecessary as well as improving dynamic performance.

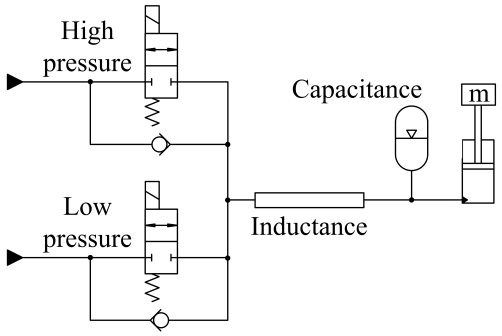

Figure 1.1: Hydraulic buck (step-down) converter [9].

Another choice for digital hydraulic flow control is to use a Digital Flow Control Unit (DFCU), which consists of parallel connected on/off valves. The valves can be coded using different methods [10]. In Pulse Code Modulation (PCM) the valves are selected according to binary series; for example, four bits in the DFCU leads to fifteen different flow rates. Hence, the coding method provides the best possible resolution with a certain number of valves. A disadvantage of PCM control is that there is the possibility of high pressure peaks during state transitions. If the parallel connected valves have equal flow capacities, the coding method is known as Pulse Number Modulation (PNM). With PNM coding, the pressure peaks can be avoided but many valves are needed to achieve satisfactory resolution. Fibonacci coding instead is a compromise between the former; pressure peaks can be avoided but still good resolution can be obtained with a reasonable number of valves.

In [11] Linjama et al. studied a cylinder drive controlled by two DFCUs; both the inflow and outflow path are controlled separately to allow independent metering. The DFCUs have five directly operated solenoid valves each and their flow ratios follow approximately the binary series. Additionally, a four-way valve is utilized for selecting the piston direction of the movement. The results imply good position tracking performance despite limited control resolution. In order to improve the tracking control of the cylinder drive, Linjama et al. has proposed a system with four DFCUs [12]. Figure 1.2 shows a diagram of the studied system; both the cylinder chambers can be connected to the supply pressure or

tank via control valves. Moreover, the flow paths can be controlled independently, which allows even all four DFCUs to be opened simultaneously. Hence, the control resolution at low velocities improves significantly compared with a system having only two DFCUs. Huova et al. also studied the energy efficiency of the four DFCU system in [13]. In addition to the distributed digital valve configuration, the cylinder drive utilizes the ELS supply pressure control and a pressurized tank line. The measurements imply that the energy losses can be reduced by $53 - 71\%$ in comparison with the traditional LS proportional controlled system.

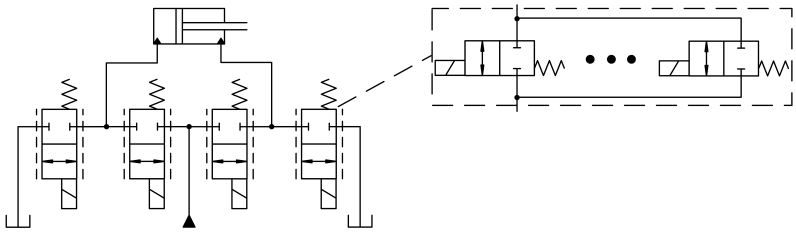

Figure 1.2: Digital hydraulic distributed valve system [12].

The Digital Valve System (DVS) can improve the reliability of the hydraulics as well. Siivonen et al. have studied the fault tolerance of the DVS in [14–16]. Different kinds of faults in valves, electronics or in electrical wires can be detected. Moreover, a single fault in a valve (jammed on or off) does not paralyze the system because the controller can adapt to the condition. A robust DVS is a worthy alternative for a sensitive servo valve as well; for example, the original tilting system of Finnish Pendolino trains will be replaced by the digital hydraulic approach [17]. The retrofit work is expected to improve the reliability of the tilting system and decrease the life cycle costs.

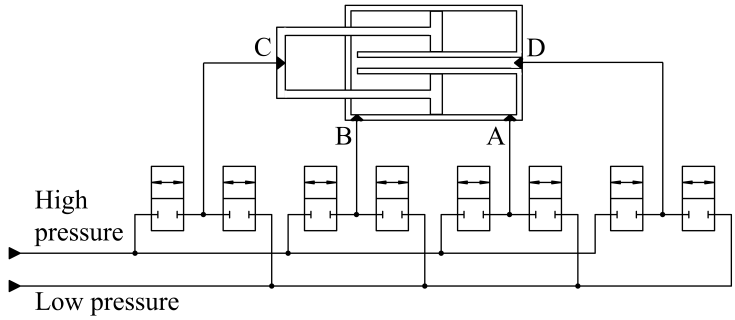

Figure 1.3: Secondary controlled multi-chamber cylinder [18].

Figure 1.3 shows a diagram of the secondary controlled multi-actuator cylinder studied by Linjama et al. in [18]. The cylinder has four chambers, each of which can be connected to the high pressure or low pressure line. As the cylinder effective areas are determined by the binary series, the cylinder can generate sixteen different force outputs. The selected supply pressure levels instead affect the maximum and minimum forces but also the force resolution. The experimental results show that the approach can save a significant amount of energy when compared with traditional solutions. However, the controllability

at low velocities is moderate and an application with high inertia can only be considered. Dell'Amico et al. have also studied a similar system in [19]. Their system consists of a four-chamber cylinder with the relative area ratios of $1 : 3 : 9 : 27$ and on/off control valves connecting the chambers either to low pressure, mid-pressure of high pressure. As a result, 81 discrete force outputs can be generated, which implies significantly improved control resolution.

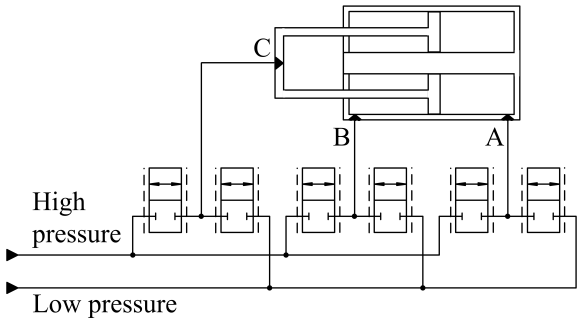

Figure 1.4: Multi-chamber cylinder with digital hydraulic distributed valve system [20].

The resistance control of a three-chamber cylinder utilizing a model-based controller has been studied by Huova et al. in [20]. A diagram of the test system is shown in Fig 1.4; the system uses distributed digital valves for the flow control of the cylinder chambers. In the case of the three-chamber cylinder there are eight different control modes on both moving directions instead of four modes which can be implemented by using the traditional cylinder. According to the experimental results, the energy losses are reduced up to 66% compared with the proportional controlled system if only restricting and balanced loadings are needed to operate.

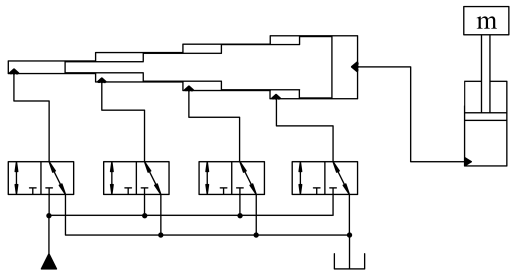

Figure 1.5: Linear digital hydraulic transformer [21].

Bishop has presented a concept of the Digital Hydraulic Transformer (DHT) in [21]. A linear transformer operates between the constant supply pressure line and the actuator in order to set the output pressure of the DHT close to the load pressure. A simplified four-bit DHT is shown in Fig 1.5. The effective areas on the input side are set according to the binary series while the area on the output side is fifteen times bigger than the smallest area on the input side. Thus, fifteen different transformation ratios can be realized. The transformation ratio is selected by controlling certain 3/2 valves. Additionally, the DHT is able to feed energy back to the supply system while the load is lowered or decelerated.

A bilaterally symmetric DHT design is discussed in [22]. The solution enables controlling a double acting cylinder in both moving directions with unlimited continuous flows. The experimental results show working fluid volume savings of $42 - 71\%$ in comparison with traditional valve controlled systems for the studied work cycle. The challenges of DHT technology mainly relate to proper design and control methods.

1.2.2 Digital pump/motor technology

The fluid commutation in traditional piston-type hydraulic pumps is realized using a valve plate, and geometric displacement is adjusted by changing the stroke of the pistons. A fundamental problem of a conventional pump is that it can operate at good efficiency only in one certain operating condition. Especially, the efficiency at partial displacements is poor because every cylinder is pressurized in a pumping cycle despite the flow rate; therefore, hydromechanical and volumetric losses become relatively higher at smaller displacements. Piston-type digital pumps, however, have actively controlled on/off valves for the fluid commutation. Hence, the displacement is adjusted by using a sufficient number of pistons while the rest are left to idle. The digital valve plate also minimizes the fluid compression losses because the valve timing can be optimized for each pressure level.

Wadsley carried out an efficiency comparison of a digital pump and conventional variable displacement pumps in [23]. The study shows that at 20% displacement (operation at 30 MPa) an overall efficiency of the digital pumping stays above 0.9 with rotational speeds between $1000 - 2500$ r/min. The corresponding number for a bent axis pump is about 0.77, whereas the efficiency of a swashplate pump varies from 0.35 to 0.62. When high powers are considered, the advantage of digital solution over traditional ones is indisputable from the point of view of losses.

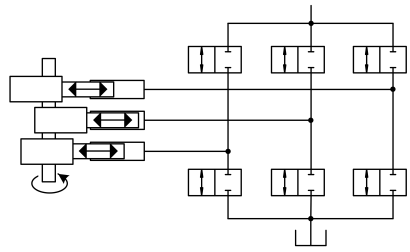

Figure 1.6: Three-piston digital hydraulic pump/motor [24].

A simplified diagram of the three-piston digital hydraulic pump/motor studied by Tammisto et al. [24] is shown in Fig. 1.6; a modified in-line pump has been tested for its efficiency and compared with the results accomplished by the original design with passive check valves. The experiments show that the units are comparable in pumping efficiency at full displacement. However, the limited flow capacity of the on/off control valves impairs the hydromechanical efficiency in the digital pump unit.

Eshan et al. [25] have introduced an approach which combines units of digital pump/motors along a common shaft, as described in Fig. 1.7. The units can serve different loads as they are separate from each other, but the shaft provides a summing junction of torque and power. Utilization of radial pump/motors leads to a compact design.

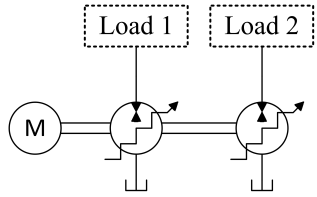

Figure 1.7: Combination of digital pump/motors along a common shaft [25].

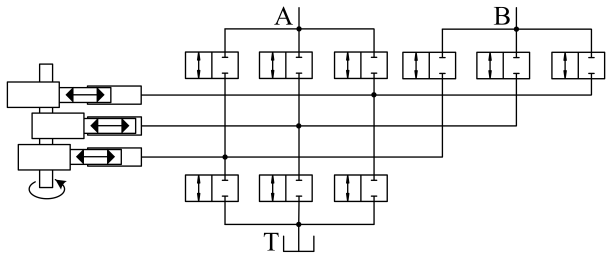

Figure 1.8: Three-piston digital hydraulic pump/motor with two independent outlets (Digital Hydraulic Power Management System) [26].

The Digital Hydraulic Power Management System (DHPMS), however, can serve several pressure outlets with distributed control valves, as presented by Linjama and Huhtala in [26]. Figure 1.8 shows a three-piston DHPMS with two independent outlets. The machine can be considered as an extended digital pump/motor; the fluid can be pumped to or motor from either one of the outlets regardless of the pressure levels. The hydraulic coupling of the outlets allows the DHPMS to be sized according to the combined maximum flow at the outlets instead of the combined maximum flow of the individual actuators. The concept of a piston-type DHPMS is discussed in more detail in Chapter 2.

Another DHPMS approach based on fixed displacement units is proposed by Linjama and Tammisto in [27]. According to the authors, the solution results in the system having fewer control valves, relaxed requirements for the valves, faster response and smoother flow in comparison with the piston-type DHPMS, but its efficiency is poorer.

1.2.3 Displacement controlled systems

A displacement controlled system using a variable displacement pump/motor can reduce the energy losses of hydraulics, as the throttling losses minimizes. Due to the direct actuation, the system pressure is always close to optimal because it is determined by the load. A simplified diagram of the displacement controlled cylinder using the variable displacement pump/motor is shown in Fig. 1.9. The approach has been studied for its efficiency by Williamson et al. in [28]; an excavator utilizing the displacement control actuators is investigated by simulations. The results indicate energy savings of 39% for a trenching maneuver when compared with the same machine using LS hydraulics.

In [29] Williamson and Ivantysynova study the power optimization of the displacement controller excavator. According to the simulations, the proposed power management

algorithm reduces the fuel consumption by up to 17% when a typical digging cycle is considered. A challenge of the displacement controlled actuation when using the variable displacement pump/motor may be an unstable switching between pumping and motoring modes. The causes and solutions for the circuit instability are studied in [30]. The measured efficiency analysis of a digging cycle has been presented by Zimmerman and Ivantysynova in [31]; the energy consumption of the displacement controlled system is half of that of the LS system.

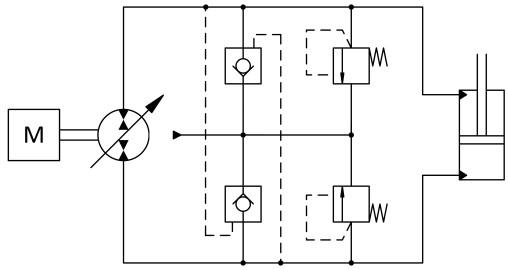

Figure 1.9: Displacement controlled actuator using a variable displacement pump/motor [29].

Traditionally, each displacement controlled actuator requires a separate pump/motor; therefore, in multi-actuator systems many components are needed, which leads to high machine production cost. Busquets and Ivantysynova have proposed a system layout shown in Fig. 1.10 as a solution [32]. A pump/motor can serve several actuators in a sequential manner based on the priority. Switching between the actuators is accomplished by the on/off valves.

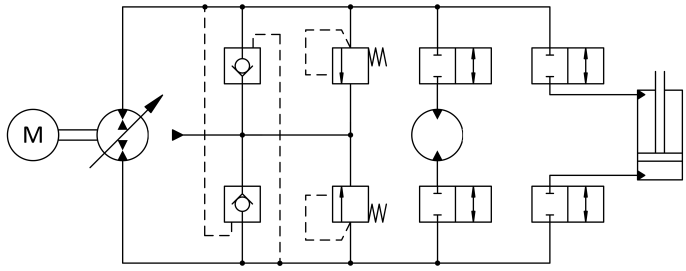

Figure 1.10: Displacement controlled actuators with pump switching [32].

A novel open circuit architecture for the displacement controlled actuation has been proposed by Ivantysyn and Weber in [33]. An original excavator utilizing open circuit hydraulics with an open center valve controlled system is used as a reference. By removing the open center control valves and by enabling the energy recuperation from the excavator boom and stick actuators, the results show energy savings of about 35%.

Minav et al. have studied a direct driven hydraulic drive in [34–36]. The principle of the setup is shown in Fig. 1.11; constant displacement pump/motors connected to a cylinder chambers are controlled by an electric motor drive. For an asymmetric cylinder, geometrical displacement of the pump/motors needs to be sized according to the area ratio. A system without a conventional oil tank has also been proposed.

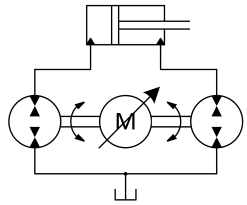

Figure 1.11: Direct-driven hydraulic drive [34].

The digital hydraulic pump control utilizing parallel connected, constant displacement units has been studied by Heitzig and Theissen in [37] and Locateli et al. in [38]. The former study also shares the idea of a multi-outlet system introduced in [27]. A displacement control approach using a piston-type DHPMS is discussed in detail in Chapter 4.

1.2.4 Hydraulic hybrids

Hydraulic hybrids utilize accumulators as energy storages. Typically, the energy is stored into compressed gas which makes the storage systems hydro-pneumatic. An advantage of hydro-pneumatic accumulators over electrical storage devices is their simple and cost-effective construction. Furthermore, the hydraulic accumulator has superior power density compared with an electric battery and it has better efficiency in frequent charging and discharging cycles [39]. However, the efficiency of a traditional gas accumulator is somewhat sensitive to operation conditions [40] but it can be further improved by new innovations. For example, the losses caused by energy exchange with the environment can be reduced by heat insulation or regeneration [41, 42]. In addition, lightweight components have been developed to achieve better suitability for mobile applications [43].

Hydraulic hybrid power trains have been considered as a worthy alternative for electric ones and they have been researched increasingly of late. Hybrids utilizing variable displacement pump/motors and hydro-pneumatic accumulators are the most common solution. Du et al. [44] have compared the fuel economy of three basic hybrid architectures: a series hybrid, a parallel hybrid, and a power-split hybrid. According to the study, power-split architecture provides the best fuel economy for a passenger car. A power management strategy of the power-split hybrid has been studied by Kumar and Ivantysynova in [45]. An instantaneous optimization based control can further improve the fuel economy of the hybrid power train. Bender et al. have studied the parallel hybrid architecture for a refuse collection vehicle in [46]. According to the simulations fuel savings of about 20% can be expected compared with a non-hybrid vehicle. A blended hybrid hydraulic power train has been studied by Sprengel and Ivantysynova in [47]. According to the results, the fuel economy of the novel solution is inferior to that of a series hydraulic hybrid but still increases the Miles Per Gallon (MPG) of a vehicle by up to 37% in comparison with a baseline automatic transmission. Moreover, a retrofittable hydraulic hybrid system utilizing a double piston accumulator is presented in [48], whereas a hybrid power train based on hydraulic transformers is studied in [49–52]; a series hybrid architecture for a passenger car can reduce the fuel consumption of the vehicle by more than 50%. An electric-hydraulic hybrid power train using fixed displacement units is proposed in [53], while digital pump/motor technology is utilized in [54–56].

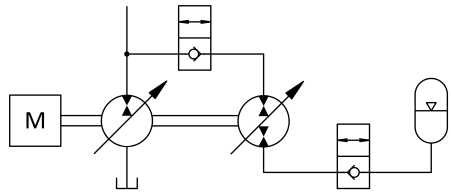

Figure 1.12: "Universal energy storage and recovery system" [57].

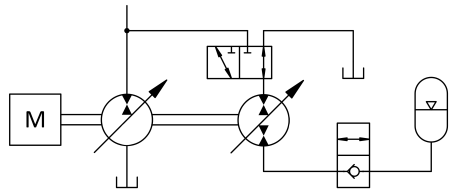

Figure 1.13: Hydraulic hybrid system of a Cut-To-Length harvester [58].

Mobile working machines utilize hydraulic actuators; therefore, hybridization by using hydraulic energy storage systems is a reasonable action to develop more energy-efficient machinery. Figure 1.12 shows a simplified diagram of "universal energy storage and recovery system" proposed by Erkkilä et al. in [57]. In addition to normal LS components, the system has a variable displacement pump/motor unit and an accumulator. The pump/motor is used to control the flow of the accumulator and it also works as a pressure transformer. Thus, the hybrid system can minimize the energy transformation losses and it is also capable of utilizing the full accumulator capacity. A similar hybrid system layout shown in Fig. 1.13 is investigated by Einola in [58, 59]. The system is proposed to serve a Cut-To-Length harvester alongside LS hydraulics. An added 3/2 valve allows the pump/motor unit to be connected to the tank; hence, the diesel engine can be assisted by using the energy stored in the accumulator.

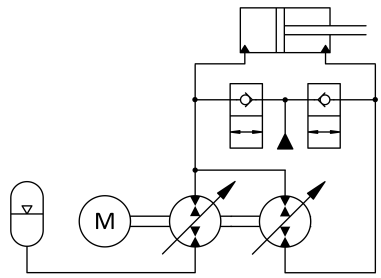

Figure 1.14: Pump controlled hybrid linear actuator [60].

Tikkanen et al. [60] have investigated a pump controlled hybrid linear actuator as shown in Fig. 1.14. The system has two pump/motor units and an accumulator. As the cylinder is controlled through the pump flow the losses minimize and allow the system to recuperate energy. Hippalgaonkar et al. have studied a hydraulic hybrid displacement controlled system in [61, 62]. A simplified diagram of the mini-excavator hydraulics is

shown in Fig. 1.15. Each working actuator (boom, stick, and bucket) has its own variable displacement pump/motor. The units are connected to the engine shaft through a belt drive allowing higher rotational speed. The pump unit feeding the swing actuator is directly driven by the engine shaft. The high pressure accumulator is used to store energy, which can be utilized to assist the engine during high power demand. The results imply a significant improvement in energy efficiency in comparison with a non-hybrid displacement controlled excavator. In addition, the hybrid system enables up to 50% engine downsizing when compared with valve controlled excavators.

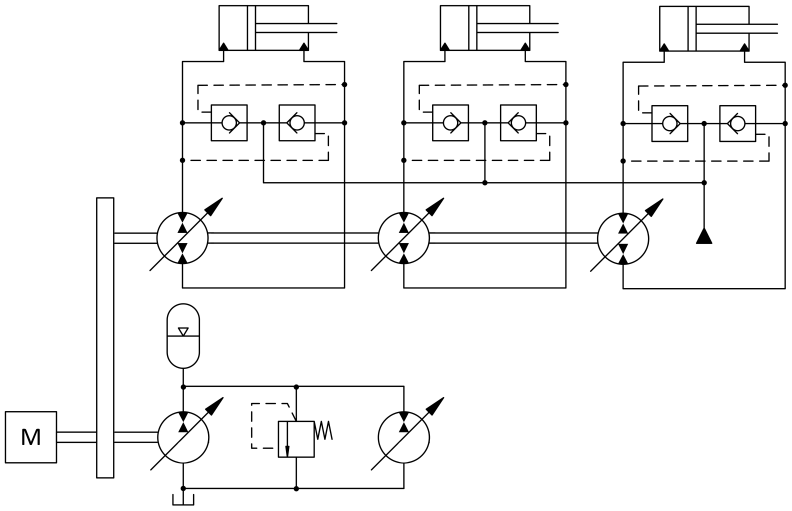

Figure 1.15: Series-parallel hydraulic hybrid excavator with displacement controlled actuators [61].

A hybrid system for the work hydraulics can be also implemented by using a common pressure rail with hydraulic energy storage systems and hydraulic transformers. The simulation results in [63] imply a 50% reduction in the fuel consumption of a wheel loader for the selected duty cycles. In addition, the fuel consumption can be greatly influenced by the control strategy, as studied in [64]. A hybrid pump drive is studied in [65]. The system layout is similar to that of Fig. 1.14, but the variable displacement pump/motors are replaced by fixed displacement units and the flow is controlled by adjusting the rotational speed of an electric motor. The results imply that the size of the electric motor can be reduced considerably by using a hybrid energy supply. However, the reduction potential depends upon the application.

A hydraulic hybrid actuator is investigated by Linjama et al. in [66]. The idea is to integrate a hydraulic accumulator into the actuator; hence, the power peaks can be handled locally at the actuator and only the mean power is needed to transmit from the outside. Additionally, the concept strongly relies on digital hydraulics. An alternative digital hydraulic solution is the Digital Hydraulic Hybrid (DHH) utilizing a piston-type DHPMS and displacement controlled actuators. The issue will be covered in Chapter 5.

1.3 Objectives of the thesis

An idea of a "lossless" hydraulic drive was proposed by Linjama and Huhtala in [26]; the approach connects the DHPMS outlets directly to the cylinder chambers. However, the authors state that the solution is demanding from the controllability point of view and requires a high number of pumping pistons and/or high rotational speed. This leads to the research question of this thesis:

"Is it possible to actuate a hydraulic cylinder without using directional control valves when a DHPMS is employed?"

Displacement controlled actuators and hybrid solutions have been widely studied, but they traditionally utilize variable displacement pump/motor units. A problem with conventional pump/motor units are their low efficiency at partial displacements. The digital pump/motors instead can provide significantly better total efficiency for a wider operation range. In addition, the number of components and overall physical size of the system can be minimized by using the digital solution. Therefore, displacement control using the DHPMS is worth studying.

The individual objectives of this thesis are summarized as follows:

- ⋆ To create a control method for the DHPMS when displacement controlled cylinders are considered
- ⋆ To create a control method for the DHH with displacement controlled actuators in order to stabilize the power of a prime mover
- ⋆ To validate the feasibility of control methods by simulations and experimental tests
- ⋆ To validate the energy saving potential of the studied approach by simulations and experimental tests

1.4 Research methods and restrictions

The research begins by constructing a simulation model for the studied systems; the direct actuation of an asymmetric cylinder is investigated in Chapter 4 and the DHH is studied in Chapter 5. A model based controller is created for each system and the validity of the proposed control algorithm is tested by simulations and measurements. Moreover, a thorough analysis of the systems under investigation is performed.

The systems are modeled using MATLAB/Simulink and the SimMechanics toolbox. The first restriction of the modeled system is that the boom is constructed by rigid bodies; hence, the model does not precisely correspond to the experimental setup. Secondly, the model of the DHPMS ignores mechanical losses. Additionally, the bulk modulus of the fluid is assumed to be unchangeable (no dissolved air). However, the system model as a whole is precise enough to reliably point out the sources of the losses.

The effect of oil temperature on boom control is not studied as the experimental tests were carried out in stable conditions. Therefore, the control accuracy would suffer due to

leakages in the prototype DHPMS as they are temperature dependent. The leakages also reduce the system efficiency which can be considered as a limitation of the test system.

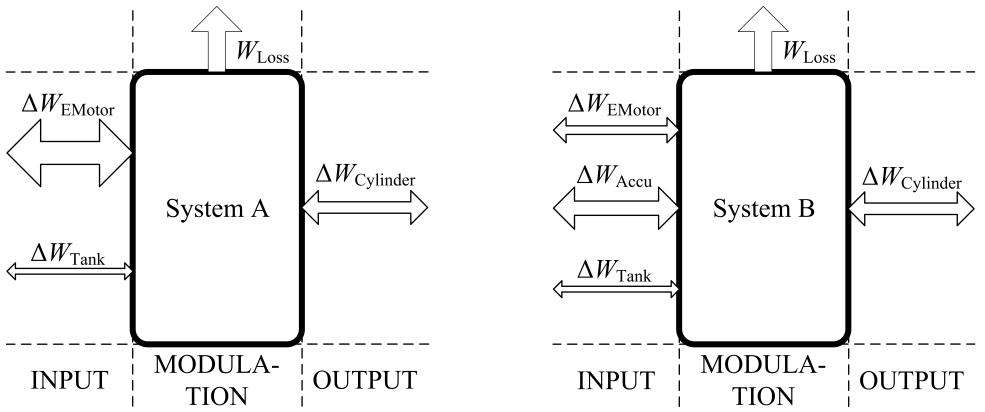

Figure 1.16: Examined energy flows and losses of the studied systems: Displacement controlled cylinder without an accumulator (System A) and with an accumulator (System B).

Figure 1.16 shows the method for determining the energy losses of the studied systems. For a displacement controlled cylinder without an accumulator (System A), a pressurized tank is considered as an energy source along an electric motor, whereas exploited energy is calculated from the actuator. For the DHH (System B) the accumulator is an additional energy source to be considered. Hence, the system losses are calculated as

$$W_{\text{Loss}} = (\Delta W_{\text{EMotor}} - \Delta W_{\text{Tank}} - \Delta W_{\text{Accu}}) - \Delta W_{\text{Cylinder}} \tag{1.1}$$

and they consist of losses in the DHPMS and supply lines. The efficiency of the accumulator charging is not studied, nor is its capability of storing energy; the inspections would not be appropriate due to the pressure/time dependent leakage losses of the DHPMS. Therefore, the accumulator is left outside of the system and is paralleled by the electric motor and the pressurized tank. Hence, only the change in the accumulator energy (hydraulic energy at the outlet) is studied during the work cycle as is the mechanical energy of the motor shaft and the hydraulic energy at the DHPMS inlet. On the other hand, the change in the output energy is calculated considering the measured cylinder pressures and the piston velocity, and therefore includes the friction forces of the actuator.

The studied prototype DHPMS has two independent outlets which allow an experimental evaluation of the displacement control approach in the case of a double-acting cylinder. However, the cylinder has to be used as a single acting one when another outlet of the DHPMS is reserved for the accumulator in the case of the hybridized system. Despite the limitations of the test system, the feasibility of the DHH can be validated from the controller point of view. Additionally, the usability of the accumulator as an additional energy source/sink can be verified. Inspections of a multi-actuator system, however, are limited to a simulation study only. However, the simulation results should correspond to a real life application as the system is an extension of the experimentally evaluated systems.

1.5 Outline and contributions of the thesis

This doctoral thesis is divided into 7 chapters. The contents of each chapter are summarized below:

Chapter 1 provides a motivation for the study and gives a review of energy efficient hydraulics. In addition, the objectives of the thesis are discussed and followed by research methods, restrictions, and contributions.

Chapter 2 introduces a piston-type DHPMS; the basic principle and control method are considered. Moreover, efficiency measurements of a prototype machine are presented and the methods of application are discussed.

Chapter 3 introduces the studied system - a small excavator boom. The test platform is presented in detail and the simulation model is also considered.

Chapter 4 investigates displacement control by using the DHPMS. First, the basic principle and the control method are explained. Then the system is verified by simulations and experimental tests. The displacement controlled system is also compared with a proportional controlled system from the energy consumption point of view. Finally, the results are analyzed.

Chapter 5 inspects the DHH. First, the basic principle and the control method are explained. Then the concept is verified by simulations and experimental tests. Moreover, the expandability for a multi-actuator system is studied by simulations. Finally, the results are analyzed.

Chapter 6 gathers the results and provides a commentary and explanation. Additionally, relevance of the results are discussed.

Chapter 7 concludes the thesis and provides recommendations for future work.

The efficiency measurements of the studied DHPMS presented in Chapter 2 have been published in [67]; the experiments were conducted in co-operation with M.Sc. Jyrki Tammisto, and D.Sc Mikko Huova contributed to the controller development. The inspections concerning direct displacement control in Chapter 4 are partially based on publications [68 – 70]. Additionally, some comparison measurements have been presented in [71], where M.Sc. Matti Karvonen contributed to the introduction of the proportional system. The research related to the DHH (Chapter 5) has been published in part in [72, 73].

The main contributions of this thesis can be listed as follows:

- ⋆ Control method of the DHPMS for a directly actuated cylinder
- ⋆ Control method for the DHH with displacement controlled actuators
- ⋆ Validation of the control methods by simulations and experimental tests
- ⋆ Energy analysis of the systems by simulations and experimental tests

2 Digital Hydraulic Power Management System

2.1 Basic principle

The DHPMS is an innovation which is based on digital pump/motor technology, but the unit has multiple outlets [26]. Moreover, the outlets are independent of each other; thus, the DHPMS can serve several arbitrary pressure levels. Power transfer between the outlets can also be implemented because the machine works as a hydraulic transformer in addition to a pump and a motor. Fig. 2.1 shows a schematic of the six-piston DHPMS with two independent outlets. Each pumping piston of the DHPMS can be connected to either one of the outlets A or B, or to the tank T via actively controlled on/off control valves.

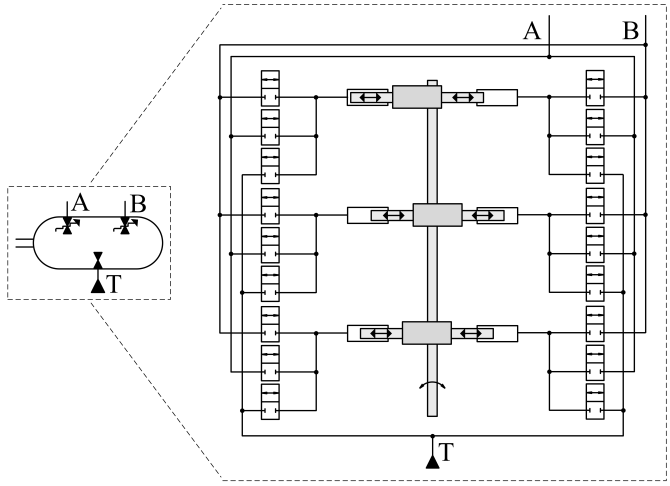

Figure 2.1: Six-piston DHPMS with two independent outlets.

In the case of two independent outlets, there are three mode options for pumping and motoring, as shown in Fig. 2.2. The fluid can be pumped to T, A, or B (subfigures (a-c) in Fig. 2.2), and it can also be motored from both the outlets and from the tank (subfigures (d-f) in Fig. 2.2). Digital technology also allows fully adjustable pressure precompression and decompression phases; hence, the energy of the compressed fluid can be recovered.

The pressure can be raised before starting to pump to, or motor from higher pressure (subfigures (g) and (h) in Fig. 2.2). Correspondingly, the pressure can be decreased before starting to pump to, or motor from lower pressure (subfigures (i) and (j) in Fig. 2.2).

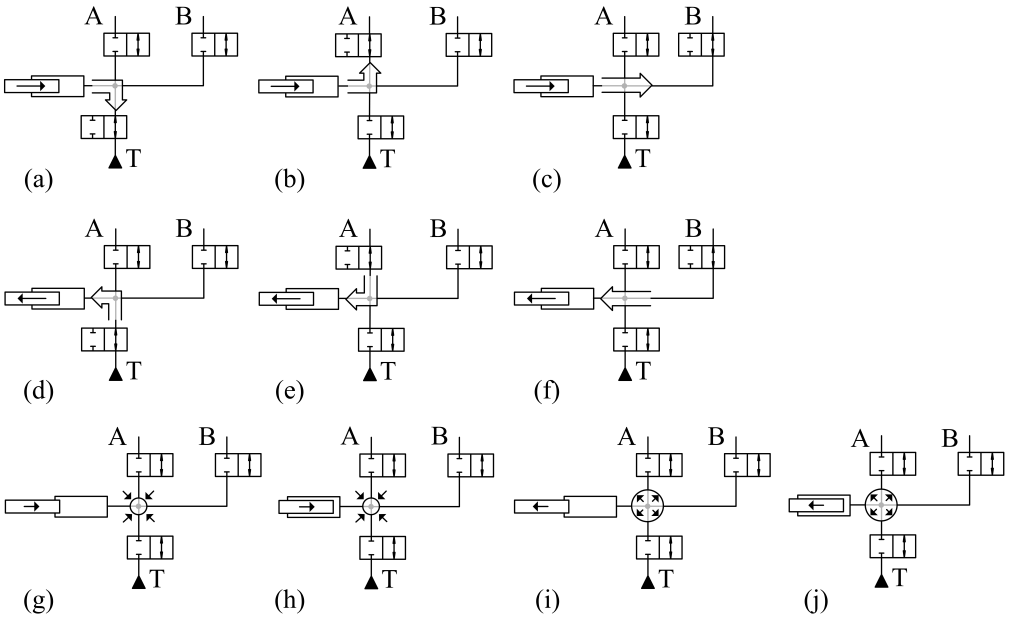

Figure 2.2: Example of DHPMS operation modes (a–f) and pressure pre-/decompression functions (g–j).

The theoretical maximum flow of the DHPMS (incompressible fluid and ideal valves) is determined by geometric displacement V_g and rotational speed according to the equation:

$$Q_\mathrm{max} = n \cdot V_\mathrm{g} \tag{2.1}$$

Hence, the flow rate of both outlets A and B can vary between $-Q_\mathrm{max}$ and Q_max on condition that the sum of the flows does not exceed these limits. Moreover, the flow rate at tank line T equals the sum of flows at the outlets. For a DHPMS that has k independent outlets, the flow limitations can be written as a generalized form:

$$\begin{cases} -Q_\mathrm{max} \leq Q_\mathrm{i} \leq Q_\mathrm{max} \\ -Q_\mathrm{max} \leq \sum_{i=1}^{k} Q_\mathrm{i} \leq Q_\mathrm{max} \\ \sum_{i=1}^{k} Q_\mathrm{i} + Q_\mathrm{T} = 0 \end{cases} \tag{2.2}$$

where Q_i is the flow rate at i:th outlet and Q_T is the flow rate at the DHPMS inlet.

2.2 Valve timing control

To operate smoothly, the DHPMS must accurately time the valve closing and opening. The pressures at the valve inlet and outlet ports must be close in value at the moment when the valve opens in order to avoid excessive pressure peaks and oscillation. Incorrect valve timing also causes additional pressure losses in the valves and lowers the efficiency of the DHPMS. Therefore, the precompression and decompression times, as well as the valve delays, must be taken into account in the valve control. [67]

The cycle of operation as a pump is shown in graph (a) in Fig. 2.3. At the beginning of the pumping stroke, the Low Pressure Valve (LPV) is closed at Bottom Dead Center (BDC) and the fluid is pressurized to a level of high pressure ($p_{\max}$ in the example). The precompression is fully adjustable and depends on the pressure levels. Pumping to high pressure starts at the moment when the High Pressure Valve (HPV) is opened. The pumping ends at the Top Dead Center (TDC) where the HPV is closed. The fluid is depressurized to the level of the low pressure (p_{T} in the example) before the LPV is opened. The decompression is also fully adjustable and valve delays can also be compensated for.

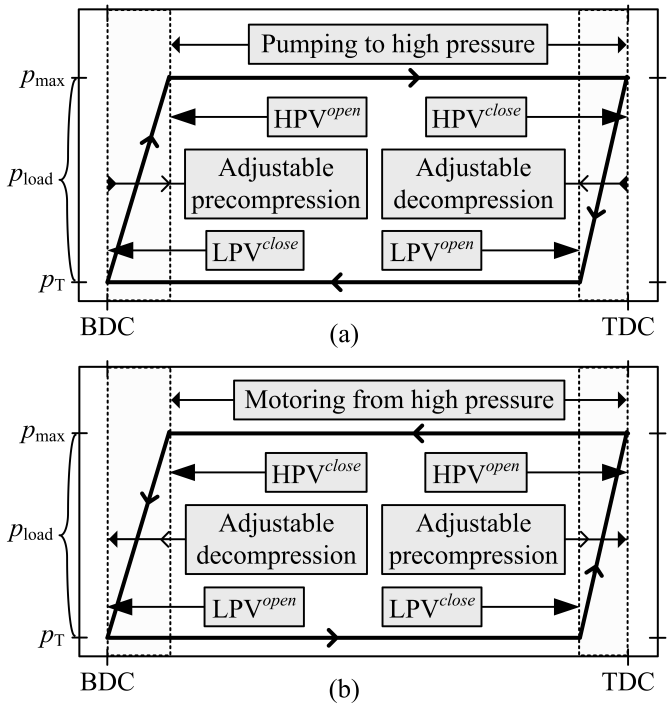

Figure 2.3: DHPMS valve timing principles for a pumping (a) and motoring (b) cycles in respect of cylinder pressures.

The cycle of operation as a motor is reverse in comparison with the pumping and is shown in graph (b) in Fig. 2.3. The motoring from high pressure starts at the TDC when the HPV is opened. At the end of the motoring stroke, the HPV is closed before reaching the BDC in order to depressurize the fluid to the level of low pressure (p_{T} in the example).

Pumping to low pressure starts at the BDC when the LPV is opened. At the end of the pumping stroke, the LPV is closed before the TDC and the fluid is pressurized to a level of high pressure ($p_{\max}$ in the example) and a new cycle starts from the beginning.

Table 2.1: Determination of optimal angles for valve opening and closing commands [67].

	Pumping cycle	Motoring cycle
HPV^{on}	$\theta_{\text{on}} = \theta_{\Delta\text{p}} - \theta_{\text{valve}}$ OR $\theta_{\text{on}} = 360° - \theta_{\text{valve}}$	$\theta_{\text{on}} = 180° - \theta_{\text{valve}}$
HPV^{off}	$\theta_{\text{off}} = 180° - \theta_{\text{valve}}$	$\theta_{\text{off}} = 360° - \theta_{\Delta\text{p}} - \theta_{\text{valve}}$
LPV^{on}	$\theta_{\text{on}} = 180° + \theta_{\Delta\text{p}} - \theta_{\text{valve}}$	$\theta_{\text{on}} = 360° - \theta_{\text{valve}}$
LPV^{off}	$\theta_{\text{off}} = 360° - \theta_{\text{valve}}$	$\theta_{\text{off}} = 180° - \theta_{\Delta\text{p}} - \theta_{\text{valve}}$

Table 2.1 shows the method that is used to determine the optimal valve command instants for the pumping and motoring cycles. In comparison with Fig. 2.3, the BDC corresponds to zero or 360 degrees while the TDC is at 180 degrees. In the equations, $\theta_{\Delta\text{p}}$ represents the pre-/decompression time in degrees and θ_{valve} the valve opening/closing delay in degrees. The timing angle calculation is unambiguous elsewhere, but in the case of the pumping cycle when the HPV is commanded on; if $\theta_{\Delta\text{p}} \geq \theta_{\text{valve}}$, the angle is calculated as $\theta_{\text{on}} = \theta_{\Delta\text{p}} - \theta_{\text{valve}}$ but otherwise from the equation $\theta_{\text{on}} = 360° - \theta_{\text{valve}}$. The valve opening/closing delay in degrees can be determined from the equation:

$$\theta_{\text{valve}} = n_{\text{filt}} \cdot d_{\text{valve}} \tag{2.3}$$

where n_{filt} is the filtered DHPMS rotational speed [°/s] and d_{valve} is the valve delay [s]. The piston movement Δx during pre-/decompression can be determined using the equation:

$$\Delta x = \Delta p_{\text{comp}} \cdot \frac{V_{\text{tot}}}{B_{\text{oil}} \cdot A_{\text{disp}}} \cdot CF \tag{2.4}$$

where Δp_{comp} is an absolute value of the pressure difference when interchanging from pumping to motoring or the other way round, V_{tot} is the overall compression volume of the cylinder, B_{oil} the bulk modulus of the fluid, A_{disp} the piston area, and CF the correction factor, which is individual for each piston at the BDC and TDC. For example, if one of the pistons is motoring from outlet A and pumping mode B is chosen for that piston, $\Delta p_{\text{comp}} = |p_{\text{A}} - p_{\text{B}}|$ and $V_{\text{tot}} = V_0 + V_{\text{disp}}$, where V_0 is the dead volume of the cylinder and V_{disp} the geometrical piston displacement. On the other hand, if the piston is currently pumping to outlet B and mode A is chosen for the motoring, $\Delta p_{\text{comp}} = |p_{\text{B}} - p_{\text{A}}|$ and $V_{\text{tot}} = V_0$.

The bulk modulus B is estimated in relation to the pressure level and temperature. With a correction factor CF, the slope can be further adjusted. The CF is used because the parameters in Eq. 2.4 cannot be determined precisely and they can even vary between the cylinders; thus, the valve timing for each cylinder can be fine-tuned by using the CFs. When the trajectory of the piston is sinusoidal, the pre-/decompression time expressed in a rotation angle can be further calculated from the equation:

$$\cos\theta_{\Delta\mathrm{p}} = \frac{-2 \cdot \Delta x}{s} + 1 \tag{2.5}$$

where the fixed parameter s is the piston stroke. Eventually, the valves are controlled based on a measured piston angle, and a valve command is executed when the estimated piston angle reaches the optimal calculated switching angle. Hence, the rotation angle and the rotational speed of the DHPMS must be known as accurately as possible. This can be done by measuring the absolute rotation angle of the shaft using the Hall effect sensor to detect rising edges from a gear ring. In this case, the rotational speed [°/s] can be calculated from the equation:

$$n_{\mathrm{pulses}} = \frac{360^\circ}{\Delta t_{\mathrm{pulses}} \cdot N_{\mathrm{pulses}}} \tag{2.6}$$

where $\Delta t_{\mathrm{pulses}}$ is the time between sequential pulses detected from the gear ring and N_{pulses} is the total number of teeth of the gear ring. However, the resolution of the gear ring is often too small to accurately time the on/off valves; therefore, a more advanced method to accurately estimate the angle and the rotational speed of the DHPMS needs to be used. The filtered rotational speed at time k can be calculated using the recursion:

$$n_{\mathrm{filt}}(k) = (1-\gamma) \cdot n_{\mathrm{filt}}(k-1) + \gamma \cdot n_{\mathrm{pulses}}(k) \tag{2.7}$$

called the Geometric Moving Average (GMA) [74]. The weight term $\gamma \in (0, 1]$ acts as a forgetting factor; hence, it defines the rate at which the previous values are forgotten. The weight term 1 means that only the last measured interval is used as the output, and that the smaller the value, the slower the dynamics of the filter become. By using filtered rotational speed, the rotation angle of the DHPMS can be reliably estimated also between the pulses detected from the gear ring. However, a separate zero pulse, which occurs once per revolution, must be used to avoid the angle measurement error in the long run. In this way, a potential measurement error may only briefly lower the performance of the DHPMS.

2.3 Measured efficiency of a prototype machine

The prototype DHPMS introduced in [67] is based on a six-piston boxer pump, which has geometric displacement of about 30 cm^3/rev. However, the original check valves are replaced with actively controlled fast two-way prototype on/off valves. Moreover, each cylinder can be connected to a second outlet via additional control valves, as shown in Fig. 2.1. The on/off valves have an opening and closing delay of around 1 ms and their flow capacity is about 23 l/min at the pressure difference of 0.5 MPa, as detailed also in Table 2.2. The prototype machine is presented in Fig. 2.4; each cylinder has a pressure relief valve in addition to the control valves, and the pressure is measured in each cylinder, as well as in the inlet and outlet ports. In order to minimize the oscillation in the pressurized tank line, it has two accumulators and low pressure hoses are used.

A test set-up has been arranged to measure the efficiency of the machine. A pressurized tank line is realized by using an auxiliary pump, and the inlet pressure is set to 1 MPa

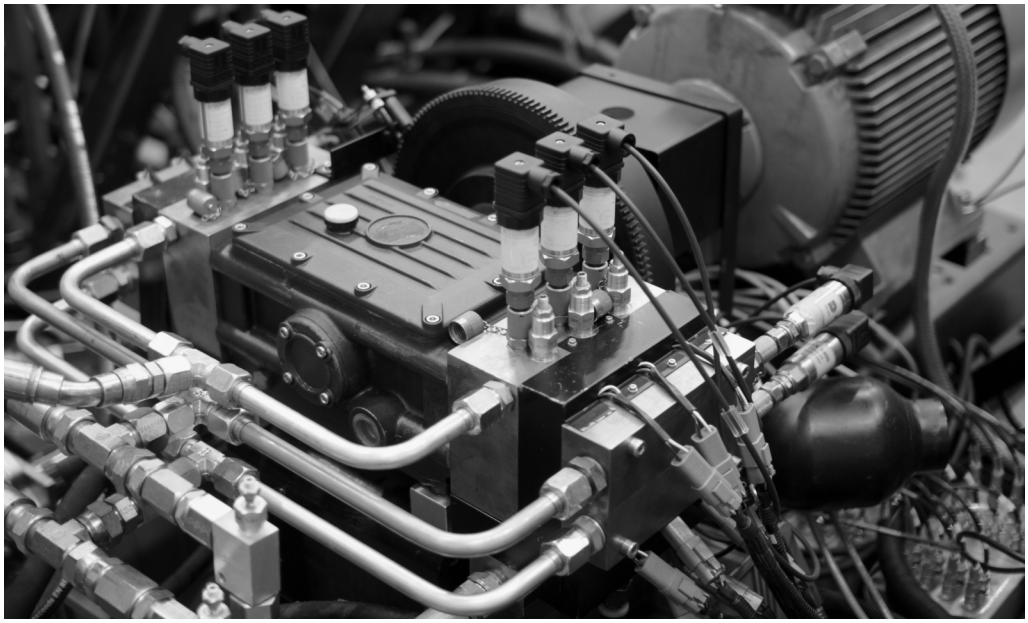

Figure 2.4: The studied DHPMS: A six-piston machine with two independent outlets.

Table 2.2: Dimensions and characteristics of the DHPMS [67].

DHPMS unit		DHPMS control valves	
Number of pistons	6	Opening delay	1 ms
Number of independent outlets	2	Closing delay	1 ms
Piston diameter	20 mm	Nominal flow	23 l/min
Piston stroke	16 mm	Nominal pressure difference	0.5 MPa

with a pressure relief valve. A pressurized tank line is used to avoid cavitation of the cylinders as the flow capacity of the on/off control valves is significantly lower than the flow capacity of the original check valves. The first supply line (A) consists of a 0.75 l accumulator and an electronically controlled proportional directional control valve, which is used to realize different loadings. The second outlet (B) has a 4 l accumulator which is used as an energy storage. In addition, both actuator lines have flow and pressure sensors near the accumulators, and the rotational speed as well as torque are measured from the rotating shaft.

Figure 2.5 shows the idle losses of the measured prototype DHPMS in relation to the rotational speed. The pistons are connected to the pressurized tank line ($p_{\mathrm{T}} = 1$ MPa); hence, the input power measured from the rotating shaft consists of parasitic losses in the control valves and friction forces. The measured loss is around 180 W at a rotational speed of 600 r/min and 630 W at a rotational speed of 1200 r/min, correspondingly. In this case, doubling the rotational speed led to 3.5 times bigger idle losses. The result implies that friction losses are directly proportional to the rotational speed, but the pressure losses in the control valves are quadratic.

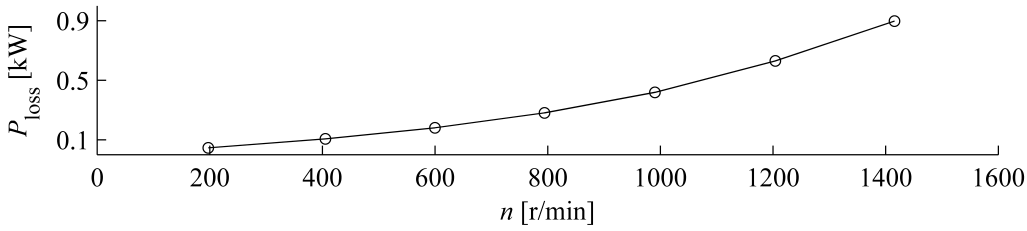

Figure 2.5: Measured idle losses of the prototype DHPMS (@ 30 °C) with respect to the rotational speed [67].

The pumping efficiency of the DHPMS at full displacement is measured using supply line A with the accumulator disengaged. The efficiencies are shown in Fig. 2.6. The results are presented in respect of the pressure difference and the measurements are carried out using an oil temperature of about 40 °C. Graph (a) in Fig. 2.6 shows the volumetric, hydromechanical, and total efficiencies at a rotational speed of 500 r/min.

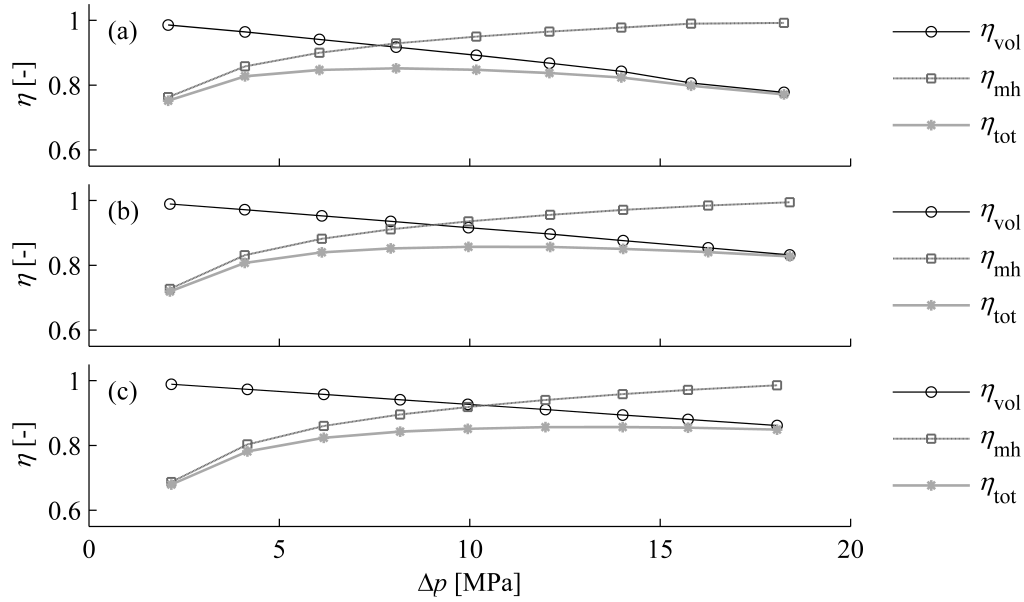

Figure 2.6: Measured full pumping efficiencies of the prototype DHPMS (@ 40 °C) with respect to the pressure difference with rotational speeds of 500 r/min (a), 750 r/min (b), and 1000 r/min (c) [67].

The volumetric efficiency is high at low pressure, but it decreases due to leakage in the control valves when the pressure difference is increased. The hydromechanical efficiency is at its lowest when the pressure difference over the DHPMS is small because the pressure losses in the control valves are relatively big in comparison with the losses at higher pressure difference. However, the measured total efficiency is above 0.8 for most of the pressure range. When the rotational speed is raised, the worsened hydromechanical efficiency decreases the total efficiency at smaller pressure levels. On the other hand,

increasing the rotational speed improves the volumetric efficiency, which can be seen as an improved total efficiency at higher pressure levels (graphs (b) and (c) in Fig. 2.6). The hydromechanical efficiency is near 1 at maximum pressure despite the parasitic losses due to its definition:

$$\eta_{\mathrm{mh}} = \frac{\Delta p \cdot V_{\mathrm{g}}}{2\pi \cdot T} \tag{2.8}$$

Hence, the hydromechanical efficiency is the ratio of the theoretical torque and the measured one (T), where the theoretical torque is a product of the pressure difference Δp over the DHPMS and the radial displacement $V_{\mathrm{g}}/2\pi$. However, the compressibility of the fluid is not considered by Eq. 2.8; therefore, the measured torque could even be smaller than that calculated according to the theoretical displacement.

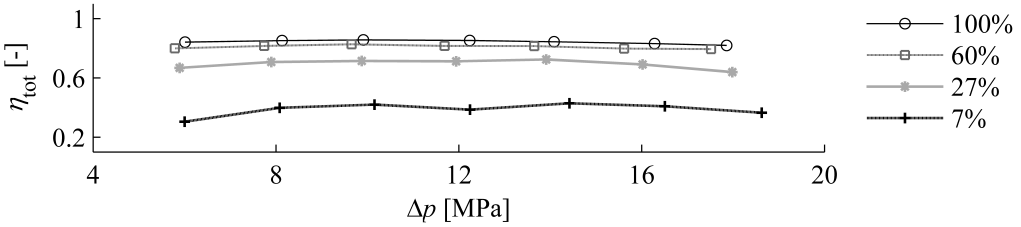

Figure 2.7: Measured partial pumping efficiencies of the prototype DHPMS (@ 30 °C) with respect to the pressure difference with a rotational speed of 500 r/min [67].

The prototype DHPMS is also measured for its efficiency at partial displacements. In the tests, the supply line accumulator is used to smooth the flow. Figure 2.7 shows the total efficiencies for pumping at a rotational speed of 500 r/min and oil temperature of 30 °C. It can be seen that the efficiency stays over 0.8 almost consistently at flows over 9 l/min (60% of the theorethical maximum flow), and is still above 0.63 at a flow of 27% of the maximum. However, at the lowest measured flow, the efficiency drops even below 0.31 owing to idle losses compared with the produced hydraulic power. In addition, the leakage is relatively higher at smaller flows, which lowers the volumetric efficiency, and thus the total efficiency decreases.

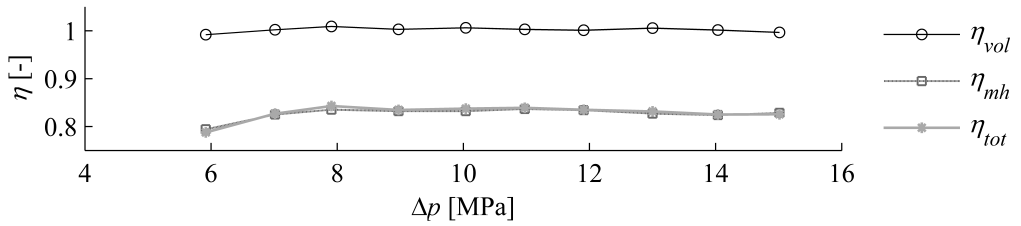

Figure 2.8: Measured full motoring efficiencies of the prototype DHPMS (@ 30 °C) with respect to the pressure difference with a rotational speed of 500 r/min [67].

The efficiencies of the DHPMS have also been measured as a motor at full displacement. An angular velocity of 500 r/min is used and the oil temperature is 30 °C in the tests.

The supply line B is used such that the pressure in the accumulator is raised to 16 MPa before starting to motor from high pressure. The efficiencies are calculated at designated times to obtain efficiency at a certain pressure difference and the results are shown in Fig. 2.8.

The volumetric efficiency is at best slightly over 1 because the volumetric efficiency is defined as:

$$\eta_{\mathrm{vol}} = \frac{n \cdot V_{\mathrm{g}}}{Q} \tag{2.9}$$

Hence, the volumetric efficiency is the ratio of the theoretical flow and the measured one (Q), where the theoretical flow is calculated by multiplying the measured rotational speed n by the geometrical displacement V_{g}. However, the compressibility of the fluid is not considered by Eq. 2.9. The dead volume of each cylinder of the DHPMS is multiple compared with the piston displacement; therefore, the measured flow can be smaller than the theoretical one despite the leakage. The hydromechanical efficiency is over 0.8 over most of the pressure range. At some points, the total efficiency is better than the hydromechanical efficiency, because the volumetric efficiency is over 1.

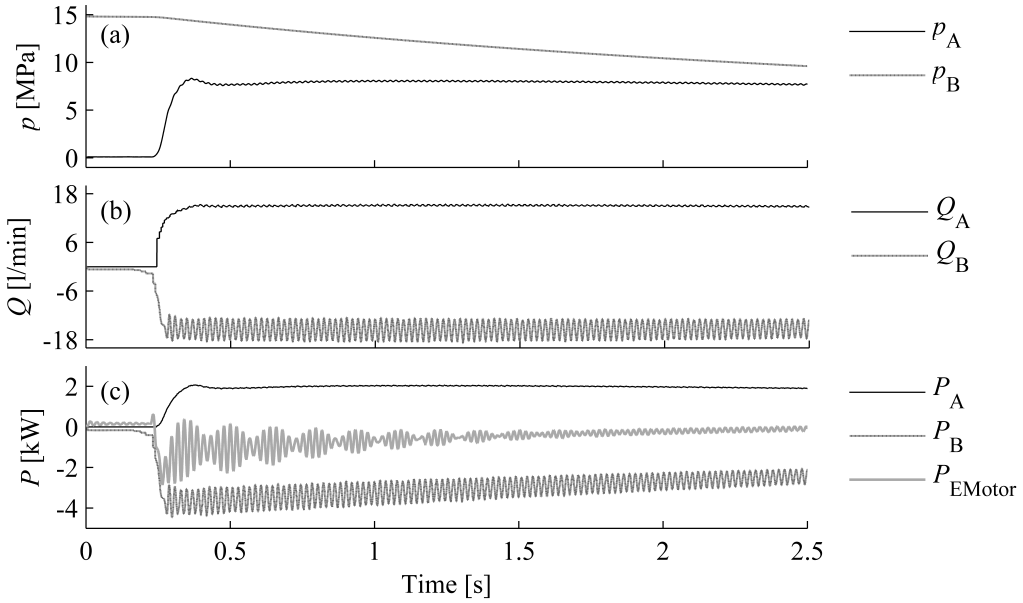

Figure 2.9: Measured pressures (a), flows (b), and powers (c) for the prototype DHPMS (@ 30 °C) when transferring power between the outlets with a rotational speed of 500 r/min [67].

Power transfer is studied with fluid being received from supply line B and pumped to supply line A; hence, the DHPMS is motoring from the accumulator outlet and pumping to another outlet where the load pressure is kept around 7.5 MPa by the proportional control valve. A rotational speed of 500 r/min is used and the oil temperature is about 30 °C during the experiment. The results are shown in Fig. 2.9.

During the power transfer, supply line A pressurizes, whereas the pressure in the accumulator line starts to decrease, as shown in graph (a) in Fig. 2.9. As the pumping and motoring take place in parallel at full displacement, the supply line B flow is negative, whereas the flow in supply line A is positive (graph (b) in Fig. 2.9). The oscillation visible in the negative flow is probably caused by the pipeline dynamics; the studied motoring cycle initiates the vibration in the accumulator line. Graph (c) in Fig. 2.9 shows the supply line power and the mechanical power measured from the rotating shaft. At full displacement, the hydraulic power taken from actuator line B is about 2.61 kW on average, and that pumped to line A is 1.67 kW, correspondingly. In addition, the shaft power transferred to the electric motor is about 0.43 kW. Hence, the losses are about 0.51 kW ($-0.43 - 1.67 + 2.61$) and the total efficiency of the power transfer is about 0.8, meaning that the efficiency of the DHPMS does not decrease in transformer mode.

2.4 Methods of application

The DHPMS is able to control separate supply line pressures, both fast and accurately, as shown by the simulations in [75, 76], while the experimental results have been presented in [77–79]. The studied systems are shown in Fig. 2.10; the proportional controlled actuation (graph (a) in Fig. 2.10) and the actuation with distributed valves (graph (b) in Fig. 2.10) are investigated in a small excavator boom. The pressure control (mode control of the DHPMS) utilizes the estimated supply line capacitances and the actuator flow estimates; hence, Model Predictive Control (MPC) is used. The pressure targets are set according to the ELS function to keep the pressure losses at a minimum.

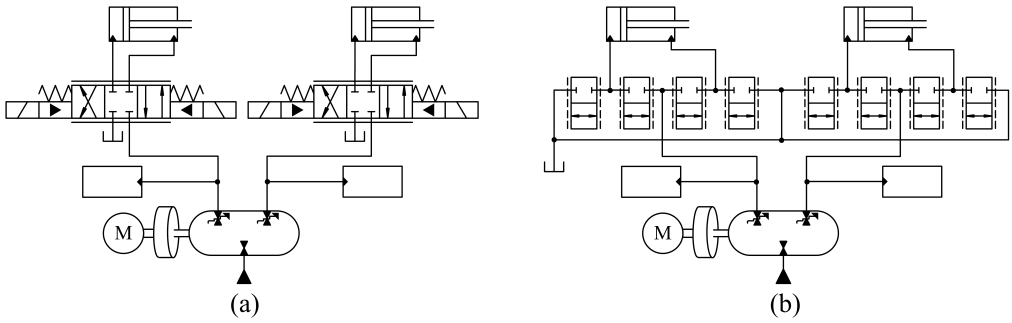

Figure 2.10: Independent actuator supply pressure control using the DHPMS: Proportional control valves (a) and a distributed valve system (b) [75, 76].

The main benefit of the DHPMS approach in multi-actuator systems is an optimized supply pressure level for each individual actuator. Therefore, the losses may significantly reduce compared with traditional LS systems, where the supply pressure is adjusted according to the highest load pressure. The simulations show a 22% reduction in losses for a proportional controlled boom when independent supply lines are used in comparison with a common LS line [75], and even more energy can be saved when distributed valve systems are used for cylinder actuation [76]. In addition to the simulations, experimental tests have validated the energy saving potential of the multi-pressure approach [77]. This doctoral thesis focuses on displacement controlled actuation by using the DHPMS, but also studies a new hydraulic hybrid concept.

3 The studied system: A small excavator boom

3.1 Test platform

In this doctoral thesis, the energy efficient actuation of a hydraulic cylinder is investigated in a small excavator boom which is presented in Fig. 3.1. The boom has an installed lift and tilt cylinders which have a piston diameter of 63 mm and their rod diameter is 36 mm correspondingly. The stroke of the lift cylinder is about 500 mm and that of the tilt cylinder about 350 mm. Due to the installation, the boom lifts up when the lift cylinder is driven inward. Hence, the load force of the lift cylinder is continuously negative whereas the load force of the tilt cylinder can change its direction. The bucket is replaced with a mount that allows testing with various load masses. The used discs weigh 25 kg each and eight of them can be engaged to the boom tip at once. In addition, a variable load mass can be tested by using additional weight discs attached to the boom by a lifting sling. The distance between the base joint and the joint connecting the lift and tilt bodies is 1590 mm, and the distance from the joint connecting the lift and tilt bodies to the boom tip is 900 mm; hence, the reach of the boom is nearly 2.5 m.

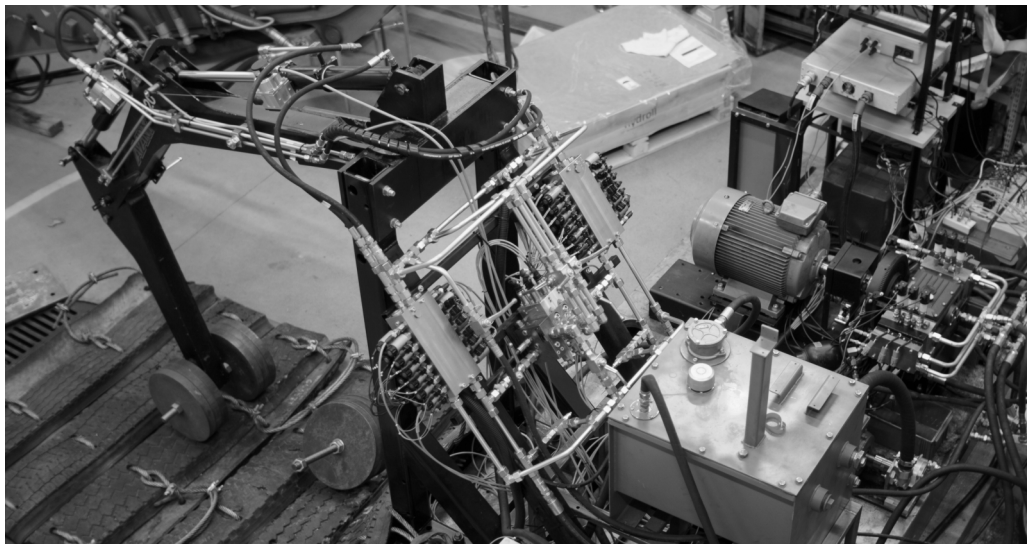

Figure 3.1: Test system: Digital hydraulic excavator boom.

The studied boom enables investigating different system layouts; therefore, the boom is equipped with numerous hydraulic components as shown in Fig. 3.2. The main components are numbered 1 – 14 and they are also enumerated in Table 3.1. Sufficient flow to the DHPMS inlet is produced by an auxiliary pump (1), while the inlet pressure is adjusted by a pressure relief valve (2). The DHPMS (5) is driven by an induction motor (3) and its rotational speed can be set by a frequency converter. A flywheel (4) installed in the rotating shaft can temporarily store the rotational energy and it also smooths out the torque.

Table 3.1: Numbered system components 1 – 14 in Fig. 3.2.

no.	Component	Details
1	Auxiliary pump	Constant flow: 27 l/min
2	Pressure relief valve	Pressure setting: 1 MPa
3	Induction motor	Rated power: 18.5 kW @ 1450 r/min
4	Flywheel	Moment of inertia: 0.15 kgm^2
5	DHPMS	Geometrical displacement: 30 cm^3
6	Added capacitance	Volume: 5 l
7	Adjustable needle valve	Damping orifices
8	Accumulator	Nominal size: 4 l, Inflation pressure: 3 MPa
9	Proportional valves	BR M4-X2 block with special spools
10	Digital valve systems	Six BR KSDER on/off valves per control edge
11	Lift cylinder	Dimensions: ⌀63/36 – 500 mm
12	Tilt cylinder	Dimensions: ⌀63/36 – 350 mm
13	Pressure relief valve	Pressure setting: 25 MPa
14	Oil filter	Return line particle filter

The supply lines are equipped with additional rigid volumes (6a, 6b) in order to constrain the maximum pressure ripple to 1 MPa. In addition, the flow of the volumes can be restricted by using adjustable needle valves (7a, 7b). A gas-charged piston accumulator (8) can also be connected to one outlet of the DHPMS. The hose volumes of the supply lines are quite large as well: approximately 1.4 l on both lines. Pressure relief valves in the supply lines and alongside the accumulator (13a, 13b, 13c) are installed for a passive fail safe feature. The hydraulic oil used in the system has grade ISO VG 32.

The boom has an installed proportional valve block (9) and DVSs (10a, 10b) by which the cylinders can be controlled. A commercial mobile valve block, provided by Bosch Rexroth (BR), is slightly modified to meet the requirements of independent supply line pressures. In addition, each control edge P-A, A-T, P-B and B-T of the DVSs consists of six on/off valves provided by BR. Orifices for the on/off valves are selected such that the flow of the control edge can be set according to the binary coding. However, the two biggest valves are the same size.

The measurement points for the transducers are numbered I – XV in Fig. 3.2. The DHPMS inlet pressure (I) is measured near the tank valves, whereas the supply line pressures are measured right after the outlet valves (II, III), but they are also measured in the DVS

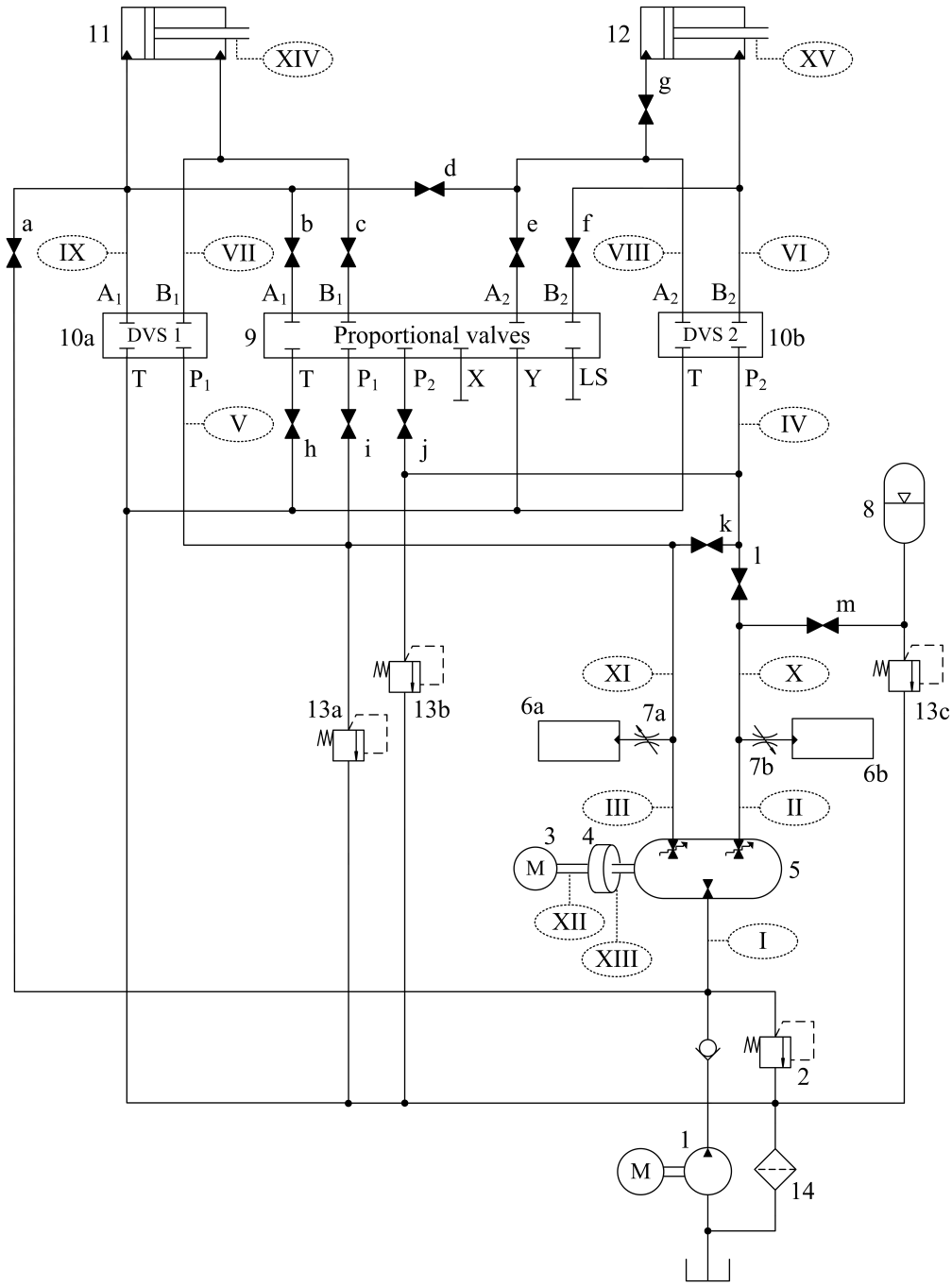

Figure 3.2: Schematic of the studied digital hydraulic excavator boom: The main components are numbered 1−14, whereas the measurement points for transducers are numbered I−XV.

blocks (IV, V). The DVS blocks also have the pressure measurement for the cylinder chambers (VI–IX). In addition, both supply lines have a gear type flow meter placed after the rigid volumes (X, XI). The input torque is measured from the rotating shaft (XII) and the transducer also has an option for an angle measurement. The rotation angle utilized by the controller is measured using a gear ring integrated into the flywheel (XIII). The distance between the cylinder joints are measured using incremental encoders (XIV, XV). The installed transducers of the test platform are also detailed in Table 3.2. For the data acquisition, a dSPACE system with boards DS1103, DS2001 and DS2004 are used. The utilized transducers for the system analysis in each experiment and the signal processing methods are considered in Appendix A: Measured quantities.

Table 3.2: Utilized transducers at numbered measurement points I–XV in Fig. 3.2.

no.	Quantity	Transducer	Range	Accuracy
I	Pressure	Druck PTX 1400	0–4 MPa	±0.25%
II	Pressure	Druck PTX 1400	0–25 MPa	±0.25%
III	Pressure	Druck PTX 1400	0–40 MPa	±0.25%
IV–IX	Pressure	Trafag NAH250.0A	0–25 MPa	±0.3%
X–XI	Flow volume	Kracht VC1	–	0.26 cm^3
XII	Shaft torque	HBM T40B	±200 Nm	±0.1%
	Rotation angle	HBM T40B	–	0.09°
XIII	Rotation angle	Honeywell 1GT1	–	2.5°
XIV–XV	Piston position	Pepperl+Fuchs RVI158N	0–1 m	20 μm

The different system layouts can be achieved by routing the flow through certain ball valves. The open flow paths in correspondence with possible system configurations are listed as follows:

- ⋆ *Proportional valve control with independent supply line pressures*
  → Ball valves: b, c, e, f, g, h, i, j, l
- ⋆ *Digital valve control with independent supply line pressures*
  → Ball valves: g, l
- ⋆ *Proportional valve control with shared supply line pressure* (accumulator engaged)
  → Ball valves: b, c, e, f, g, h, i, j, k, (m)
- ⋆ *Digital valve control with shared supply line pressure* (accumulator engaged)
  → Ball valves: g, k, (m)
- ⋆ *Direct control of a double-acting lift cylinder*
  → Ball valves: d, l; DVS 1: P_1-B_1; DVS 2: P_2-A_2
- ⋆ *Direct control of a single-acting lift cylinder* (accumulator engaged)
  → Ball valves: a, (m); DVS 1: P_1-B_1

This doctoral thesis, however, exclusively concentrates on displacement controlled systems with the exception of the comparison measurements carried out by using a proportional controlled system. Nonetheless, only the lift cylinder actuation is studied with the test platform.

3.2 Simulation model

A model of the studied system has been created using MATLAB/Simulink and the SimMechanics toolbox [68, 72, 76]. The boom is modeled according to the dimensions shown in Fig. 3.3 and the mechanics consist of five bodies: a base, a two-part lift body, a tilt body, and a load mass. The massless base is fixed to the global origin; hence, only the coordinates for a lift boom joint and lift cylinder joint need to be defined. The lift boom is connected to the base by using a revolute joint and, in order to imitate the original shape of the boom, it is modeled by joining two bodies together using a weld. Furthermore, a revolute joint is utilized to connect the lift and tilt bodies together.

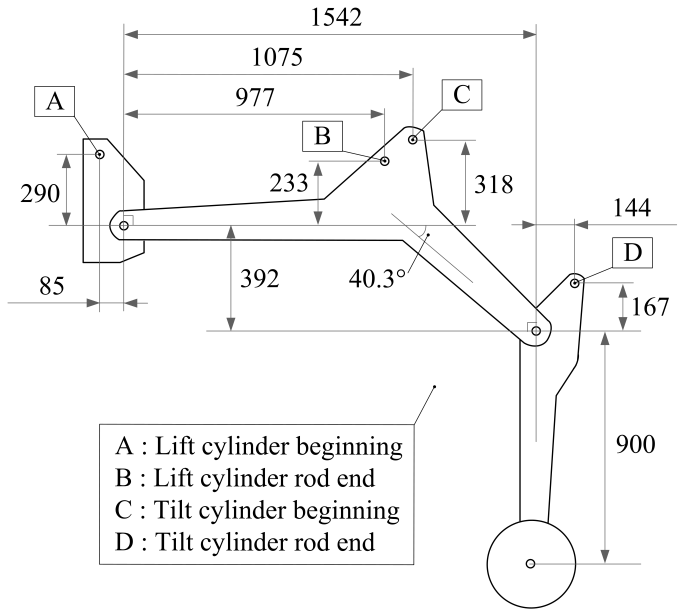

Figure 3.3: Boom dimensions (in millimeters) utilized in the SimMechanics model.

The bodies are modeled as slender rods and the moment of inertia matrices are determined as:

$$I = \begin{bmatrix} 0 & 0 & 0 \\ 0 & \dfrac{m \cdot L^2}{12} & 0 \\ 0 & 0 & \dfrac{m \cdot L^2}{12} \end{bmatrix} \tag{3.1}$$

where m is the mass of a rod and L is the rod length. For lift bodies, the lengths are 1 m and 0.69 m, and the masses are 50 kg and 40 kg respectively. On the other hand, the length of the tilt body is 0.9 m and it has a mass of 30 kg. The load mass welded to the tilt boom end is considered as a point mass at the distance of 0.1 m from the adjoining. The lift and tilt cylinders are modeled as force vectors in the mechanical model; thus, the moment of inertia caused by the cylinders is not considered in the boom model. The magnitudes of the force vectors are determined in a hydraulic model and the direction of the vectors are calculated according to the relative position of the cylinder joint coordinates. In addition, the cylinder lengths and velocities are determined from those coordinates as well.

An interaction between the system blocks in the simulation models is presented in Fig. 3.4 The most important equations for modeling the hydraulics are based on the compressibility of a fluid and the turbulent flow. A derivative of the pressure as the fluid volume changes can be solved from the equation:

$$\frac{dp}{dt} = \frac{B_{\text{eff}}}{V} \cdot \left(\sum Q - \frac{dV}{dt} \right) \tag{3.2}$$

where B_{eff} is the effective bulk modulus, V the total fluid volume, and Q the fluid flow involved in the volume. The flow through an orifice depends on the pressure difference and can be written as:

$$Q = \begin{cases} K_{\text{v}} \cdot \operatorname{sgn}(p_1 - p_2) \cdot \sqrt{|p_1 - p_2|} & : |p_1 - p_2| > p_{\text{tr}} \\ \dfrac{K_{\text{v}} \cdot (p_1 - p_2)}{2 \cdot \sqrt{p_{\text{tr}}}} \cdot \left(3 - \dfrac{|p_1 - p_2|}{p_{\text{tr}}} \right) & : |p_1 - p_2| \leq p_{\text{tr}} \end{cases} \tag{3.3}$$

where K_{v} is the orifice flow factor determined from the nominal characteristics and p_{tr} the transition pressure between the turbulent and laminar flow. Hence, at a small pressure difference, the model mimics the laminar flow in order to avoid infinite derivative when the pressure difference equals zero [80]. The volume model is used to simulate the lift and tilt cylinders, hose volumes of the system, damping volumes, and the DHPMS piston chambers. On the other hand, the flow model mimics the phenomena in the cylinder port orifices, damping orifices, and in the orifices of the DHPMS control valves. The dynamics of the control valves are modeled using a series connected delay and rate limit. Moreover, a dynamic friction model is applied to realistically imitate the seal friction of the lift and tilt cylinders [81].

The modeled DHPMS is assumed to be leakage-free and the mechanical friction forces are also ignored. The cylinder volumes, which are connected to the supply lines or to the tank throughout the on/off control valves, change in relation to the rotation angle. For a sinusoidal piston trajectory, the position of each pumping piston can be solved from the equation:

$$x_{\text{i}} = \frac{s}{2} \cdot \left[1 - \cos\left(\omega t - 2\pi \cdot \frac{i-1}{N_{\text{pistons}}} \right) \right] \tag{3.4}$$

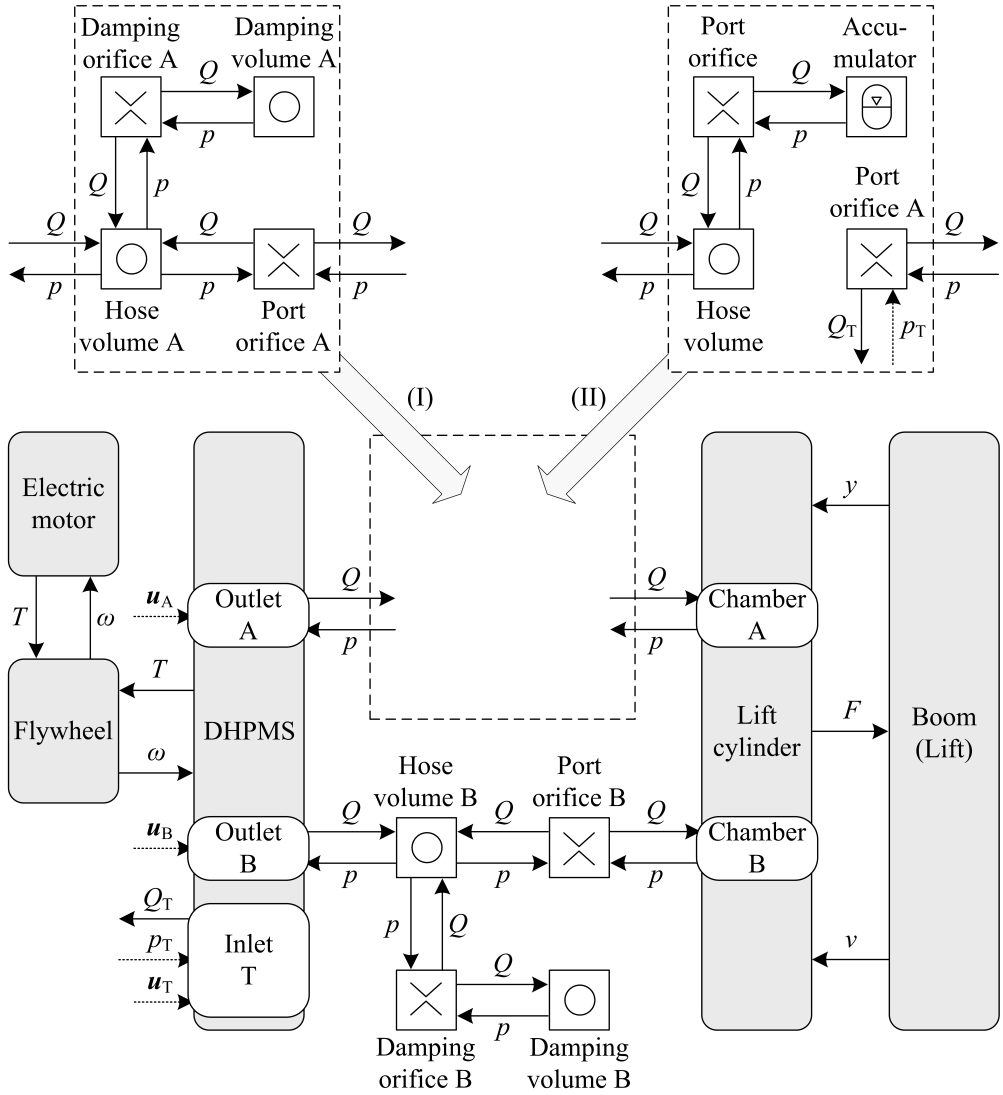

Figure 3.4: Interaction between the system blocks in simulation models: The displacement control of a double-acting lift cylinder by using a DHPMS (I) and the displacement control of a single-acting lift cylinder by using a hybridized DHPMS (II).

where ω is the angular velocity of the rotating shaft, s the stroke of a pumping piston, ω the angular velocity, N_{pistons} the piston count of the DHPMS, and i an integer: $i \in [1, N_{\text{pistons}}]$. The velocity for the pistons can be further calculated as a derivative of the position:

$$v_{\text{i}} = \frac{s}{2} \cdot \sin\left(\omega t - 2\pi \cdot \frac{i-1}{N_{\text{pistons}}}\right) \cdot \omega \tag{3.5}$$

The power produced by a piston i can be determined as a product of the force and the velocity; hence, the equation can be written as:

$$P_{\mathrm{i}} = p_{\mathrm{i}} \cdot A_{\mathrm{disp}} \cdot v_{\mathrm{i}} \tag{3.6}$$

where, p_{i} is the pressure in the pumping cylinder i and A_{disp} the area of the pumping piston. Because the torque can be calculated by dividing the power by the angular velocity, it validates for the DHPMS:

$$T_{\mathrm{DHPMS}} = \frac{P}{\omega} = \frac{\sum_{i=1}^{N_{\mathrm{pistons}}} P_{\mathrm{i}}}{\omega} \tag{3.7}$$

The electric motor is again modeled as a torque source and the torque is determined from the equation:

$$T_{\mathrm{EMotor}} = \frac{T_{\mathrm{N}}}{s_{\mathrm{N}}} \cdot (n_{\mathrm{s}} - n) \tag{3.8}$$

where T_{N} is the nominal torque of the motor, s_{N} the nominal slip, n_{s} the synchronous speed, and n the shaft rotating speed. When the affecting torques have been determined, the angular acceleration of the rotating shaft can be calculated as:

$$\alpha = \frac{1}{I} \cdot (T_{\mathrm{EMotor}} - T_{\mathrm{DHPMS}}) \tag{3.9}$$

where I is the moment of inertia of the flywheel. Furthermore, the angular velocity is an integral of the angular acceleration.

In this doctoral thesis two different system configurations are studied and they are shown in Fig. 3.4: the displacement controlled double-acting lift cylinder (I) is investigated in Section 4.3 and the displacement controlled single-acting lift cylinder with a hydraulic energy storage system (II) is reviewed in Section 5.3. The accumulator in the latter system configuration is modeled according to the ideal gas law:

$$p_0 \cdot V_0^{\kappa} = p_1 \cdot V_1^{\kappa} = p_2 \cdot V_2^{\kappa} \tag{3.10}$$

where p_0 is the gas inflation pressure, p_1 the gas initial pressure, p_2 the instantaneous gas pressure, and V_0, V_1, and V_2 the corresponding gas volumes. The process is assumed to be adiabatic, and the heat capacity ratio is therefore $\kappa = 1.4$.

An extended system model is studied in Section 5.5, which consists of a DHPMS with five independent outlets and it controls both the lift and tilt cylinders, and an accumulator. Hence, the model is created by doubling the supply lines of the system (I) and adding the accumulator line of the system (II). Of course, the additional outlets had to be inserted in the DHPMS model as well. The utilized simulation parameters can be found in Appendix B: Simulation parameters.

4 Displacement control using the DHPMS

4.1 Direct connection

Direct connection is a way to control an actuator by using the DHPMS [68]. In this approach, the DHPMS outlets are directly connected to the cylinder chambers and the cylinder actuation is based on the flow control of the supply lines. Figure 4.1 shows the system configuration studied in this chapter; the lift cylinder of the boom is controlled by the DHPMS while the tilt cylinder is hydraulically locked near to its minimum length throughout the tests. In theory, the method of actuation is free of hydraulic losses because the cylinder flows are not controlled by throttling and the energy can be also recovered.

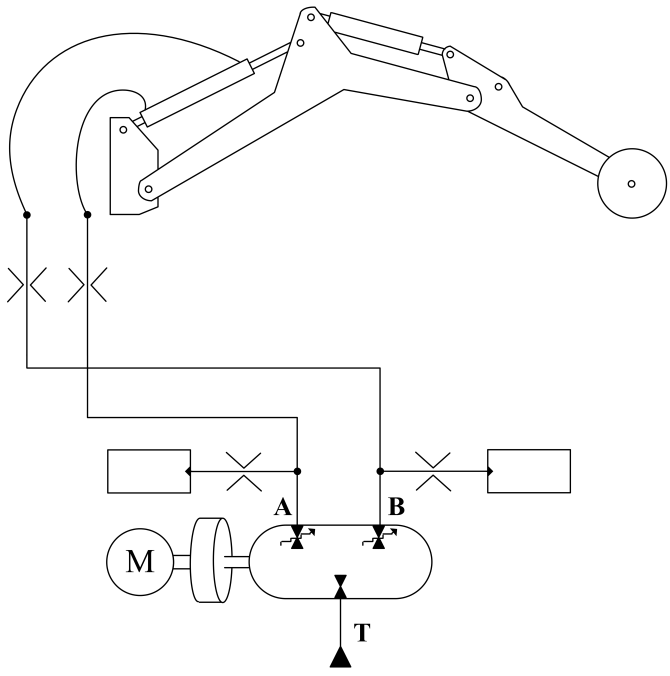

Figure 4.1: Displacement controlled boom (direct connection) using the DHPMS [71].

As the DHPMS is simultaneously pumping to one outlet and motoring from another, the direct connection can be regarded as a closed circuit system. In the case of an asymmetric cylinder, the maximum actuator velocity is the same at both moving directions and it is determined by the cylinder area at the maximum flow. Moreover, the accurate position tracking of the cylinder piston can be realized without utilizing a position feedback thanks to the stroke-by-stroke control of the pumping pistons. However, the positioning has a certain resolution that can be determined as:

$$\Delta y = \frac{V_{\text{disp}}}{A_{\text{cyl}}} \tag{4.1}$$

where V_{disp} is displacement of a pumping piston and A_{cyl} the effective area of the cylinder piston. In the studied boom, the load force is constantly negative. Therefore, the resolution depends on the rod side area and is about 2.4 mm in the worst case. If the resolution is enhanced by decreasing the piston displacement, either the number of pumping pistons needs to be added to or the rotational speed of the DHPMS must be increased in order to keep the maximum flow unchanged. In addition, the variation on the back-pressure of the cylinder also affects the position tracking accuracy.

4.2 Control algorithm

The principle of direct displacement control is to minimize the fluid volume errors (tracking error) in the cylinder chambers by choosing the best modes for pumping and motoring at each mode selection instant. A control block diagram for the mode selection logic is shown in Fig. 4.2. The target values for the actuator fluid volumes are calculated from the piston velocity reference taking the effective cylinder areas into consideration:

$$V_{\text{ref}} = (\pm) \int v_{\text{ref}} \cdot A_{\text{cyl}} \tag{4.2}$$

where the velocity reference v_{ref} is positive for an extending movement. Hence, the equation has a negative sign for the rod side volume as it increases, while the velocity reference is negative. The Euler method is used for the numerical integration and the change in volume is extrapolated until the stroke end assuming that the rotational speed is constant between the mode selection instants.

As the pumping and motoring modes are chosen in tandem, the volume errors are determined for all mode combinations using geometric piston displacement, as shown in Table 4.1. Finally, the optimal mode vector $\mathbf{M}_{\text{tmp}} = [M_{\text{P.tmp}}, M_{\text{M.tmp}}]$ is selected according to the minimizing function:

$$M_{\text{idx}} = \min_{idx}\{V_{\text{err.1}}, V_{\text{err.2}}, V_{\text{err.3}}, V_{\text{err.4}}, V_{\text{err.5}}, V_{\text{err.6}}, V_{\text{err.7}}\} \tag{4.3}$$

For example, if $M_{\text{idx}} = 4$ then the modes $\mathbf{M}_{\text{tmp}} =$ [“A”,“B”] will be preselected (see Table 4.1). Thereafter, the cumulative volume estimates V_{cyl} used in the error calculation (see Fig 4.2) are determined according to the preselected modes by considering the compression volume of the fluid:

Table 4.1: Determination of the combined fluid volume errors for all mode combinations.

M_P	M_M	Approximated total fluid volume error
T	T	$V_{\mathrm{err.1}} = \lvert V_{\mathrm{err.A}}\rvert + \lvert V_{\mathrm{err.B}}\rvert$
A	T	$V_{\mathrm{err.2}} = \lvert V_{\mathrm{err.A}} - V_{\mathrm{disp}}\rvert + \lvert V_{\mathrm{err.B}}\rvert$
T	B	$V_{\mathrm{err.3}} = \lvert V_{\mathrm{err.A}}\rvert + \lvert V_{\mathrm{err.B}} + V_{\mathrm{disp}}\rvert$
A	B	$V_{\mathrm{err.4}} = \lvert V_{\mathrm{err.A}} - V_{\mathrm{disp}}\rvert + \lvert V_{\mathrm{err.B}} + V_{\mathrm{disp}}\rvert$
B	T	$V_{\mathrm{err.5}} = \lvert V_{\mathrm{err.A}}\rvert + \lvert V_{\mathrm{err.B}} - V_{\mathrm{disp}}\rvert$
T	A	$V_{\mathrm{err.6}} = \lvert V_{\mathrm{err.A}} + V_{\mathrm{disp}}\rvert + \lvert V_{\mathrm{err.B}}\rvert$
B	A	$V_{\mathrm{err.7}} = \lvert V_{\mathrm{err.A}} + V_{\mathrm{disp}}\rvert + \lvert V_{\mathrm{err.B}} - V_{\mathrm{disp}}\rvert$

$$\Delta V_{\mathrm{comp}} = \Delta p_{\mathrm{comp}} \cdot \frac{V_{\mathrm{tot}}}{B_{\mathrm{oil}}} \cdot CF \tag{4.4}$$

where Δp_{comp} is the measured pressure difference (absolute value) at the crossover from pumping to motoring or the other way round, V_{tot} the compression volume in the DHPMS pumping cylinder and B_{oil} the bulk modulus of the oil. The correction factor CF is individual for the BDC and TDC and it depends on the operation (pumping or motoring). Hence, the controller utilizes four correction factors in total: $CF_{\mathrm{pump.BDC}}$, $CF_{\mathrm{motor.BDC}}$, $CF_{\mathrm{pump.TDC}}$, and $CF_{\mathrm{motor.TDC}}$.

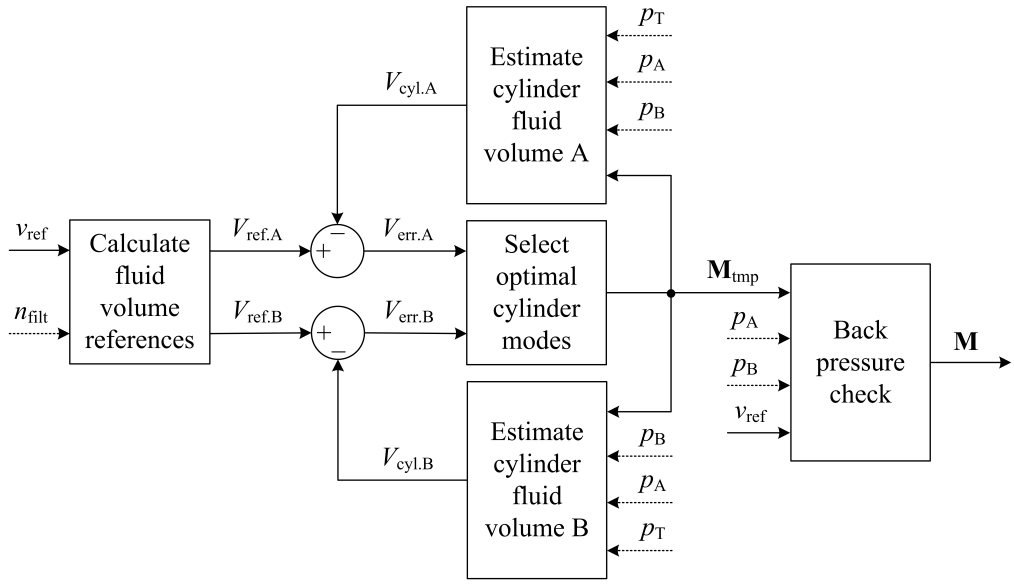

Figure 4.2: Block diagram for the displacement control of a double-acting cylinder [70].

Both cylinder chambers should be constantly pressurized to prevent cavitation and to maintain the stiffness of the system. Therefore, the final modes $\mathbf{M} = [M_\mathrm{P}, M_\mathrm{M}]$ are selected in order to keep the minimum pressure of the cylinder within the user-defined

Table 4.2: Rules for final mode selection in the case of too low and too high cylinder pressure.

Rule	Condition	Decision
1	$p_{\text{back}} = p_{\text{B}}$ AND $\min\{p_{\text{A}}, p_{\text{B}}\} < p_{\min}$ AND $v_{\text{ref}} \geq 0$	$\mathbf{M} = [\text{“A”}, M_{\text{M.tmp}}]$
2	$p_{\text{back}} = p_{\text{B}}$ AND $\min\{p_{\text{A}}, p_{\text{B}}\} < p_{\min}$ AND $v_{\text{ref}} < 0$	$\mathbf{M} = [M_{\text{P.tmp}}, \text{“T”}]$
3	$p_{\text{back}} = p_{\text{A}}$ AND $\min\{p_{\text{A}}, p_{\text{B}}\} < p_{\min}$ AND $v_{\text{ref}} > 0$	$\mathbf{M} = [M_{\text{P.tmp}}, \text{“T”}]$
4	$p_{\text{back}} = p_{\text{A}}$ AND $\min\{p_{\text{A}}, p_{\text{B}}\} < p_{\min}$ AND $v_{\text{ref}} \leq 0$	$\mathbf{M} = [\text{“B”}, M_{\text{M.tmp}}]$
5	$p_{\text{back}} = p_{\text{B}}$ AND $\max\{p_{\text{A}}, p_{\text{B}}\} > p_{\max}$ AND $v_{\text{ref}} > 0$	$\mathbf{M} = [\text{“T”}, M_{\text{M.tmp}}]$
6	$p_{\text{back}} = p_{\text{B}}$ AND $\max\{p_{\text{A}}, p_{\text{B}}\} > p_{\max}$ AND $v_{\text{ref}} \leq 0$	$\mathbf{M} = [M_{\text{P.tmp}}, \text{“A”}]$
7	$p_{\text{back}} = p_{\text{A}}$ AND $\max\{p_{\text{A}}, p_{\text{B}}\} > p_{\max}$ AND $v_{\text{ref}} \geq 0$	$\mathbf{M} = [M_{\text{P.tmp}}, \text{“B”}]$
8	$p_{\text{back}} = p_{\text{A}}$ AND $\max\{p_{\text{A}}, p_{\text{B}}\} > p_{\max}$ AND $v_{\text{ref}} < 0$	$\mathbf{M} = [\text{“T”}, M_{\text{M.tmp}}]$

values. The pressure can change due to change in the load force which affects the chamber volume via compressibility. The back-pressure can also drift due to uncertain controller parameters, such as the oil bulk modulus. In addition, the leakages can be compensated for by controlling the back-pressure.

Table 4.2 shows the rules for the final mode selection. The final pumping and motoring modes depend on the velocity reference and the direction of the load force. The mode selection is made such that the effect on the position tracking is as small as possible. In the case of extending movement and restricting load force, for example, the back-pressure is raised by adding fluid volume in the chamber A (Rule 1). On the other hand, the pressure is decreased by restricting the flow to chamber A (Rule 5). The controller utilizes filtered chamber pressures (filtered by the GMA algorithm) and the maximum rate of the mode changes can be set by the user.

4.3 System verification by simulations

The simulated characteristics of the displacement controlled boom can be seen in Fig. 4.3. In this test, the load mass at the boom tip is 200 kg and the damping orifices have big flow capacity: 100 l/min at the pressure difference of 0.5 MPa. In addition, the rotational speed of the electric motor is set to 750 r/min. The piston of the lift cylinder is first driven 0.2 m inward and then back to its initial position. Hence, the boom is lifted up first and then lowered down again. The trapezoidal velocity reference of the piston has a maximum speed of 0.1 m/s. Graph (a) in Fig. 4.3 shows the position tracking through the trajectory; the maximum open-loop positioning error is within the theoretical accuracy, but slight oscillation can be seen during the movements. The oscillation is more visible in the velocity curve, as seen in graph (b) in Fig. 4.3. The oscillation is caused by the poor damping characteristics of the displacement controlled system. The boom damping mainly depends on mechanical friction because the flow is only slightly throttled at port orifices.

Graph (c) in Fig. 4.3 shows the simulated lift cylinder pressures during trajectory. The back-pressure (p_{A} in the studied case) is not controlled, but the pressure level stays stable because the load force only slightly changes during the trajectory. The pressure in chamber B is affected by the load force and is around 13 MPa, but p_{B} also oscillates on the natural

frequency of the system especially during the lifting movement. In addition, a slight ripple can be seen in the pressures due to the flow ripple produced by the DHPMS. Graph (d) in Fig. 4.3 shows that the rotational speed decreases when the boom is lifted because the required torque builds up. On the other hand, the rotational speed increases when the boom is lowered. Thus, the energy recovered during the boom lowering accelerates the electric motor. The irregular torque of the DHPMS can be seen as frequent peaks in the rotational speed in spite of the flywheel attached to the system.

The simulated input power fed by the electric motor and the output power of the lift cylinder are shown in graph (e) in Fig. 4.3. The power losses while the DHPMS is idling are about 69 W. The power of the electric motor has rather high peaks during the movement; however, its average value is close to the output power through the trajectory. The output power is about 2.5 kW at its highest during the lifting and about -2 kW at its lowest during the boom lowering. It is notable that the DHPMS feeds power to the electric motor when the boom is lowered down. The corresponding energies are shown in graph (f) in Fig. 4.3. The trajectory consumes about 0.4 kJ because work is done against the friction forces. The energy consumed by the electric motor is about 1 kJ and it mainly results from losses in the DHPMS as the energy of the DHPMS is close to the cylinder energy at the end of the trajectory. The DHPMS energy is calculated considering the tank line as well; due to the asymmetric cylinder, the use of the inlet depends on the moving direction. Therefore, the lifting seems to require additional energy, but that energy is recovered during the boom lowering. Graph (g) in Fig. 4.3 shows the utilization rate of the DHPMS outlets. The rate is a value between -1 and 1 and describes the selected modes during one revolution; hence, the rates have thirteen levels including zero. For example, if the pumping mode is selected twice in a revolution for an outlet, the rate is 0.33. The negative rate represents the chosen motoring modes. The utilization rate of outlet A is higher than the rate of outlet B due to the cylinder area ratio. Therefore, the full pumping and motoring sequences are decided only for outlet A. The total number of valve switchings (opening and closing) is 1222 for the simulated trajectory.

The system damping can be improved by throttling the flow of the additional volumes [69]. Figure 4.4 shows the simulated response when the damping orifices have a nominal flow capacity of 1.4 l/min at the pressure difference of 0.5 MPa. It can be seen that the position tracking improves (graph (a) in Fig. 4.4), but more significantly, the oscillation in the velocity is almost totally dampened (graph (b) in Fig. 4.4). On the other hand, a higher frequency ripple is more visible in this case and the ripple can be clearly seen in the cylinder pressures as well (graph (c) in Fig. 4.4). The improved damping characteristics also affect the rotational speed (graph (d) in Fig. 4.4) and the shape of the power curves is more angular (graph (e) in Fig. 4.4). The system losses ($W_{\mathrm{EMotor}} - W_{\mathrm{Cylinder}}$) increase about 55 J in comparison with the lightly damped system (graph (f) in Fig. 4.4), even though the control mode sequences are almost identical (graph (g) in Fig 4.4).

A simulated trajectory with a load mass of 50 kg is shown in Figure 4.5. The position tracking accuracy is as good as in the case of higher inertial load (graph (a) in Fig. 4.5). However, the velocity ripple has increased (graph (b) in Fig. 4.5), and the ripple in the pressures is more visible as well (graph (c) in Fig. 4.5). The rotational speed is less affected (graph (d) in Fig. 4.5) because the power level is lower (graph (e) in Fig. 4.5). Nevertheless, the losses for the trajectory are of the same size independent of the load mass (graph (f) in Fig. 4.5) as the mode sequences are alike (graph (g) in Fig. 4.5).

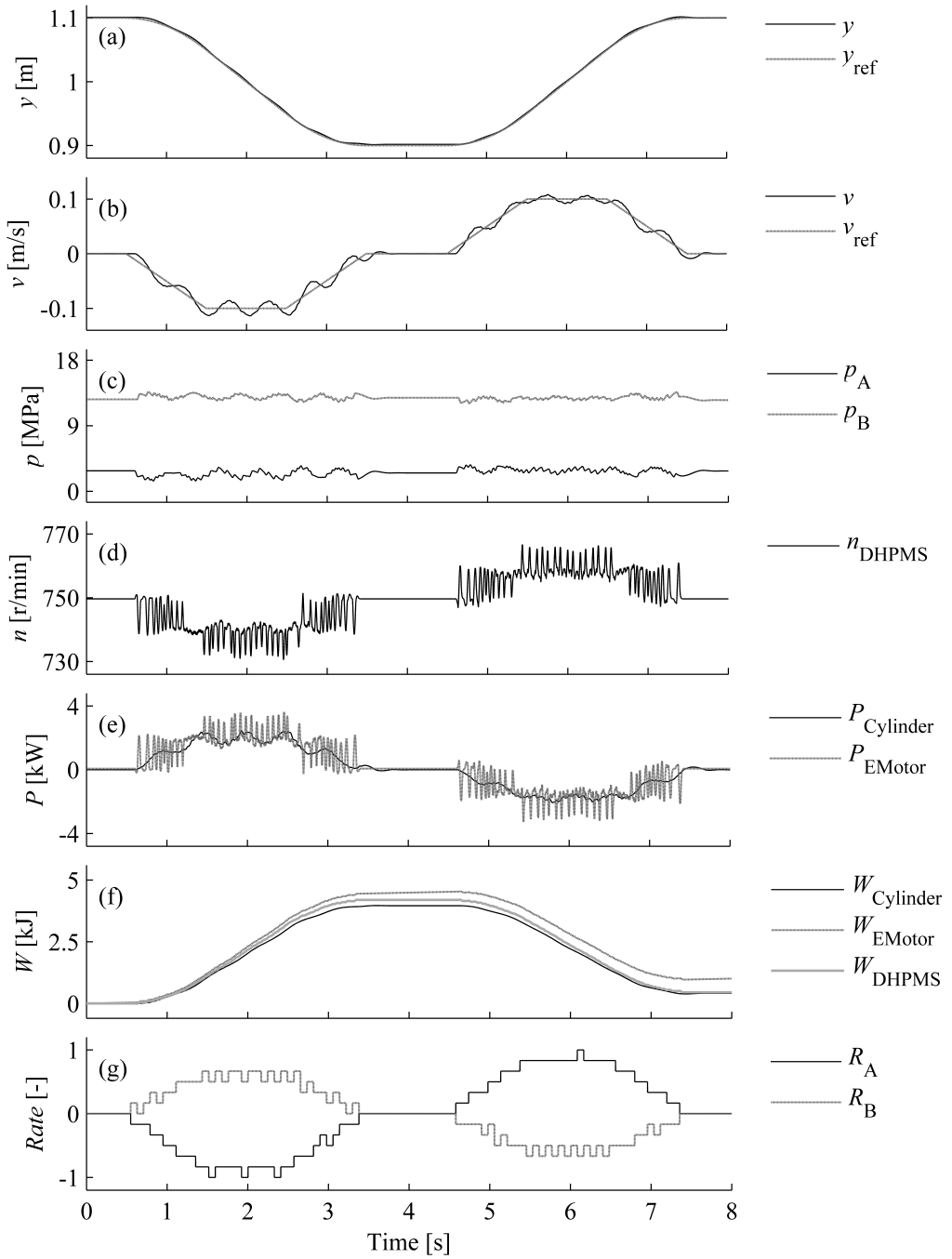

Figure 4.3: Simulated characteristics of a lightly damped system with a load mass of 200 kg: Piston position (a), piston velocity (b), cylinder pressures (c), rotational speed (d), powers (e), energies (f), and outlet utilization rates (g).

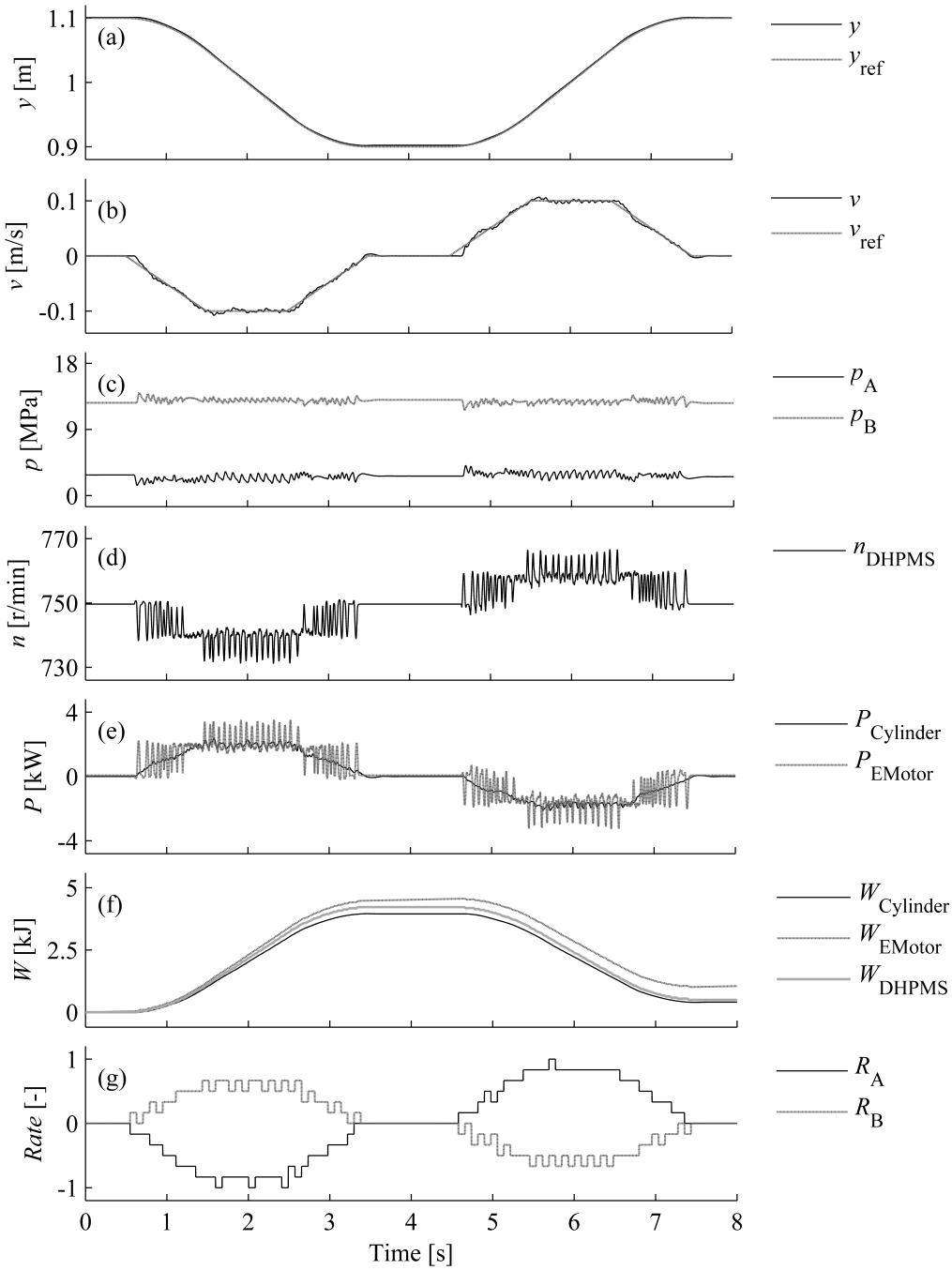

Figure 4.4: Simulated characteristics of a damped system with a load mass of 200 kg: Piston position (a), piston velocity (b), cylinder pressures (c), rotational speed (d), powers (e), energies (f), and outlet utilization rates (g).

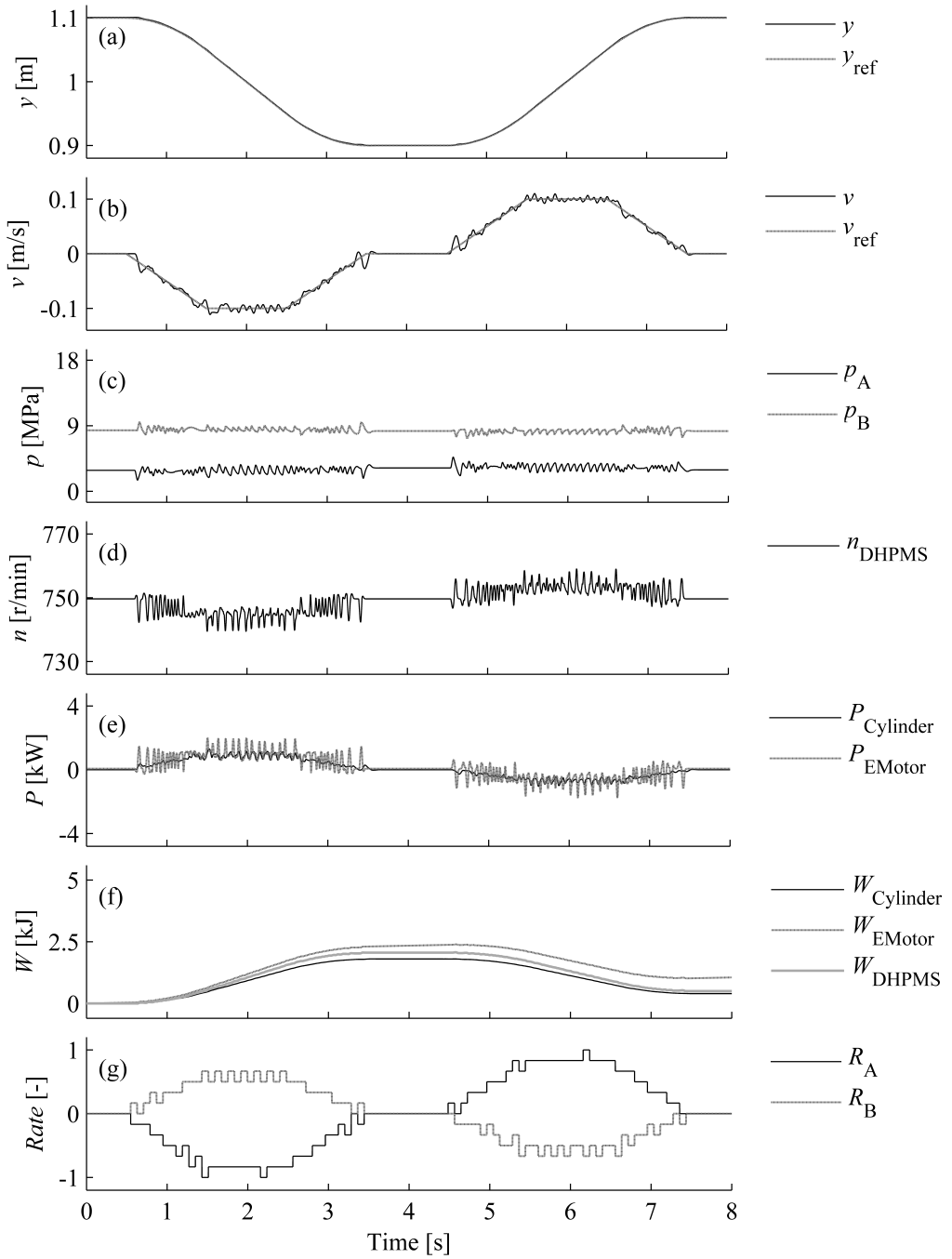

Figure 4.5: Simulated characteristics of a damped system with a load mass of 50 kg: Piston position (a), piston velocity (b), cylinder pressures (c), rotational speed (d), powers (e), energies (f), and outlet utilization rates (g).

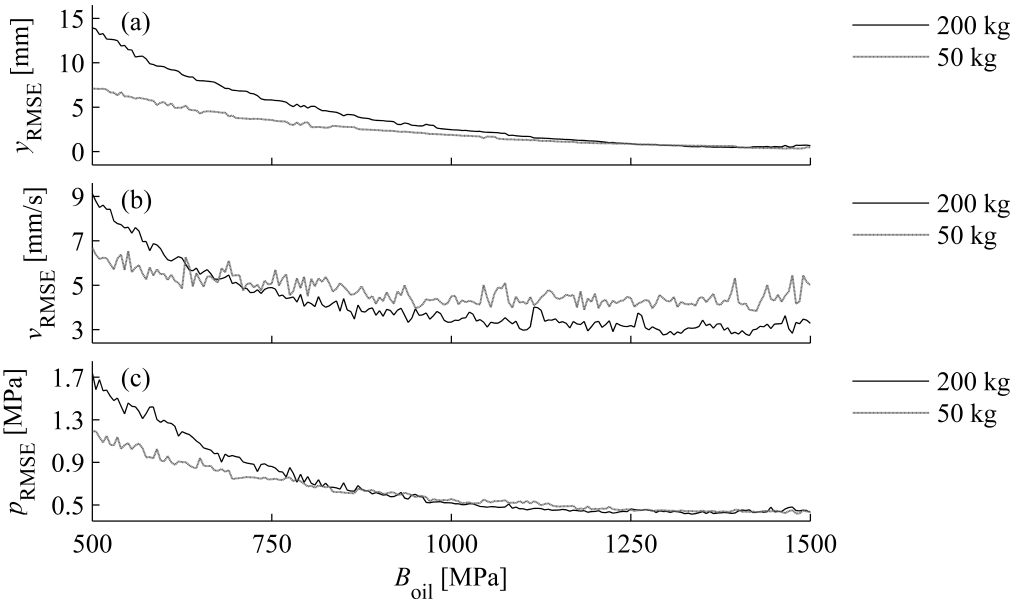

Figure 4.6: Simulated RMSE of a position tracking (a), velocity tracking (b), and back-pressure (c) for the studied trajectory: A sensitivity analysis in regard to the bulk modulus parameter.

The studied system utilizes a model based control algorithm to estimate the change in actuator fluid volumes during an operation; thus, for a good control performance the dimensions of the actuator and DHPMS must be known. In addition, the oil bulk modulus affects the compressibility, which is considered also by the controller. Unlike the geometrical dimensions of components, however, the value for the bulk modulus is difficult to determine due to unknown amount of dissolved air in the oil. The modeled system has a value of 1500 MPa for the oil bulk modulus. This value is also used by the controller in the previous simulations; thus, the position tracking accuracy is good in the studied cases. Figure 4.6 shows an impact of the bulk modulus parametrization to the control performance; the studied trajectory has been simulated using different values for the bulk modulus utilized by the controller. To analyze the parameter sensitivity, a Root Mean Square Error (RMSE) for the position, velocity, and pressure is examined.

Graph (a) in Fig. 4.6 shows the RMSE for the position tracking. Both the load mass of 50 kg and 200 kg are studied. With the correct parameter value, 1500 MPa, the RMSE is less than 0.7 mm for the both cases. The RMSE exceeds 1 mm when the bulk modulus utilized by the controller has values lower than 1230 MPa; hence, the parameter can have 18% smaller value that the fluid has and the effect on the position tracking is insignificant. It can also be seen that a greater load mass is more sensitive to the bulk modulus parameter than a smaller one due to a higher pressure level. Graph (b) in Fig. 4.6 shows the RMSE for the velocity tracking in respect of the bulk modulus parameter. For the most part, the smaller load mass causes a greater error. This is due to higher velocity ripple involved in a small inertia. Graph (c) in Fig. 4.6 shows the RMSE for the back-pressure (the back-pressure control is disabled). The error is calculated by using an initial value of the pressure as a reference. An imprecise parameter value for

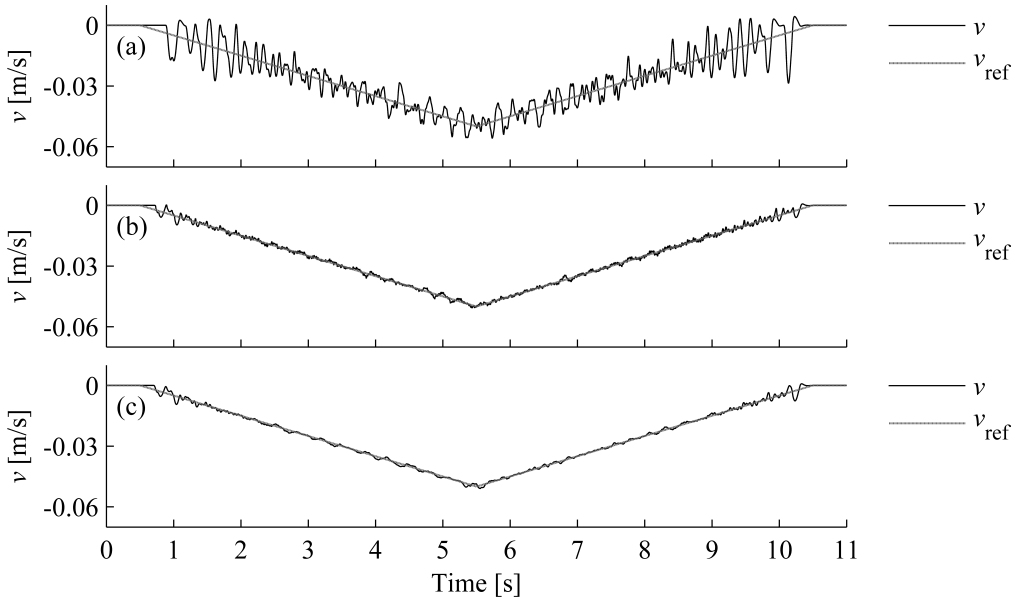

Figure 4.7: Simulated velocity ramp with a load mass of 50 kg: Original DHPMS (a), a 6-piston DHPMS with one third of original geometrical piston displacement and a rotational speed of 2250 r/min (b), and an 18-piston DHPMS with one third of original geometrical piston displacement and a rotational speed of 750 r/min (c).

the oil bulk modulus causes the back-pressure to drift. Nevertheless, the RMSE for the back-pressure is somewhat constant when using the parameter values over 1230 MPa.

The simulated trajectories show that the controllability of the boom is at its worst at low velocities, especially when the inertial load is small. However, the controllability can be improved by decreasing geometrical displacement of the DHPMS pumping pistons, as shown in Fig. 4.7. A load mass of 50 kg is used and the lift cylinder is driven inward according to a slow velocity ramp that goes from zero to -50 mm/s in six seconds. Graph (a) in Fig. 4.7 shows the simulated velocity response when the studied DHPMS is used; hence, geometrical displacement of the six-piston DHPMS is 30 cm^3 and the rotational speed is set to 750 r/min. The velocity curve is quite rough and high peaks occur especially at negative velocity references greater than -20 mm/s. Occasionally, the velocity even has positive values.

In the case of graph (b) in Fig. 4.7 the modeled six-piston DHPMS has a geometrical displacement of 10 cm^3 but the rotational speed is set to 2250 r/min in order to keep the maximum flow unchangeable. It can be seen that the velocity tracking improves significantly: velocities under -10 mm/s have only a small ripple. Increasing the number of pumping pistons also has a similar effect to the velocity tracking performance, as shown in graph (c) in Fig. 4.7. The geometrical displacement of the DHPMS is 30 cm^3 in this case, but the DHPMS has 18 pistons; thus, a rotational speed of 750 r/min can be used to achieve the same maximum flow that six-piston machines have. The reduced phase shift between the pumping pistons enables an even smoother velocity curve.

4.4 Proof of concept by measurements

The feasibility of direct connection is also tested by measurements. In the experiments, position feedback is not utilized by the controller, but the compressed fluid volume is estimated according to the measured cylinder pressures. The back-pressure of the cylinder is also controlled. The controller parameters utilized in the tests are shown in Table 4.3. For fluid volume control the geometrical piston displacement is set to 5 cm^3 while the dead volume of each pumping cylinder is estimated to be 40 cm^3. The estimate for the oil bulk modulus is 1300 MPa. In addition, rather drastic correction factors for the compression volumes need to be used in order to achieve good position tracking; inaccuracy in the model parameters and especially the leakages through the DHPMS control valves distract the fluid volume control of the outlets. The minimum limit for the back-pressure is set to 2 MPa, whilst the maximum allowed back-pressure is 4 MPa. The pressures utilized by the back-pressure controller are only slightly filtered to allow fast leakage volume compensation. However, the back-pressure controller cannot interfere with the fluid volume controller more often than every 13th mode decision. The oil temperature is about 30 °C throughout the measurements.

Table 4.3: Utilized controller parameters.

Fluid volume control		Back-pressure control	
Actuator piston side area	31 cm^2	Actuator piston side area	31 cm^2
Actuator rod side area	21 cm^2	Actuator rod side area	21 cm^2
DHPMS piston displacement	5 cm^3	Minimum pressure	2 MPa
DHPMS cylinder dead volume	40 cm^3	Maximum pressure	4 MPa
Oil bulk modulus	1300 MPa	GMA forgetting factor	0.5
CFs for pumping	1.5	Waiting period after decision	12
CFs for motoring	0.5		

The measured characteristics of the displacement controlled boom without added damping can be seen in Fig. 4.8. The flow capacity of the damping orifices is adjusted to 13 l/min at the pressure difference of 0.5 MPa. A load mass of 200 kg is used at the boom tip and the rotational speed of the electric motor is set to 750 r/min. The same reference trajectory is used as in the previous simulations; the piston of the lift cylinder is first driven 0.2 m inward and then back to its initial position. Graph (a) in Fig. 4.8 shows that the position tracking is good despite the poor damping characteristics; the tracking error is about 4 mm at worst. The oscillation in the velocity is perceptible, as shown in Graph (b) in Fig. 4.8.

Graph (c) in Fig. 4.8 shows the lift cylinder pressures during trajectory. It can be seen that the back-pressure p_A occasionally goes below the set minimum value during the movement, but rises back to the desired level. The load pressure p_B is almost 15 MPa at its highest during the lifting movement but drops under 10 MPa during the boom lowering. Hence, the friction forces strongly depend on the direction of the movement. In addition, a slight ripple can be seen in the pressures due to the uneven flow produced by the DHPMS. The irregularity of the flow also affects the rotational speed, as shown in graph (d) in Fig. 4.8. Moreover, the electric motor races during the boom lowering.

Graph (e) in Fig. 4.8 shows the input power fed by the electric motor and the output power of the lift cylinder for the studied trajectory. The output power is around 2.6 kW at its highest during the boom lifting, whereas the number is about −2 kW when the boom is lowered. The constant power loss of the DHPMS (idling loss) is about 270 W. The maximum power needed from the electric motor is about 5.3 kW, but during the recuperative boom lowering the power flows towards the electric motor. Graph (f) in Fig. 4.8 shows that the trajectory requires about 1.1 kJ of energy as calculated from the actuator outputs. However, the energy needed from the electric motor is around 6.4 kJ at the end of the measurement. The hydraulic energy measured from the DHPMS outlets is 1.8 kJ. The energy of the pressurized tank line can be estimated according to the decided modes and the measured tank pressure. An estimated 0.1 kJ is taken from the tank line when geometrical piston displacement is used in the calculation.

The highest power peaks are caused by back-pressure control during the boom lifting. The preselected mode is changed eleven times due to low back-pressure when the lift cylinder piston is driven inward, as shown in graph (g) in Fig. 4.8 (black plus sign). During the boom lowering the preselected mode is changed five times correspondingly. The leakage is also compensated when the velocity reference is zero; therefore, the pumping rate of outlet B is higher than the motoring rate of the outlet. The utilization rate of outlet A also slightly differs when comparing the pumping and motoring rates due to the estimated compression volume.

Figure 4.9 shows the measured response of the system with enhanced damping properties. The nominal flow capacity of the damping orifices is set to 2 l/min at the pressure difference of 0.5 MPa. It can be seen that the position tracking of the cylinder piston improves (graph (a) in Fig. 4.9) and the amplitude of the velocity oscillation decreases (graph (b) in Fig. 4.9). In addition, the cylinder pressures are more stable compared with those of the lightly damped system (graph (c) in Fig. 4.9). The improved damping only has a slight effect on the rotational speed (graph (d) in Fig. 4.9) but the power curves are more like the velocity reference in shape (graph (e) in Fig. 4.9). However, high peaks occur in the power of the electric motor due to the back-pressure control. The lift cylinder energy is around 1.1 kJ at the end of the measurement, whereas the electric motor output is about 6.5 kJ (graph (f) in Fig. 4.9). The hydraulic energy of the DHPMS outlets is 1.8 kJ, while the estimated change in the inlet energy is about −0.1 kJ at the end of the measurement. The utilization rate of the outlets is similar to those in the slightly damped system; the back-pressure control interferes eleven times during the boom lifting and five times during the boom lowering (graph (g) in Fig. 4.9).

Figure 4.10 shows the tested trajectory with a load mass of 50 kg. The position and velocity tracking do not deteriorate compared with the case of higher inertial load (graphs (a) and (b) in Fig. 4.10). The pressure level of cylinder B chamber is lower due to the smaller load force (graph (c) in Fig. 4.10) and the rotational speed is steadier (graph (d) in Fig. 4.10) because the power level is lower in this case (graph (e) in Fig. 4.10). The measured output energy, hydraulic energy of the outlets and the input energy are 0.9 kJ, 1.6 kJ, and 4.8 kJ, respectively, as shown in graph (f) in Fig. 4.10. The estimated change in the inlet energy is around −0.1 kJ. The utilization rate of outlet B is lower than in the case of bigger load mass due to the smaller leakage flow; the back-pressure control interferes seven times during the boom lifting and twice during the boom lowering (graph (g) in Fig. 4.10).

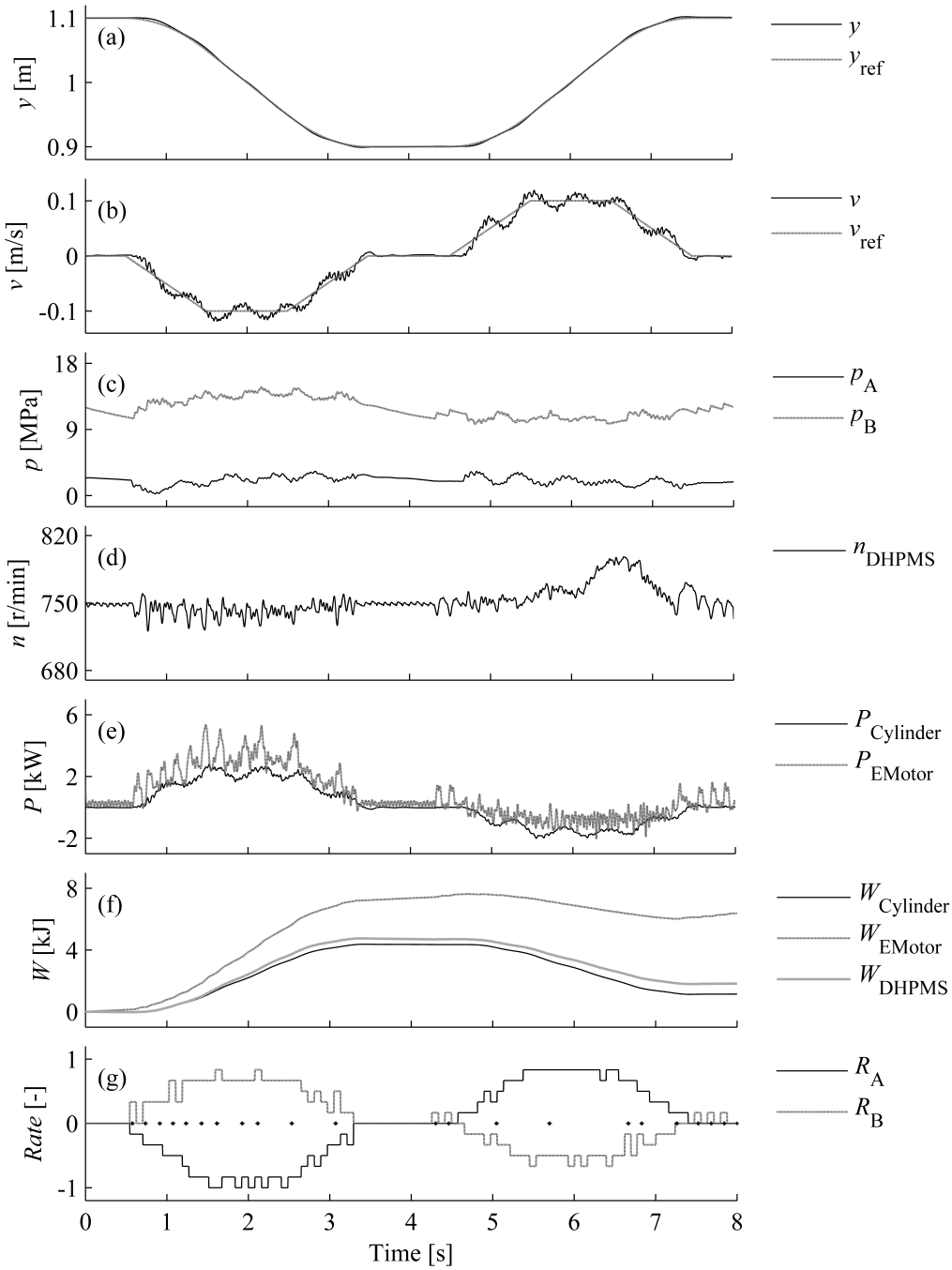

Figure 4.8: Measured characteristics of a lightly damped system with a load mass of 200 kg: Piston position (a), piston velocity (b), cylinder pressures (c), rotational speed (d), powers (e), energies (f), and outlet utilization rates (g).

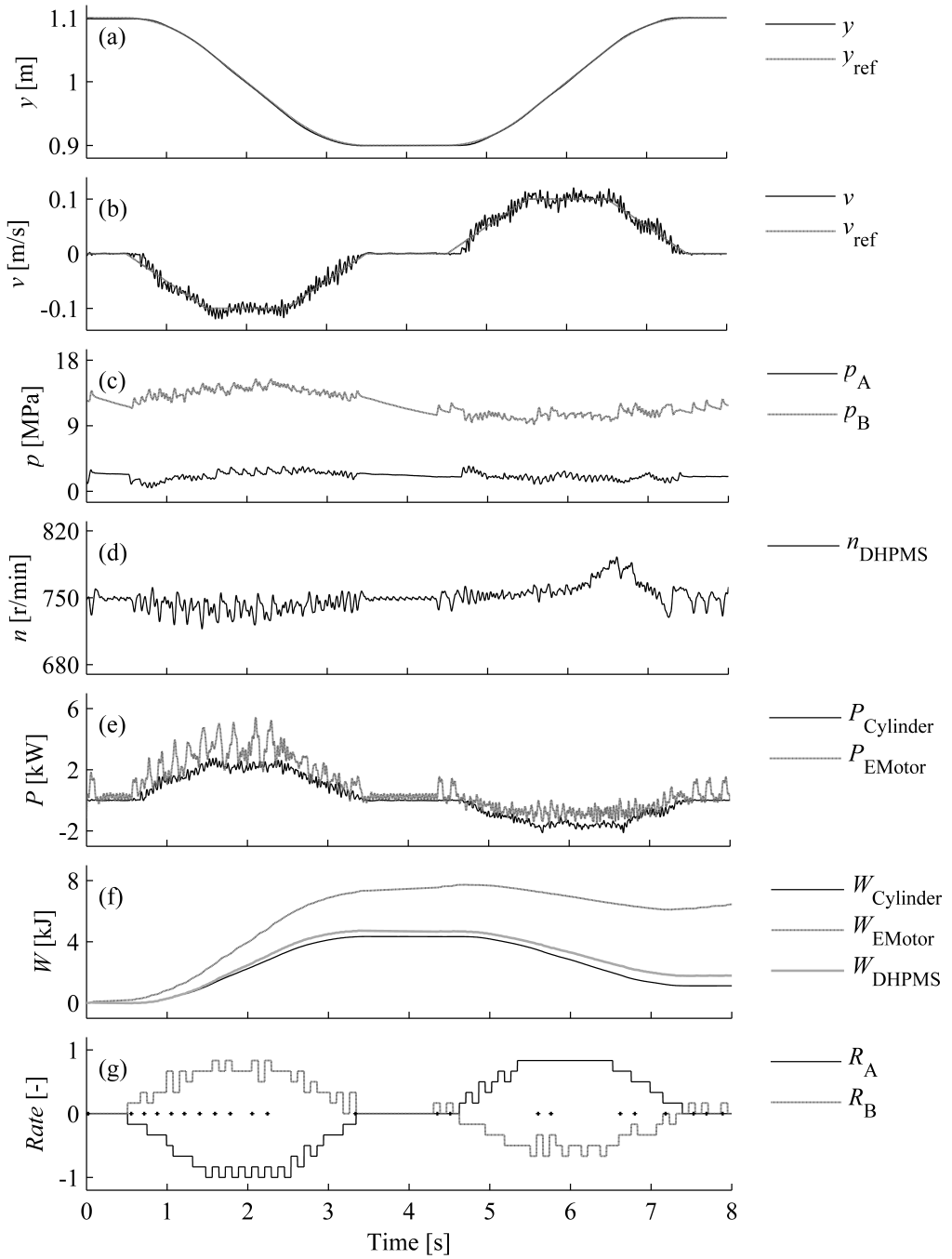

Figure 4.9: Measured characteristics of a damped system with a load mass of 200 kg: Piston position (a), piston velocity (b), cylinder pressures (c), rotational speed (d), powers (e), energies (f), and outlet utilization rates (g).

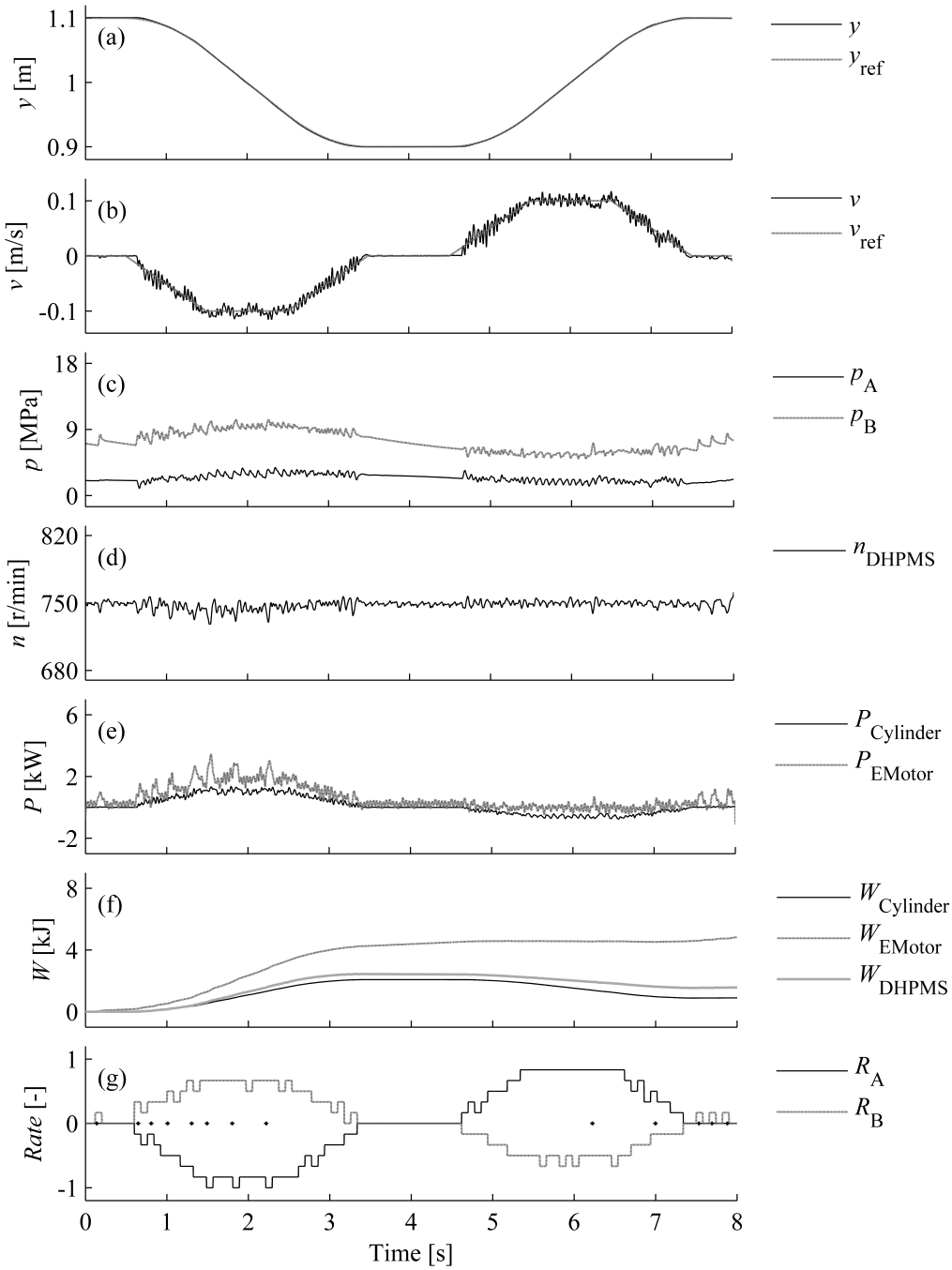

Figure 4.10: Measured characteristics of a damped system with a load mass of 50 kg: Piston position (a), piston velocity (b), cylinder pressures (c), rotational speed (d), powers (e), energies (f), and outlet utilization rates (g).

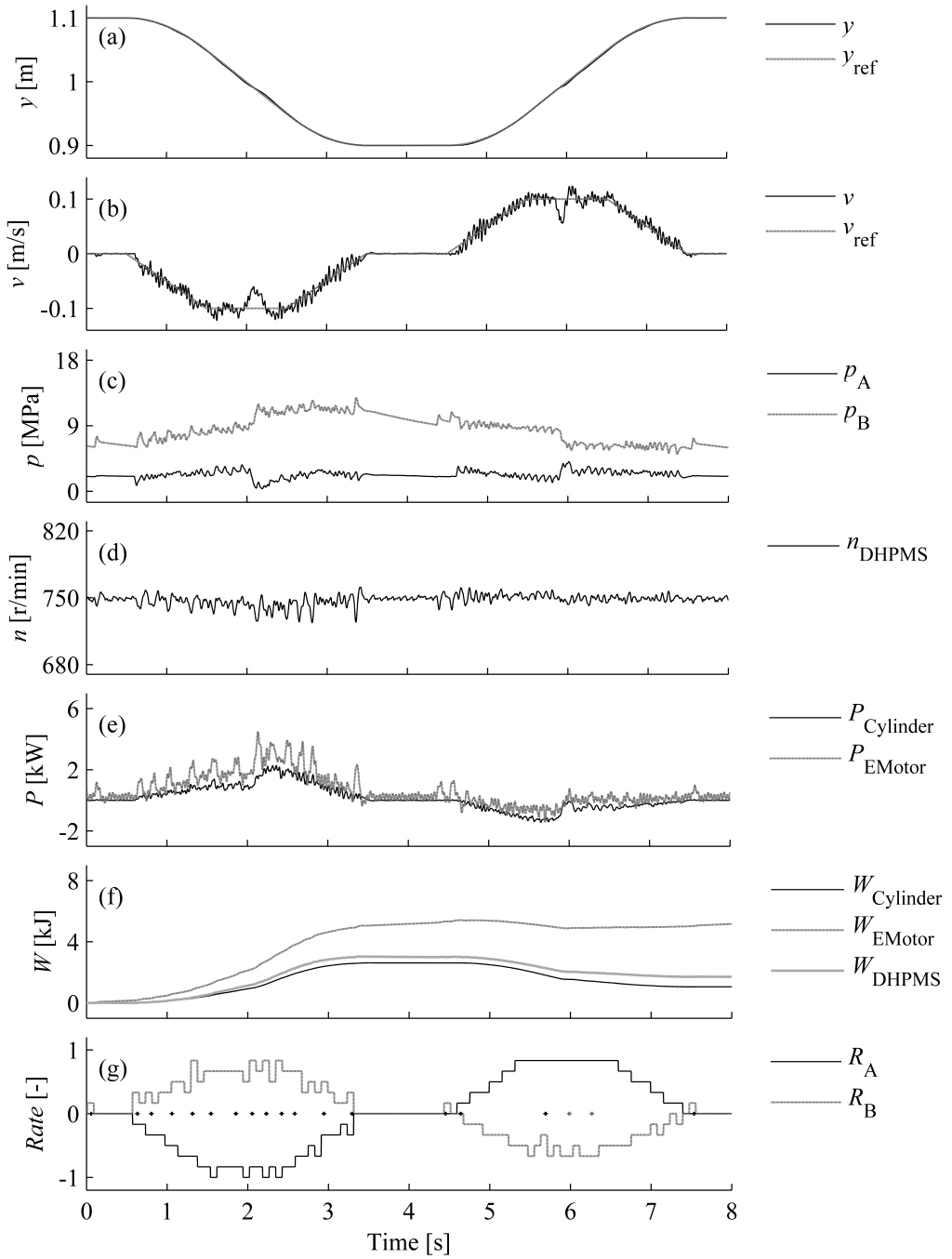

Figure 4.11: Measured characteristics of a damped system with a changing load mass: Piston position (a), piston velocity (b), cylinder pressures (c), rotational speed (d), powers (e), energies (f), and outlet utilization rates (g).

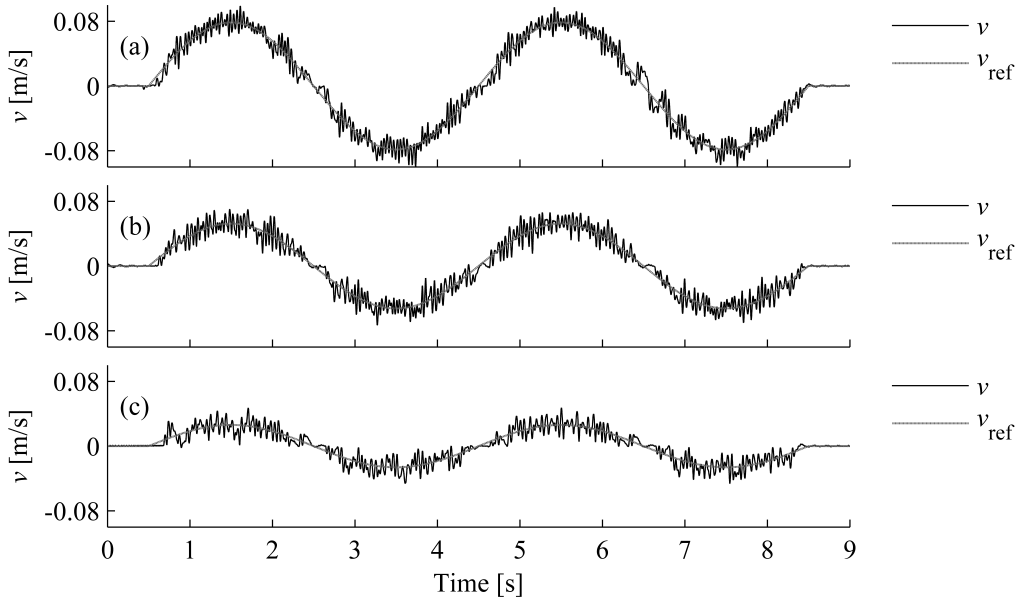

Figure 4.12: Measured velocity tracking of a sinusoidal reference with a load mass of 50 kg: Frequency of 0.25 Hz and amplitude of 79 mm/s (a), frequency of 0.25 Hz and amplitude of 52 mm/s (b), and frequency of 0.25 Hz and amplitude of 26 mm/s (c).

An experiment with a changing load mass is shown in Fig. 4.11. Initially, the boom tip has a load of 50 kg and an extra load of 150 kg is attached to the boom midway through the lifting movement. The extra load is disengaged again during the boom lowering. A lifting sling is used to realize the load change. Graph (a) in Fig. 4.11 shows that the load change causes a temporary disturbance to the position tracking; however, the positioning accuracy does not deteriorate. The effect on the velocity instead can be clearly seen due to the large compression volume of the supply lines (graph (b) in Fig. 4.11). At the moment when the load mass increases, the back-pressure of the lift cylinder drops close to zero but rises again to its target level (graph (c) in Fig. 4.11). By contrast, the back-pressure rises when the extra load disengages.

Graph (d) in Fig. 4.11 shows that the rotational speed is only mildly affected by the load change. The cylinder power doubles during the lifting movement and halves during the lowering movement as a result of the load change (graph (e) in Fig. 4.11). The energy taken from the electric motor is about 5.1 kJ, whereas the lift cylinder energy is around 1 kJ as shown in graph (f) in Fig. 4.11. The energy of the DHPMS outlets is 1.7 kJ and the estimated change in the inlet energy is about 0.1 kJ. Graph (g) in Fig. 4.11 shows the utilization rate of the outlets according to the selected modes. The back-pressure is raised twelve times during the boom lifting and twice during the boom lowering (black plus sign). Additionally, the back-pressure control interferes twice due to exceeding of the maximum limit at the moment when the extra load mass disengages (gray plus sign).

Figure 4.12 shows the measured velocity responses to a sinusoidal reference signal with the frequency of 0.25 Hz. The load mass is 50 kg and the rotational speed of the DHPMS

is set to 750 r/min. The maximum reference velocities for the lift cylinder piston are 79 mm/s (a), 52 mm/s (b), and 26 mm/s (c). It can be seen that the ripple amplitude is about 15 mm/s for the studied velocities. Relatively speaking, an instantaneous velocity error is at its highest at low speeds.

4.5 Advantages over a proportional controlled system

4.5.1 ELS pressure control using the DHPMS

The DHPMS can also be used for supply pressure control in a proportional controlled system [75]. Figure 4.13 shows the system which is compared with the displacement controlled system. The supply line pressure (DHPMS outlet B) is controlled according to the target value set by the ELS function, whereas outlet A of the DHPMS is not used. The additional volume is needed to increase the hydraulic capacitance of the supply line. By using a rigid wall volume a linear pressure response can be achieved [82]. The piston displacement volume of the DHPMS raises the supply line pressure about 1 MPa at maximum.

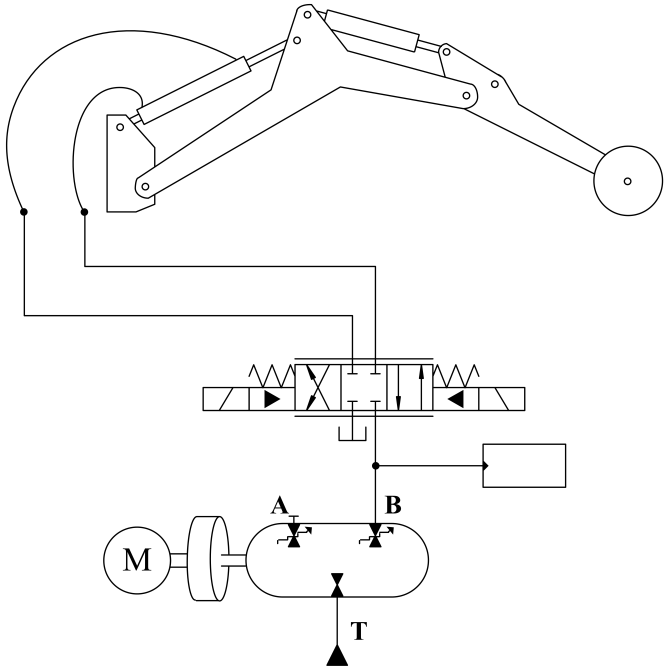

Figure 4.13: Proportional controlled boom using the DHPMS [71].

The pressure control logic is shown in Fig. 4.14. The block diagram presents a model predictive mode selection for a pair of pistons which have an opposite phase [76]. The change in the supply line fluid volume is estimated first considering the previously selected modes and the actuator flow. Linear extrapolation as a function of the piston angles is used to determine the additional fluid volume due to the uncompleted piston strokes.

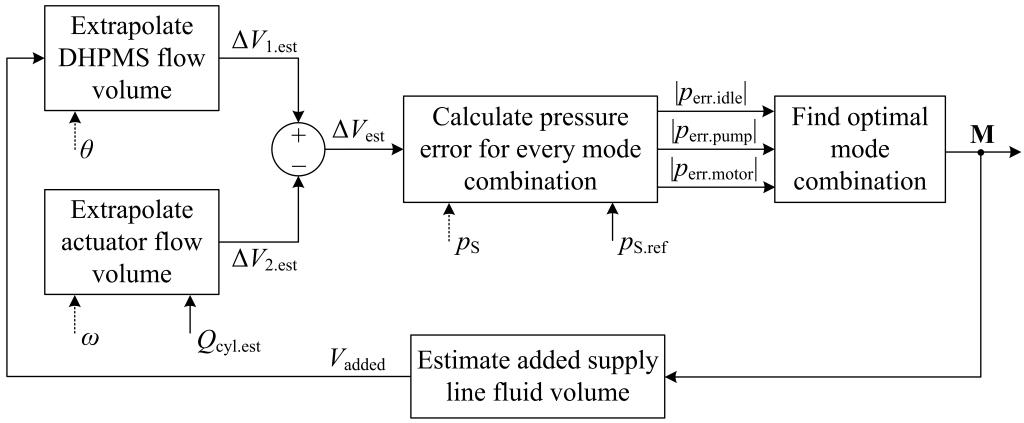

Figure 4.14: ELS pressure control logic using the DHPMS [71].

Table 4.4: Rules for mode selection in order to minimize supply pressure error.

Rule	Condition	Decision
1	$M_{\text{idx.opt}} = 1$	$\mathbf{M}_{\text{opt}} = [\text{“T”},\text{“T”}]$
2	$M_{\text{idx.opt}} = 2$	$\mathbf{M}_{\text{opt}} = [\text{“B”},\text{“T”}]$
3	$M_{\text{idx.opt}} = 3$	$\mathbf{M}_{\text{opt}} = [\text{“T”},\text{“B”}]$

As a result, the volume estimate $\Delta V_{1.\text{est}}$ is formed. Similarly, the change in the actuator flow volume $\Delta V_{2.\text{est}}$ is calculated according to the actuator velocity reference, assuming that the actuator flow stays unchangeable until the pumping/motoring stroke is finished. Apart from the measured supply pressure p_{S}, the effective change in the supply line fluid volume is utilized in the pressure error estimation; the error is calculated for every mode based on the supply line capacitance C_{h} and the geometrical piston displacement V_{disp}:

$$\begin{cases} p_{\text{err.idle}} = p_{\text{S.ref}} - p_{\text{S}} - \dfrac{\Delta V_{\text{est}}}{C_{\text{h}}} \\ p_{\text{err.pump}} = p_{\text{S.ref}} - p_{\text{S}} - \dfrac{\Delta V_{\text{est}} + V_{\text{disp}}}{C_{\text{h}}} \\ p_{\text{err.motor}} = p_{\text{S.ref}} - p_{\text{S}} - \dfrac{\Delta V_{\text{est}} - V_{\text{disp}}}{C_{\text{h}}} \end{cases} \tag{4.5}$$

The target value for $p_{\text{S.ref}}$ is determined by the ELS function considering the filtered cylinder pressures; the eligible pressure difference over the main spool of the proportional valve is 2 MPa [75, 79]. The rules for selecting the optimal mode vector $\mathbf{M}_{\text{opt}} = [M_{\text{P}}, M_{\text{M}}]$ are shown in Table 4.4, where the optimal mode index is solved from the minimizing function:

$$M_{\text{idx.opt}} = \min_{idx}\{|p_{\text{err.idle}}|, |p_{\text{err.pump}}|, |p_{\text{err.motor}}|\} \tag{4.6}$$

Table 4.5: Utilized controller parameters.

ELS pressure control		Cylinder position control	
Supply line capacitance	$4.2 \cdot 10^{-12}$ m^3/Pa	Feed-forward gain	0.6
DHPMS piston displacement	5 cm^3	P-gain	2 1/s

Thus, the decision is made between the pumping and motoring modes for the supply line outlet, or alternatively the DHPMS is let idle. The controller of the proportional valve consists of a feed-forward component determined by the velocity target, and a P-component for controlling the position; hence, the feedback signal of the piston position is utilized. The controller parameters are tuned such that the response corresponds to the behavior of the displacement controlled system. The utilized parameters in the pressure control and position control are shown in Table 4.5.

4.5.2 Experimental results

The proportional controlled system is experimentally tested using the same trajectory as in the case of the displacement controlled system, and an oil temperature of 30 °C is used. Figure 4.15 shows the measurement, where the load mass of 200 kg is utilized. The controller of the proportional valve is tuned such that there is no overshoot in the positioning in order to imitate the response of the displacement controlled system (graph (a) in Fig. 4.15). Graph (b) in Fig. 4.15 shows that the flow throttling makes the velocity curve smooth. The supply line pressure and the lift cylinder pressures are shown in graph (c) in Fig. 4.15. The pressure in chamber A is about 1.6 MPa during the boom lifting, but it drops even to zero at the end of the lowering movement. Thus, the cylinder momentarily cavitates. The pressure level of chamber B is about 12 MPa for the lifting and 8 MPa for the lowering, correspondingly. The supply line pressure is controlled in respect of chamber B pressure during the boom lifting, and chamber A when the boom is lowered.

The rotational speed of the electric motor is set to 750 r/min. The greatest disturbance occurs after the lifting movement when the rotational speed momentarily rises to 800 r/min and then drops to 710 r/min before it stabilizes again (graph (d) in Fig. 4.15). Graph (e) in Fig. 4.15 shows the power of the electric motor and the cylinder power during the trajectory. The fast pressurization of the supply line causes a positive peak to the input power at the beginning of the lifting movement. Conversely, a negative power peak occurs due to the depressurization when the uppermost orientation is reached. The power of the electric motor is around 4 kW for the retracting piston movement and 0.6 kW for the extending movement. The corresponding numbers for the cylinder power are 2.2 kW and −1.6 kW. Measured from the cylinder, the trajectory requires about 1.1 kJ of energy. However, 10.4 kJ is consumed according to the energy outputted by the electric motor, whereas the DHPMS outputs 7.7 kJ of hydraulic energy; the energy cannot be recuperated during the boom lowering, but the energy of compressed fluid can be utilized by the DHPMS during the depressurization (graph (f) in Fig. 4.15). In addition, an estimated 1 kJ is taken from the pressurized tank line. The utilization rate of the supply line outlet is higher during the extending piston movement than it is during the retracting movement due to the piston ratio, as shown in graph (g) in Fig. 4.15.

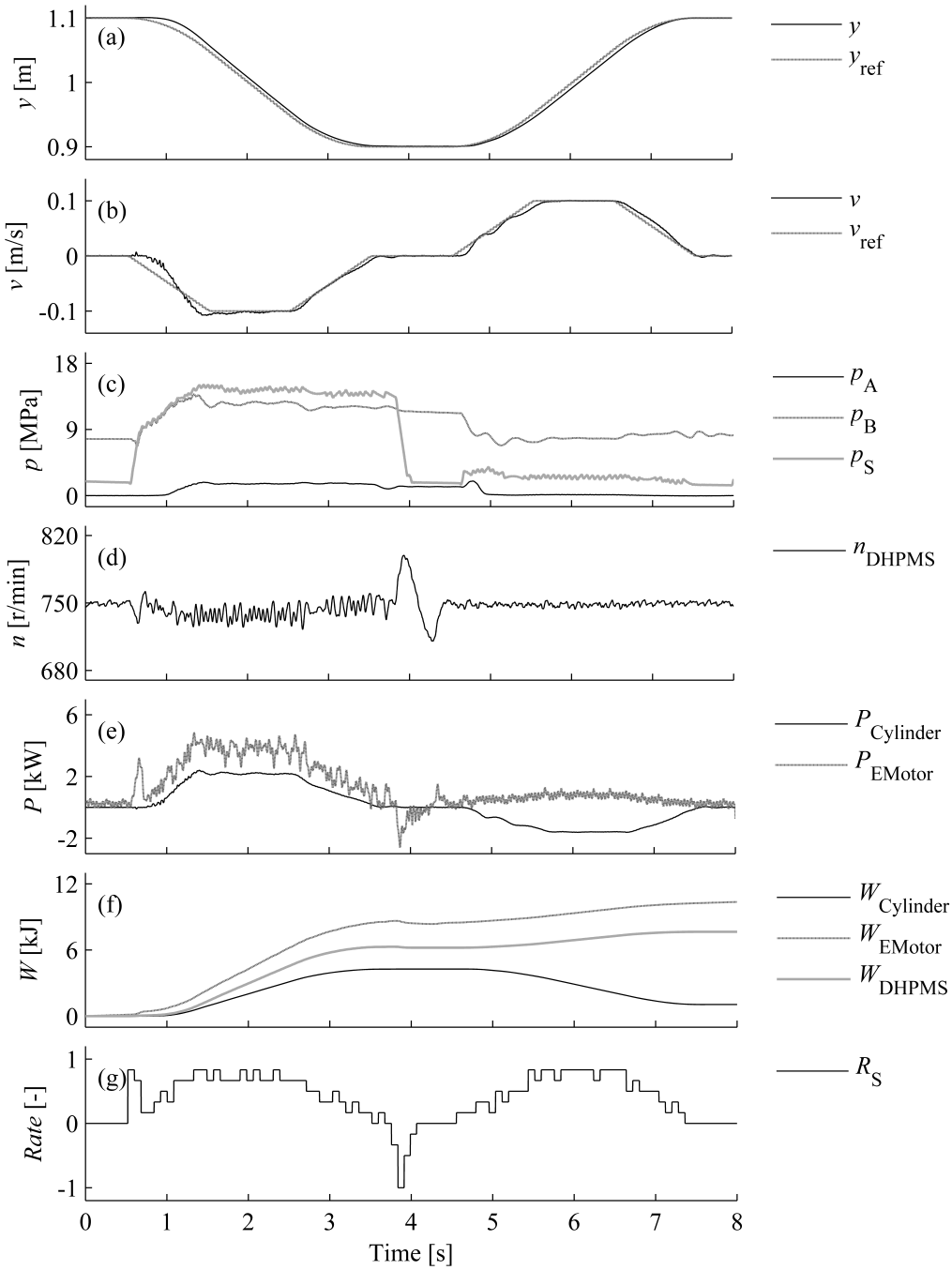

Figure 4.15: Measured characteristics of a proportional system with a load mass of 200 kg: Piston position (a), piston velocity (b), pressures (c), rotational speed (d), powers (e), energies (f), and outlet utilization rates (g).

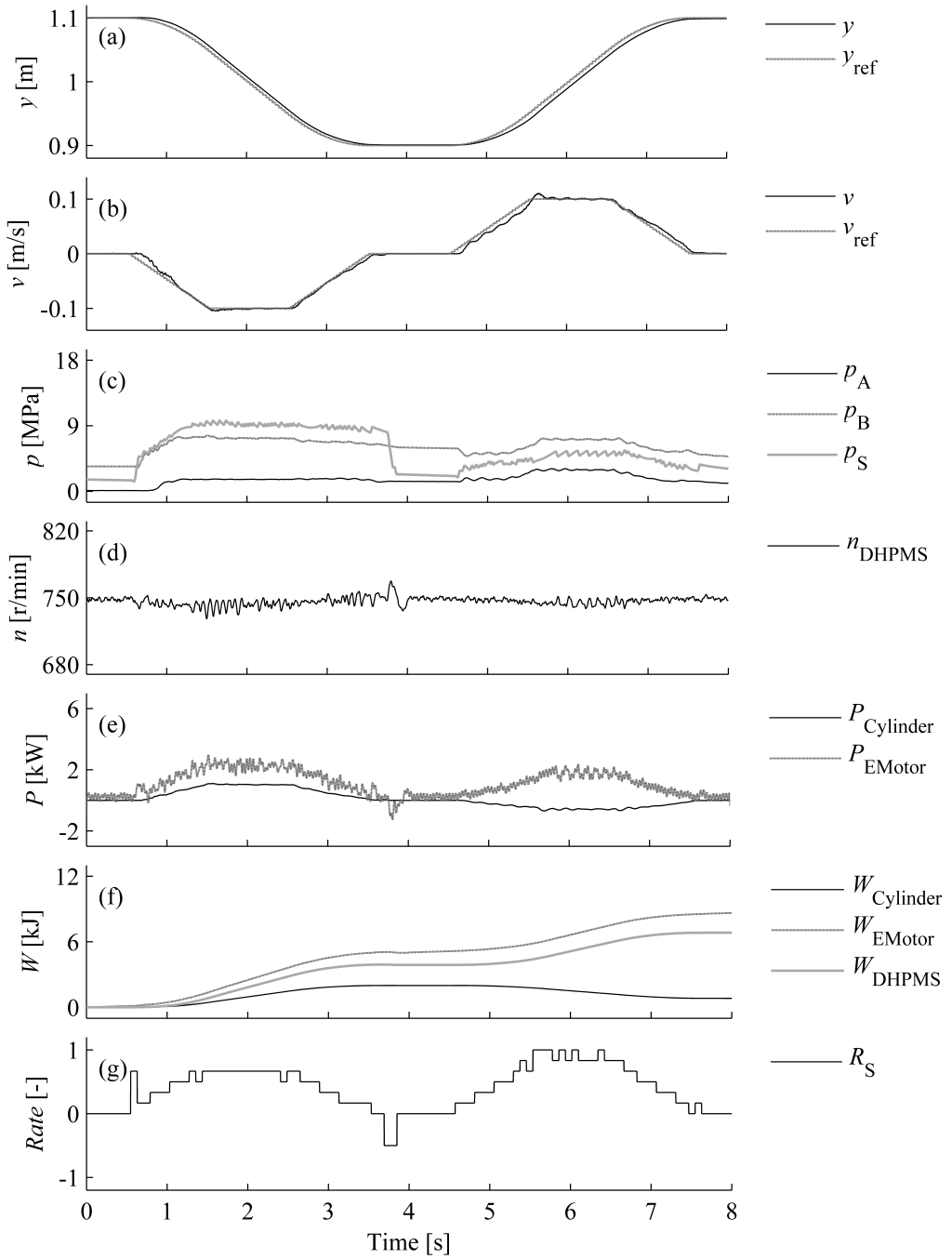

Figure 4.16: Measured characteristics of a proportional system with a load mass of 50 kg: Piston position (a), piston velocity (b), pressures (c), rotational speed (d), powers (e), energies (f), and outlet utilization rates (g).

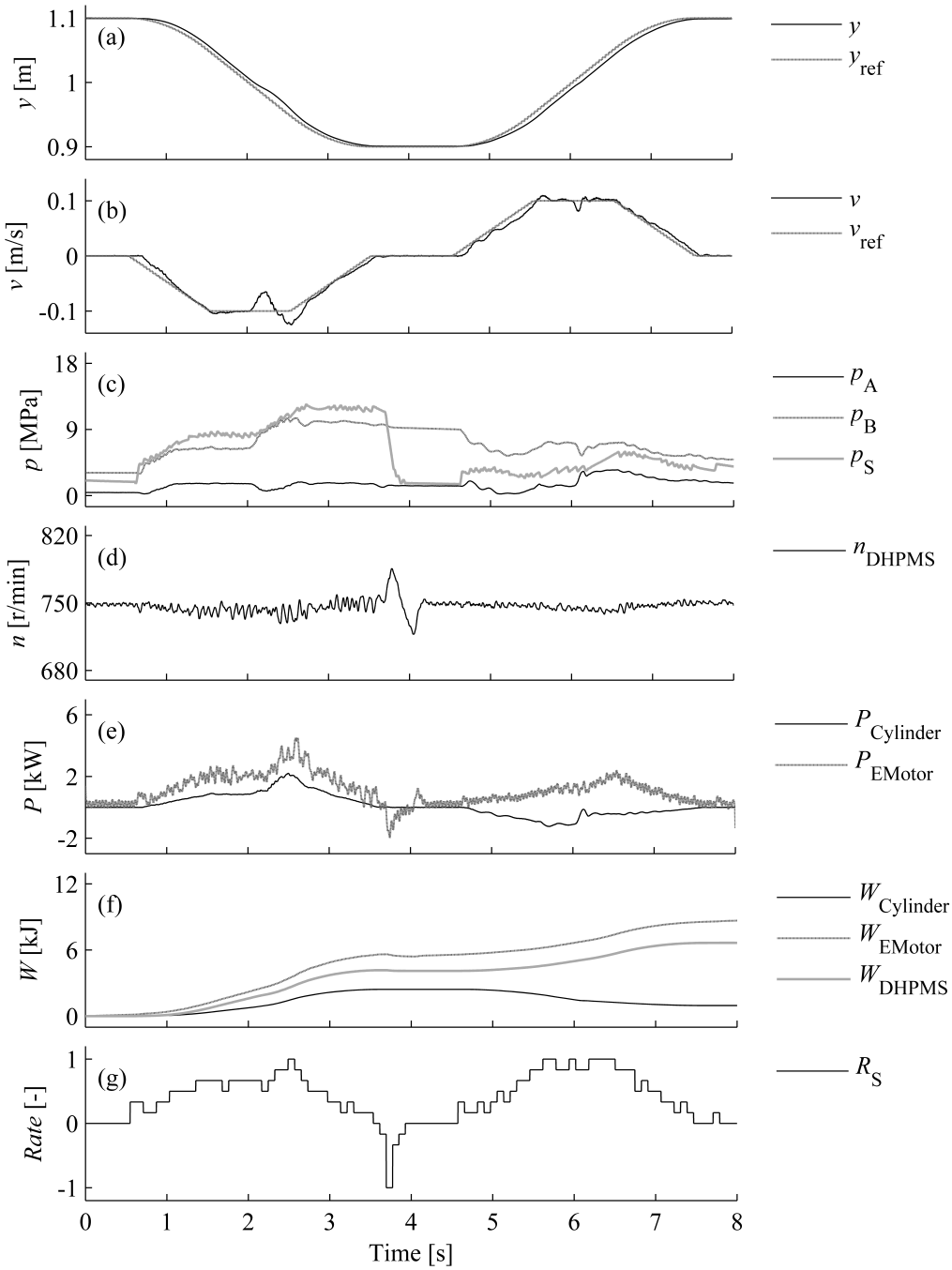

Figure 4.17: Measured characteristics of a proportional system with a changing load mass: Piston position (a), piston velocity (b), pressures (c), rotational speed (d), powers (e), energies (f), and outlet utilization rates (g).

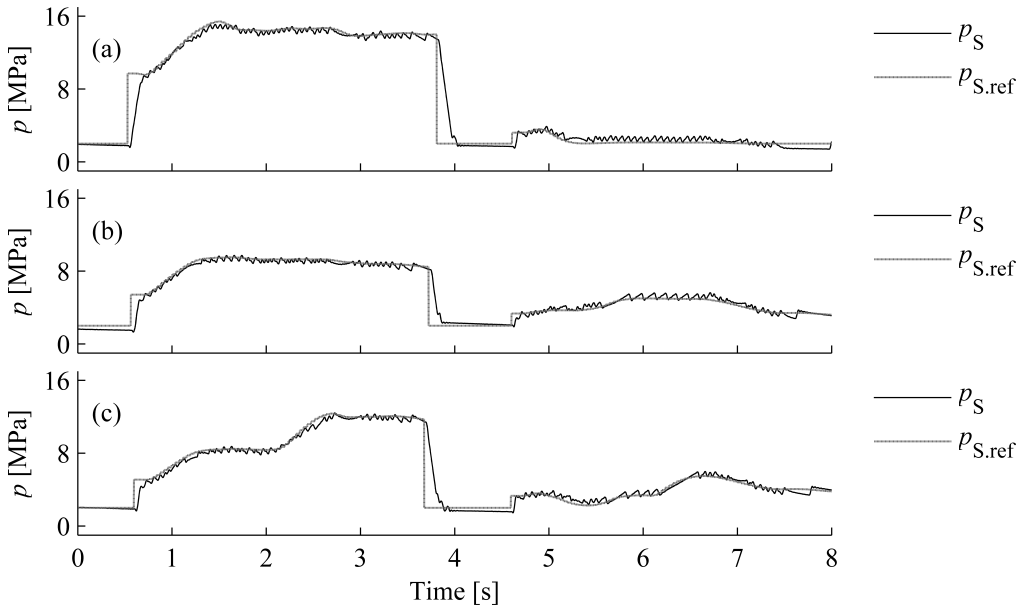

Figure 4.18: Measured pressure control performance of the DHPMS for the tested cases: Load mass of 200 kg (a), load mass of 50 kg (b), and changing load mass (c).

Also the proportional controlled system is tested with a load mass of 50 kg and the results are shown in Fig. 4.16. The position and velocity responses are similar to those of the trajectory with the bigger load mass (graphs (a) and (b) in Fig. 4.16). The cylinder pressures differ from the pressures in the previous case; during the lowering movement, chamber A pressure rises to 3 MPa, whereas the pressure is 1.6 MPa during the lifting movement (graph (c) in Fig. 4.16). Chamber B pressure is about 7 MPa during the movement and the supply line pressure is controlled according to the cylinder pressures. In this case, the depressurization of the supply line has less effect on the rotational speed, as shown in graph (d) in Fig. 4.16. The cylinder output power is about 1 kW during the boom lifting and −0.6 kW when the boom is lowered (graph (e) in Fig. 4.16). For the power of the electric motor the numbers are around 2.2 kW and 1.8 kW, respectively. Graph (f) in Fig. 4.16 shows the measured energies for the trajectory. The energy outputted by the cylinder is about 0.8 kJ as against 8.6 kJ taken from the electric motor. The DHPMS outputs 6.8 kJ of hydraulic energy, whereas an estimated 1 kJ is taken from the pressurized tank line. The utilization rate of the DHPMS supply line outlet is shown in graph (g) in Fig. 4.16; the proportional system requires positive flow also for the extending movement of the cylinder.

Figure 4.17 shows an experiment where the load mass rapidly changes from 50 kg to 200 kg and back during the movement. The increase in the load force while the boom is lifted clearly affects both the position and the velocity (graphs (a) and (b) in Fig. 4.17). In contrast, the effect is slight at the moment when the extra load disengages while the boom is lowered. Chamber B pressure builds up when the load mass increases, while chamber A pressure drops, as shown in graph (c) in Fig. 4.17. The smaller load causes higher pressure in chamber A during the extending piston movement. As regards the

rotational speed, the change in the load mass has no effect (graph (d) in Fig. 4.17) but in the power curves the influence is perceivable (graph (e) in Fig. 4.17). During the lowering movement the power consumption increases at the moment when the extra load disengages. The actuator energy is around 1 kJ at the end of the trajectory whereas the DHPMS has fed about 6.6 kJ to the supply line (graph (f) in Fig. 4.17). The energy taken from the electric motor is about 8.7 kJ, while an estimated 1 kJ is taken from the pressurized tank line. The compensation for the position error can be seen in the utilization rate of the DHPMS outlet during the retracting piston movement; the rate temporarily increases after the extra load engages (graph (g) in Fig. 4.17).

Figure 4.18 shows the pressure control performance of the DHPMS for the tested cases. With a load mass of 200 kg a stepwise change in the LS pressure target occurs in the beginning of the lifting movement (graph (a) in Fig. 4.18). The supply line pressure rises 8 MPa in 0.2 s as the DHPMS pumps to the outlet. After the lifting movement the supply line is depressurized rapidly by motoring; the rate of the pressure release is as fast as in the pressurization. The ripple in the pressure is about 1 MPa at maximum. Additionally, the leakage through the DHPMS control valves causes the supply pressure to go down slowly also in the static situation. The response is similar also at the lower pressure level, as shown in graph (b) in Fig. 4.18. In addition, the pressure can be controlled accurately even if the load changes during the movement (graph (c) in Fig. 4.18).

4.6 Analysis of the results

Displacement control approach using the DHPMS has been studied in this chapter. The boom actuation method minimizes the number of required components as the cylinder is directly controlled by the DHPMS. However, quite large supply line volumes are needed in order to decrease the pressure pulsation amplitude. The amplitude is determined by the supply line capacitance and the displacement volume of a single piston of the DHPMS. In the studied system, the volumes are chosen such that the maximum pressure fluctuation is less than 1 MPa. Additionally, separate damping orifices have to be used because of the poor damping characteristics of a displacement controlled system.

The simulations show that the developed control algorithm could allow accurate position tracking control without using the position feedback. The velocity reference of the piston is converted to the fluid volume references of the cylinder chambers. And further, the volume errors are minimized by controlling the flow at the DHPMS outlets. Good control accuracy can be achieved regardless of the load pressure by considering the compressibility of the fluid; since the parameters of the modeled system are on record, setting the controller parameters is straightforward. However, the position tracking accuracy degrades only little in the case an imprecise parameter value is used for the oil bulk modulus. Moreover, when the load force is stable the back-pressure is not affected and the piston movement is smooth.

In the experimental test system, the controller parameter tuning is more challenging. Although, the dimensions of the DHPMS pistons and the actuator are known, for example the value for the oil bulk modulus is somewhat a guess due to the unknown amount of dissolved air. In addition, the dead volume in the DHPMS cannot be determined precisely; therefore, correction factors need to used when estimating the compression volume. Excessive leakage through the DHPMS control valves also impedes the actuator

control. However, the leakage flow can be quite effectively compensated by controlling the back-pressure; the controller responds to the decreased pressure by selecting a mode combination which minimizes the effect of the leakage volume on the position tracking. In addition, the disturbance caused by the change in the load force can be compensated by using the back-pressure control.

The results show that achieving a smooth movement at low actuator speeds is challenging, although good position tracking accuracy can be realized. A restriction is the displacement volume of a single pumping piston; the larger displacement the poorer the controllability. Hence, to achieve smooth operation geometric piston displacement should be small while the flow demands are met by the larger number of pumping pistons or increased rotational speed. The simulations show that reducing the geometrical piston displacement to one third of the original one will allow good velocity tracking without an excessive ripple. Increasing the piston number is slightly more beneficial than increasing the rotational speed from the velocity ripple point of view: the more the pumping pistons the smaller the phase shift and flow ripple.

Passive damping orifices are an effective way to increase the damping characteristics of the displacement controlled digital hydraulic system. Furthermore, the orifices are easy to implement in the experimental system. In the simulated case the losses are about 8% higher for the system with added damping in comparison with the lightly damped system. However, the absolute difference is only 49 J because the total losses are small; the losses mainly consist of the constant parasitic loss in the DHPMS. Hence, minimizing the DHPMS losses should minimize the system losses. Control valves with sufficiently large flow capacity are therefore needed. In addition to the small energy loss in the supply lines, the system is able to effectively recuperate the energy when the boom is lowered down. Simulations show that the losses are somewhat constant despite the operation mode of the DHPMS.

The experimental tests also show the effect of the damping orifices: oscillations can be restrained but at the expense of increased losses. Added damping results in 94 J bigger losses in the studied case. However, the increase in the number is only 2%. The measured losses are over eight times bigger than the simulation model indicates. The constant power loss of the prototype DHPMS is much higher, about 270 W, due to the hydro-mechanical losses. In addition, leakage through the on/off control valves causes significant volumetric losses; the leakage needs to be compensated by increasing the pumping flow during the boom lifting and limiting the motoring flow during the boom lowering, correspondingly. Therefore, the estimated tank energy is negative (energy is taken also from the pressurized tank line) although the profile of the studied trajectory is symmetric (lifting-lowering).

The proportional controlled system was measured for comparison purposes; the DHPMS controls the ELS pressure, while the boom actuation is realized by the proportional valve. The position feedback is utilized in the system and the controller parameters are tuned such that a similar response is gained in comparison with the displacement controlled system. The results show that the DHPMS is capable of fast and accurate pressure control as well - the ripple in the supply pressure is less than 1 MPa. The flaws of the proportional controlled system are rather high flow throttling losses and inability for energy recuperation while lowering the boom. In addition, the losses depend on the loading because the valve spool is optimized for a certain point of operation.

The energy consumption of the displacement controlled system (System 1) and the

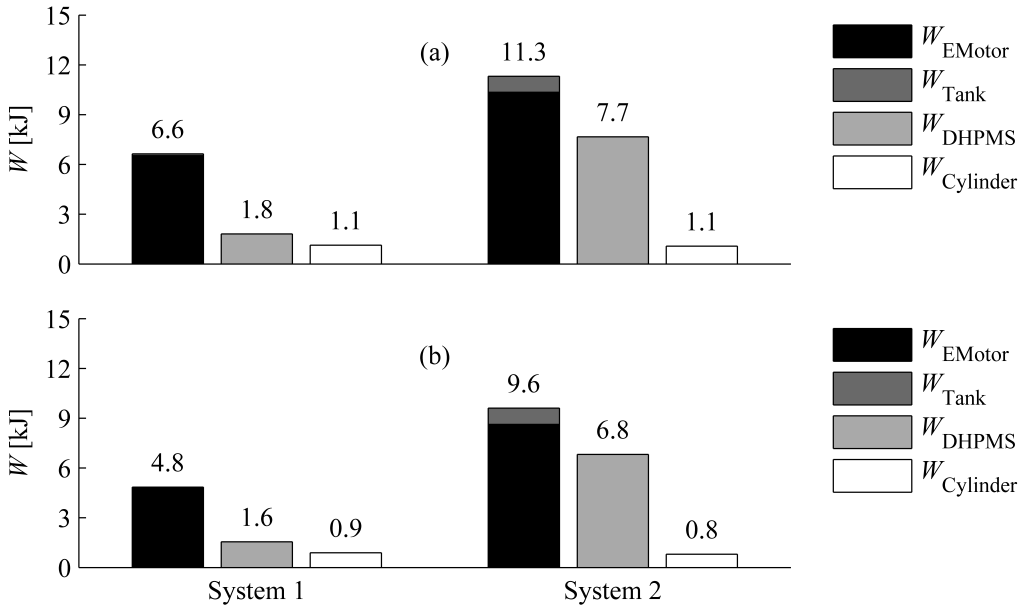

Figure 4.19: Measured energy consumption (averages of three repetitions) of the displacement controlled system (System 1) and the proportional controlled system (System 2) for the studied trajectory with load masses of 200 kg (a) and 50 kg (b).

proportional controlled system (System 2) is studied in Fig. 4.6. It can be seen that System 1 has significantly smaller losses between the DHPMS and the cylinder. On the other hand, System 2 has smaller DHPMS losses; the leakage loss is bigger in System 1 because the supply lines are constantly affected by the load pressure. It can also be seen that the energy does not recuperate to the tank in System 2 as it does in System 1. All in all, System 1 has 46% smaller losses than System 2 in the studied trajectory with a load mass of 200 kg (graph (a) in Fig. 4.6). Correspondingly, the figure is 56% when a load mass of 50 kg is used (graph (b) in Fig. 4.6). The reduction in hydraulic losses is about 89% and 88% respectively.

Table 4.6: Estimated energy consumption of DHPMS control valves for the studied trajectory (averages of three repetitions) according to the number of switchings.

Case	Number of switchings	Electrical energy
System 1 (200 kg)	1269	1.3 kJ
System 1 (50 kg)	1245	1.2 kJ
System 2 (200 kg)	1014	1.0 kJ
System 2 (50 kg)	989	1.0 kJ

Table 4.6 shows an estimated energy consumption of DHPMS control valves for the studied cases. It can be noted that the electrical energy losses are rather moderate compared to the other losses in the DHPMS.

5 Digital hydraulic hybrid

5.1 Hybridization of the DHPMS

A hybrid system assumes a secondary power source that can cover the peak power of the system, and an energy storage that can store the energy recovered from the system. In a DHH, a hydraulic accumulator meets both preconditions: the accumulator capacity can be effectively used because the DHPMS also functions as a transformer. Figure 5.1 shows the studied DHH, where the DHPMS directly controls a single acting lift cylinder and the tilt cylinder is hydraulically locked near to its minimum length. The damping volume and orifice are also used. In addition, an accumulator is attached to another DHPMS outlet and it can be used as an energy source/sink. Hence, the power can be taken from the accumulator during the boom lifting and the recovered energy can be stored in the accumulator when the boom is lowered down.

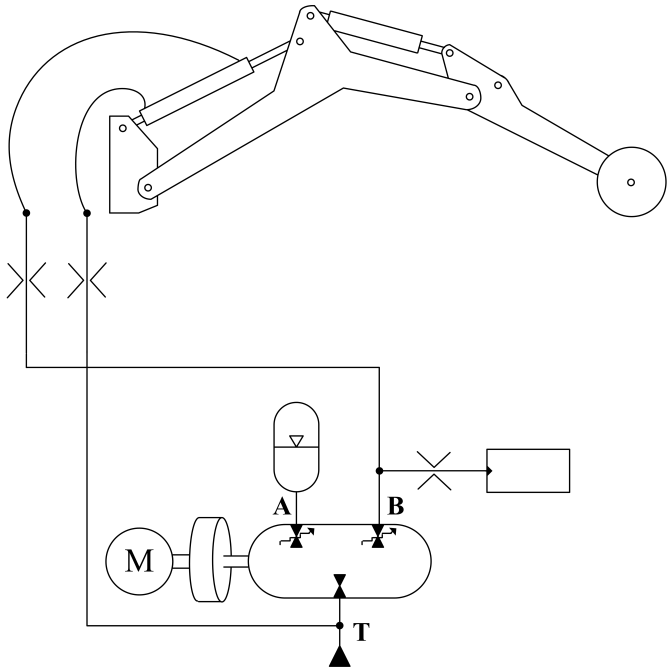

Figure 5.1: Displacement controlled DHH [72].

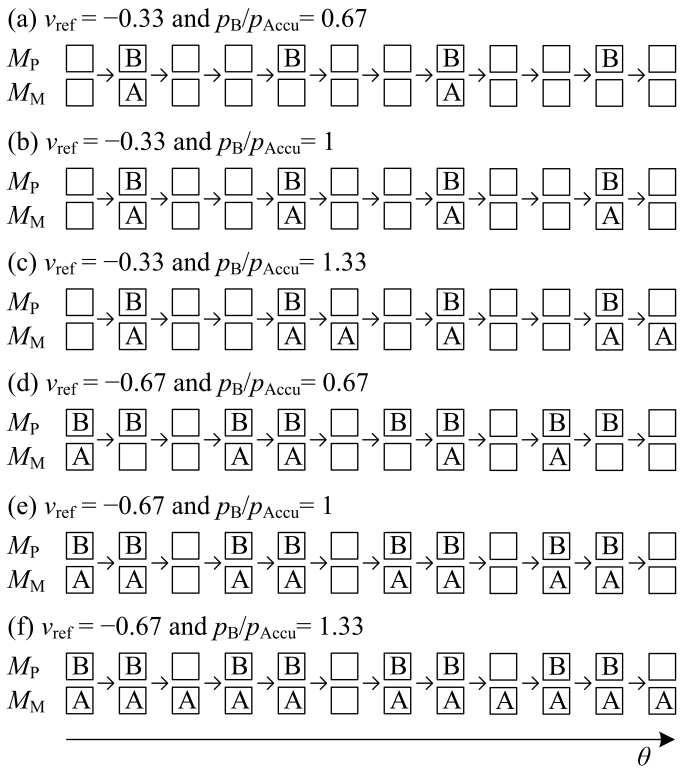

Figure 5.2: Example of mode selection sequences of the DHH with different pressure ratios.

The prime mover power in the DHH can be balanced because the DHPMS works as a discrete transformer. The operation principle is illustrated in Fig. 5.2; the charts describes the mode selection logic during the boom lifting when it is attempted to keep an average of the input power close to zero. In this case, the pumping mode decisions depend upon the relative velocity of the lift cylinder piston. The motoring mode is chosen for accumulator (A) every time the pumping mode is selected for cylinder (B) if the pressure ratio is one (Fig. 5.2 (b) and (e)). The motoring from the accumulator is decided less frequently than the pumping to the cylinder when the accumulator pressure is higher than the cylinder pressure (Fig. 5.2 (a) and (d)). Correspondingly, the accumulator needs to be used more often if the pressure ratio is over one (Fig. 5.2 (c) and (f)). Due to the discrete nature of the DHPMS, the maximum pressure ratio that can be used to balance the input power depends on the actuator velocity. For example, at maximum speed the ratio cannot be more than one in order to keep the average power of the prime mover close to zero. The same principles apply also to energy recovery during the boom lowering.

5.2 Control algorithm

The basic idea of controlling the DHH is as follows: firstly, the actuator fluid volume error is minimized and secondly, the hydraulic energy of the outlets is balanced [72]. The mode selection logic for the DHH is shown in Fig. 5.3. The displacement controlled actuation is

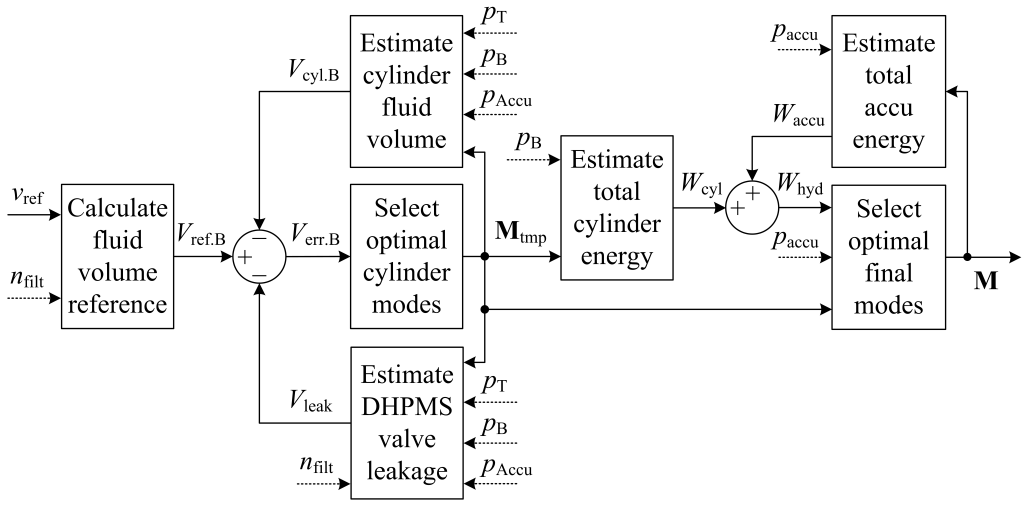

Figure 5.3: Control block diagram of the DHH.

used for the single-acting lift boom cylinder. A temporary mode vector $\mathbf{M}_{\text{tmp}}$ is chosen in order to minimize the volume error at the actuator outlet. The fluid volume reference V_{ref} is calculated based on the velocity reference v_{ref} and effective piston area A_{cyl} as presented in Section 4.2 (Eq. 4.2). The volume extrapolation is also utilized to make the velocity tracking more sensitive. The compressibility of the fluid is considered when calculating $V_{\text{cyl.B}}$ (Eq. 4.4). Chamber A of the lift cylinder is connected to the pressurized tank line; hence, the leakage cannot be compensated for by monitoring the back pressure. Therefore, the leakage volume from the actuator line during the selected mode ΔV_{leak} is estimated for each piston as:

$$\Delta V_{\text{leak}} = C_{\text{leak}} \cdot \frac{180^\circ}{n_{\text{filt}}} \cdot (p_1 - p_2) \tag{5.1}$$

where C_{leak} is the valve leak coefficient, n_{filt} is the filtered angular velocity of the DHPMS in degrees, and $(p_1 - p_2)$ is the measured pressure difference over a valve. The rules for selecting the optimal mode vector $\mathbf{M}_{\text{tmp}} = [M_{\text{P.tmp}}, M_{\text{M.tmp}}]$ are shown in Table 5.1 when the optimal mode index is solved from:

$$M_{\text{idx.cyl}} = \min_{idx}\{|V_{\text{err.B}}|, |V_{\text{err.B}} - V_{\text{disp}}|, |V_{\text{err.B}} + V_{\text{disp}}|\} \tag{5.2}$$

It is attempted to utilize the energy of the accumulator in a way that balances the prime mover power. The estimated actuator energy consumption W_{cyl} is calculated according to the selected mode. The change in energy is estimated as a product of the geometric piston displacement V_{disp} and the measured actuator pressure p_{B}:

$$\Delta W_{\text{cyl}} = (\pm) V_{\text{disp}} \cdot p_{\text{B}} \tag{5.3}$$

Table 5.1: Rules for temporary mode selection in order to minimize cylinder outlet volume error.

Rule	Condition	Decision
1	$M_{\text{idx.cyl}} = 1$	$\mathbf{M}_{\text{tmp}} = [\text{“T”},\text{“T”}]$
2	$M_{\text{idx.cyl}} = 2$	$\mathbf{M}_{\text{tmp}} = [\text{“B”},\text{“T”}]$
3	$M_{\text{idx.cyl}} = 3$	$\mathbf{M}_{\text{tmp}} = [\text{“T”},\text{“B”}]$

The sign is determined by the operation (pumping or motoring). The actuator energy is added to the estimated accumulator energy W_{accu}, which is calculated as a product of the geometric piston displacement V_{disp} and the measured accumulator pressure p_{accu}, respectively. An optimal index is selected such that the total hydraulic energy W_{hyd} is close to zero:

$$M_{\text{idx.accu}} = \min_{idx}\{|W_{\text{hyd}}|, |W_{\text{hyd}} + V_{\text{disp}} \cdot p_{\text{accu}}|, |W_{\text{hyd}} - V_{\text{disp}} \cdot p_{\text{accu}}|\} \tag{5.4}$$

Table 5.2: Rules for final mode selection in order to balance the hydraulic energy.

Rule	Condition	Decision
1	$M_{\text{idx.accu}} = 1$	$\mathbf{M} = \mathbf{M}_{\text{tmp}}$
2	$M_{\text{idx.accu}} = 2$ AND $\mathbf{M}_{\text{tmp}} = [\text{“T”},\text{“T”}]$	$\mathbf{M} = [\text{“A”},\text{“T”}]$
3	$M_{\text{idx.accu}} = 2$ AND $\mathbf{M}_{\text{tmp}} = [\text{“B”},\text{“T”}]$	$\mathbf{M} = \mathbf{M}_{\text{tmp}}$
4	$M_{\text{idx.accu}} = 2$ AND $\mathbf{M}_{\text{tmp}} = [\text{“T”},\text{“B”}]$	$\mathbf{M} = [\text{“A”},\text{“B”}]$
5	$M_{\text{idx.accu}} = 3$ AND $\mathbf{M}_{\text{tmp}} = [\text{“T”},\text{“T”}]$	$\mathbf{M} = [\text{“T”},\text{“A”}]$
6	$M_{\text{idx.accu}} = 3$ AND $\mathbf{M}_{\text{tmp}} = [\text{“B”},\text{“T”}]$	$\mathbf{M} = [\text{“B”},\text{“A”}]$
7	$M_{\text{idx.accu}} = 3$ AND $\mathbf{M}_{\text{tmp}} = [\text{“T”},\text{“B”}]$	$\mathbf{M} = \mathbf{M}_{\text{tmp}}$

The final mode $\mathbf{M} = [M_{\text{P}}, M_{\text{M}}]$ is selected as per the rules shown in Table 5.2. In case of a mode conflict, the selected mode for the actuator is kept unchanged as stipulated by rules 3 and 7.

5.3 System verification by simulations

A simulated response of the displacement controlled single-acting lift cylinder is shown in Fig. 5.4. The load mass at the boom tip is 200 kg and the rotational speed of the electric motor is set to 750 r/min in the test. The boom is first lifted up and then lowered down again to its original position. The piston movement during the position trajectory is 0.2 m and the response can be seen in graph (a) in Fig. 5.4. The position tracking is accurate considering that the controller does not utilize the position feedback; the positioning error is within the theoretical accuracy. However, slight oscillation occurs in the piston velocity, as shown in graph (b) in Fig. 5.4.

The accumulator is disengaged during the reference simulation; therefore, the accumulator pressure is zero, as shown in graph (c) in Fig. 5.4. The pressure in the cylinder chamber

A is 1 MPa because the chamber is connected to the pressurized tank line. The load pressure p_{B} is about 10 MPa and it has a perceivable ripple due to the uneven flow of the DHPMS. The effect can also be seen as a ripple in the simulated rotational speed (graph (d) in Fig. 5.4). Graph (e) in Fig. 5.4 shows that the trajectory requires about 2 kW during the boom lifting (P_{Cylinder}) and the recoverable power during the lowering movement is about 1.8 kW. The input power P_{EMotor} is close to the output power but it has quite high peaks during the movement. Due to the friction forces, the simulated trajectory consumes about 0.4 kJ of energy, while the total input energy taken from the electric motor is around 1 kJ, as shown in graph (f) in Fig. 5.4. The utilization rates of the DHPMS outlets are shown in graph (g) in Fig. 5.4; only the cylinder outlet is used as the accumulator is disengaged.

Figure 5.5 shows simulated characteristics of the hybridized DHPMS when the initial pressure of the accumulator is 8 MPa. It can be seen that the position tracking (graph (a) in Fig. 5.5) as well as the velocity tracking (graph (b) in Fig. 5.5) are similar to the simulated curves in the case of the disengaged accumulator. Graph (c) in Fig. 5.5 shows that the accumulator pressure p_{Accu} decreases about 2.8 MPa during the boom lifting, but increases again when the boom is lowered down. The rotational speed still has a ripple during the piston movement, but the level of the rotational speed is steadier, as shown in graph (d) in Fig. 5.5. The input power P_{EMotor} is close to zero on average, but it has a slight upward trend during the lifting movement because the pressure ratio of the cylinder and the accumulator becomes too high in relation to the actuator velocity. In addition, frequent peaks occur in the power of the electric motor (graph (e) in Fig. 5.5). However, the required peak power is lower than the output power P_{Cylinder} during the lifting movement. Graph (f) in Fig. 5.5 shows that the required energy for the boom lifting is taken from the accumulator and the energy is recuperated to the accumulator during the boom lowering; thus, the curve of the accumulator energy W_{Accu} is a mirror image of the cylinder energy W_{Cylinder}. The losses for the trajectory ($W_{\mathrm{EMotor}} - W_{\mathrm{Accu}} - W_{\mathrm{Cylinder}}$) are about 0.6 kJ also in this case. The utilization rate of the outlets (graph (g) in Fig. 5.5) shows how the DHPMS operates as a transformer; the pressure level of the accumulator is lower than the cylinder load pressure, which is why the motoring rate of the accumulator outlet is higher than the pumping rate of the cylinder outlet during the boom lifting. The motoring rate even saturates to 100%. Correspondingly, the fluid can be pumped more often to the accumulator than it is received from the cylinder during the boom lowering.

The effect of higher accumulator initial pressure is shown in Figs. 5.6 and 5.7. The pressure level has no influence on the position tracking or the velocity tracking (graphs (a) and (b) in Figs. 5.6 and 5.7). The accumulator pressure decreases about 3.7 MPa during the boom lifting when the pressure is initially 12 MPa (graph (c) in Fig. 5.6). On the other hand, the pressure in the accumulator drops 4.9 MPa during the lifting movement when the initial pressure of the accumulator is 18 MPa (graph (c) in Fig. 5.7). The rotational speed has only a slight ripple when the accumulator pressure and the load pressure are close in value (graph (d) in Fig. 5.6). At a greater pressure level, the ripple is quite high (graph (d) in Fig. 5.7). The same impact can be seen in the power of the electric motor as well; the power curve is smooth at a favorable pressure ratio $p_{\mathrm{B}}/p_{\mathrm{Accu}} \approx 1$, but large peaks occur when the DHPMS transforms the hydraulic power (graph (e) in Figs. 5.6 and 5.7). However, the accumulator energy is used similarly, independent of the accumulator pressure level (graph (f) in Figs. 5.6 and 5.7), although the motoring and pumping rates are lower for the accumulator at higher pressure levels (graph (g) in Figs. 5.6 and 5.7).

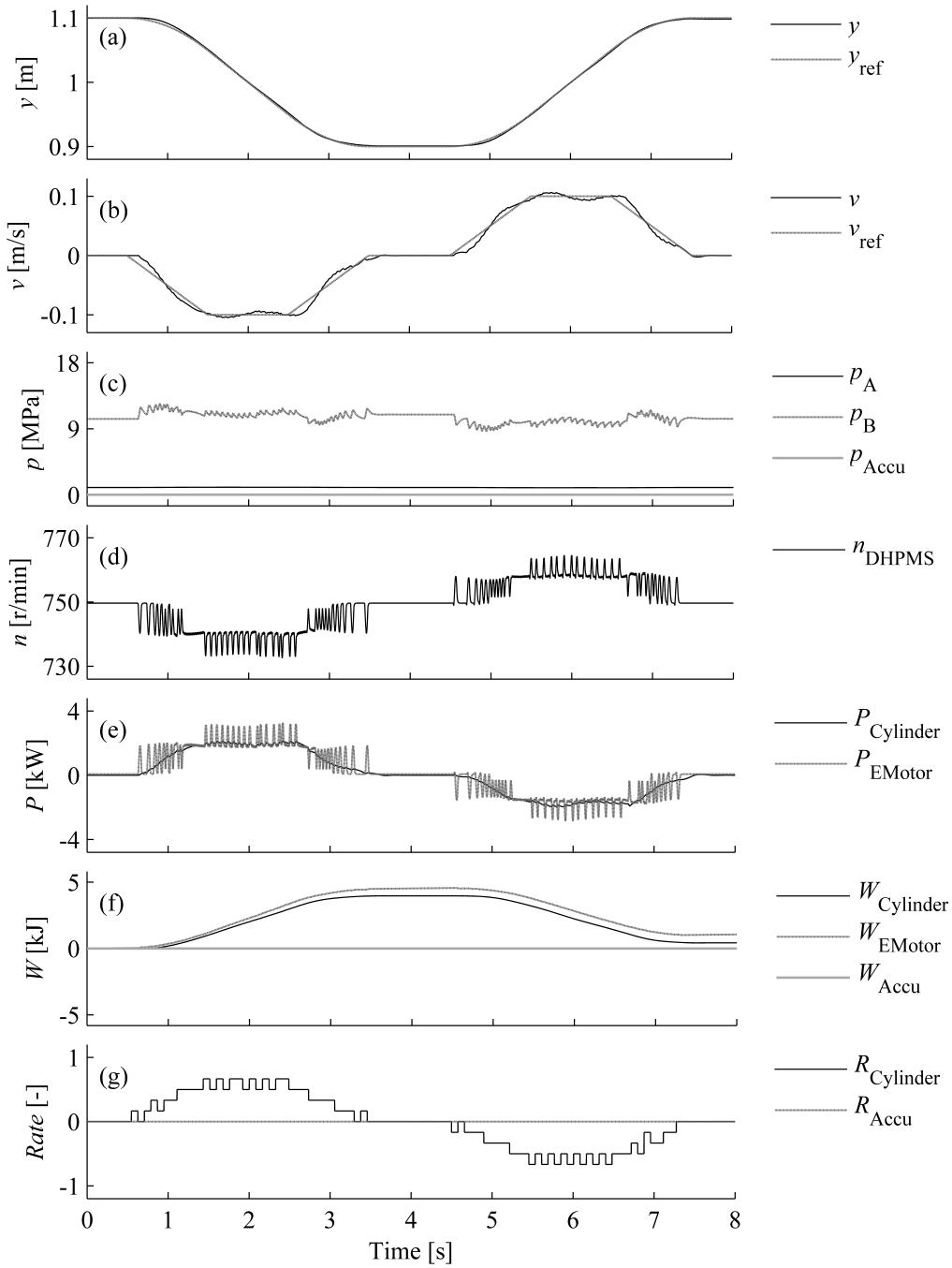

Figure 5.4: Simulated characteristics of a reference system (accumulator not used) using a load mass of 200 kg: Piston position (a), piston velocity (b), pressures (c), rotational speed (d), powers (e), energies (f), and outlet utilization rates (g).

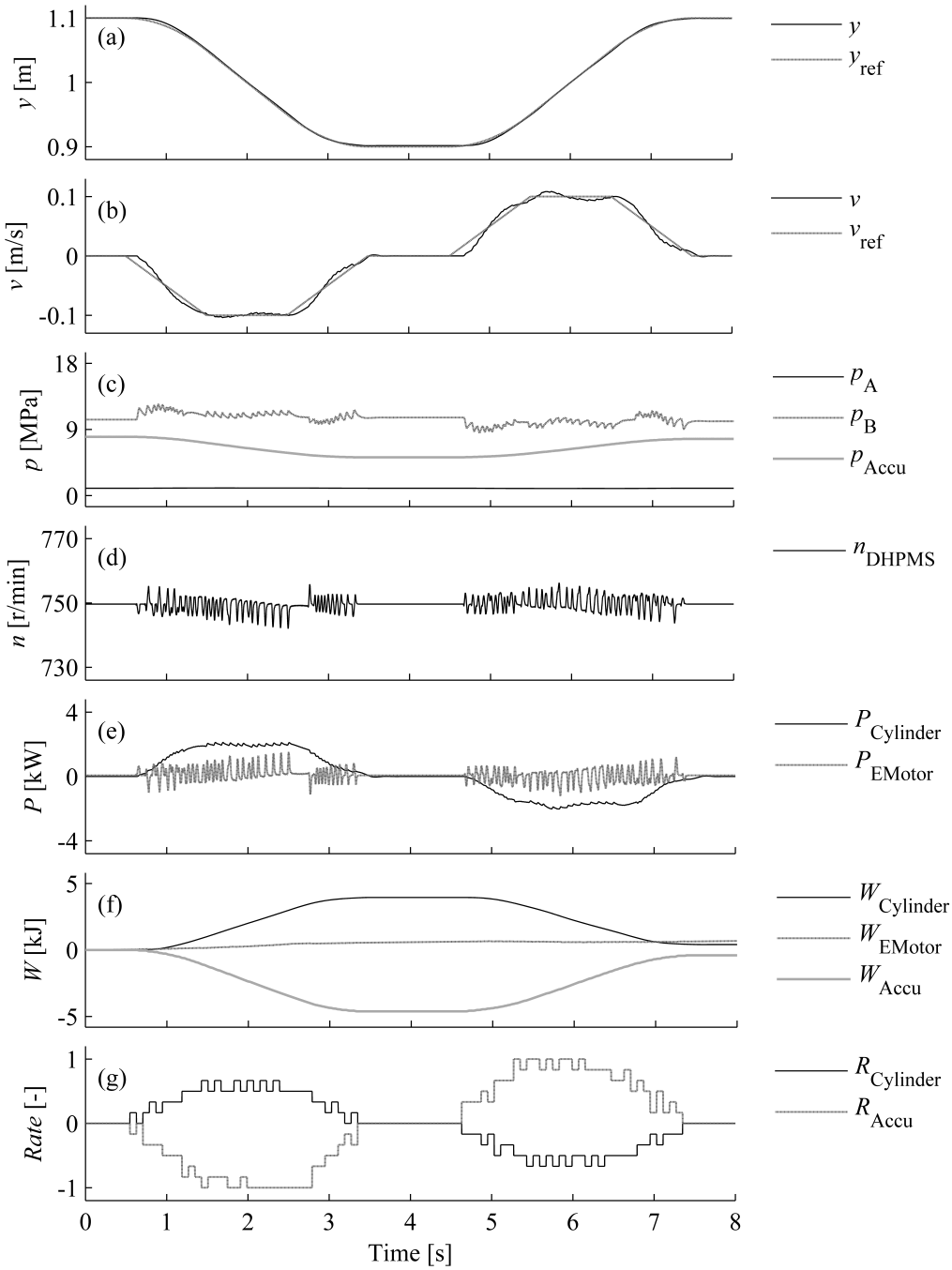

Figure 5.5: Simulated characteristics of the DHH (initial pressure of the accumulator is 8 MPa) with a load mass of 200 kg: Piston position (a), piston velocity (b), pressures (c), rotational speed (d), powers (e), energies (f), and outlet utilization rates (g).

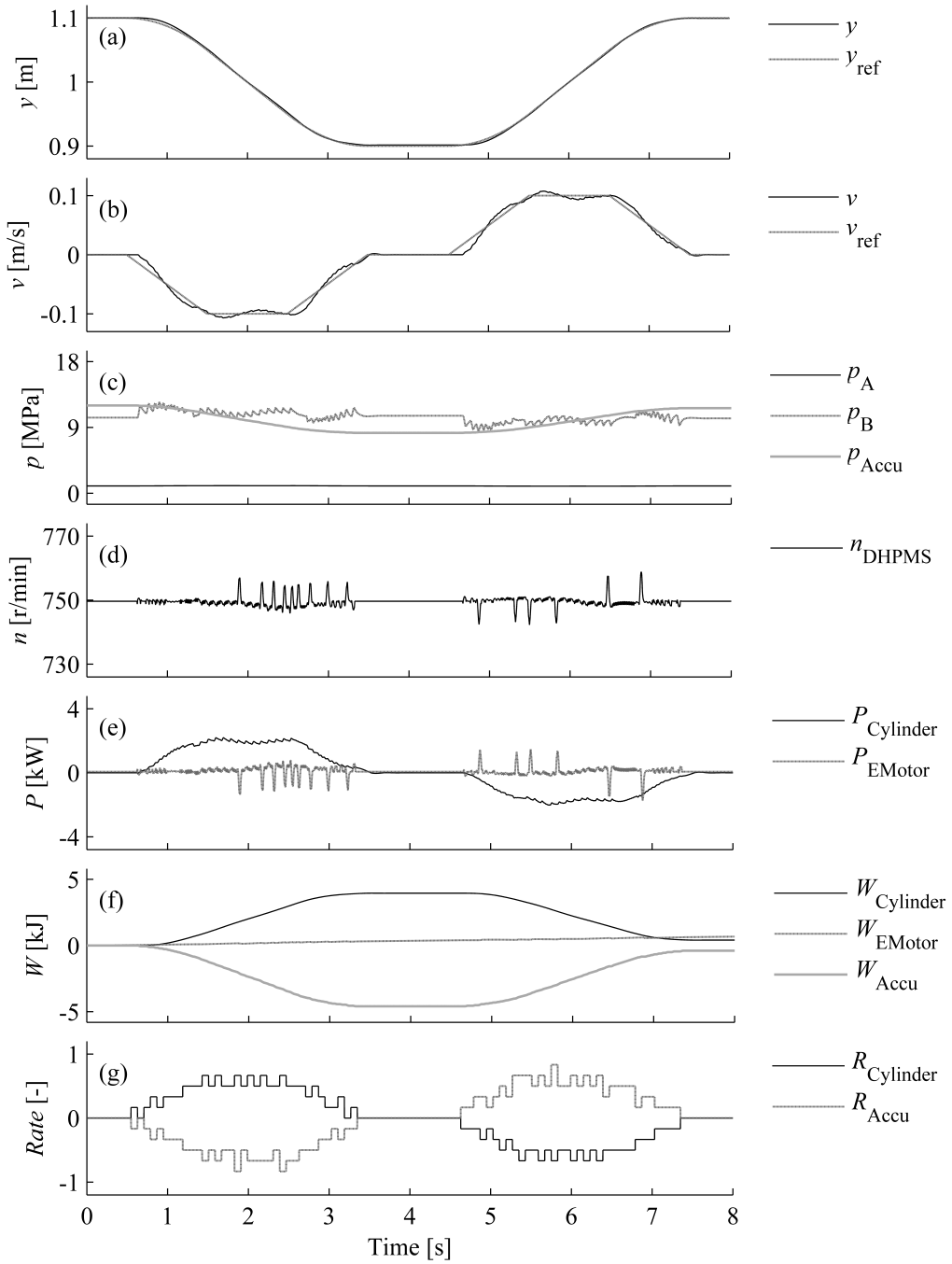

Figure 5.6: Simulated characteristics of the DHH (initial pressure of the accumulator is 12 MPa) with a load mass of 200 kg: Piston position (a), piston velocity (b), pressures (c), rotational speed (d), powers (e), energies (f), and outlet utilization rates (g).

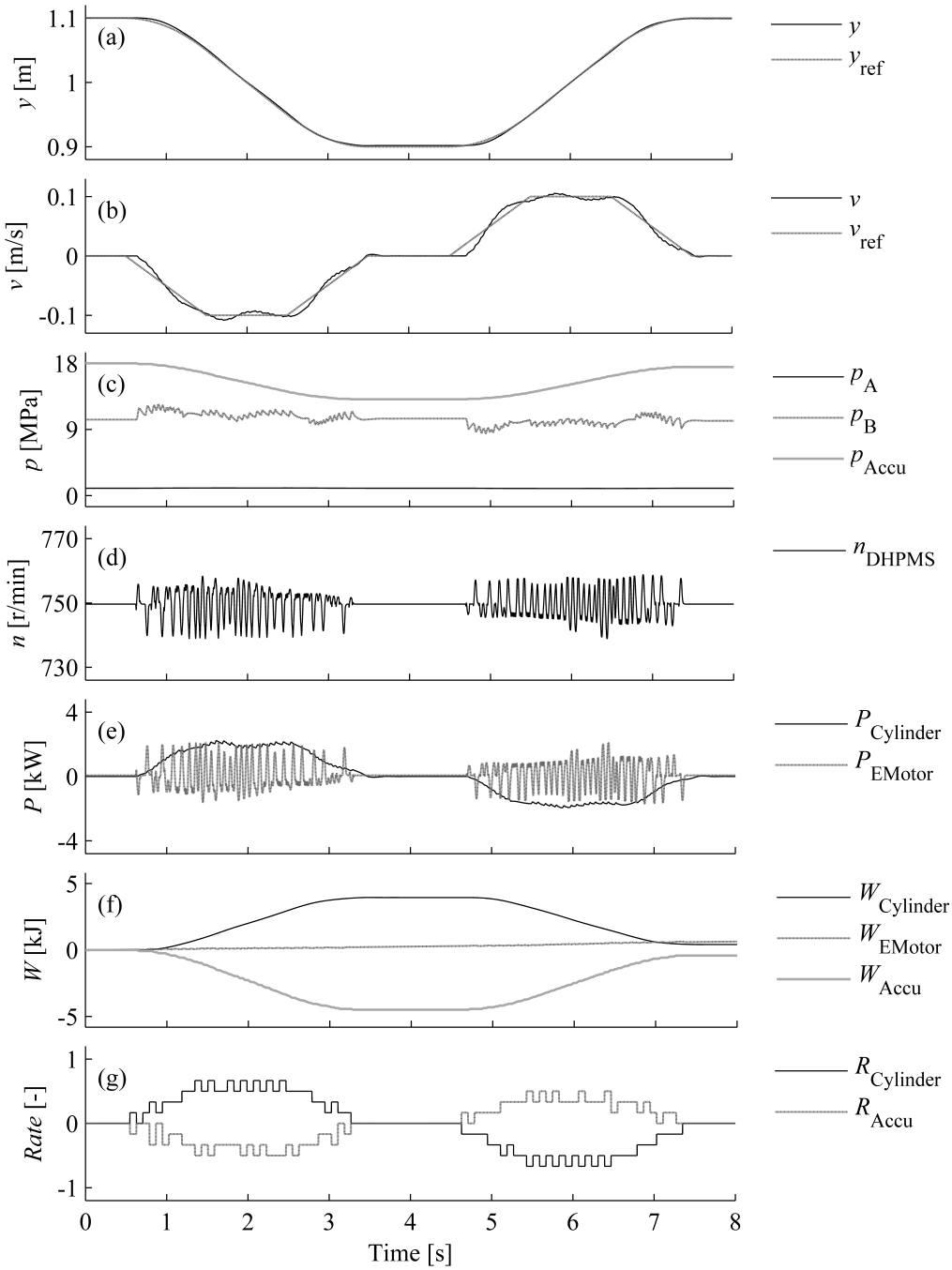

Figure 5.7: Simulated characteristics of the DHH (initial pressure of the accumulator is 18 MPa) with a load mass of 200 kg: Piston position (a), piston velocity (b), pressures (c), rotational speed (d), powers (e), energies (f), and outlet utilization rates (g).

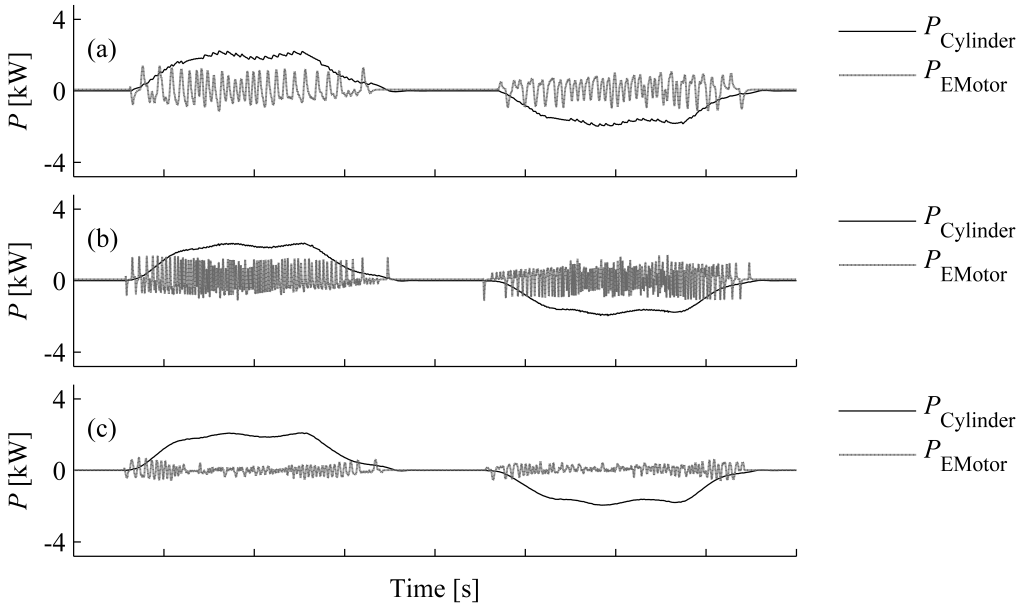

Figure 5.8: Simulated input and output power with a load mass of 50 kg: Original DHPMS with three times bigger moment of inertia of the flywheel (a), a 6-piston DHPMS with one third of original geometrical piston displacement and rotational speed of 2250 r/min (b), and an 18-piston DHPMS with one third of original geometrical piston displacement and rotational speed of 750 r/min (c).

The simulated trajectories show that the amplitude of the input power ripple increases in relation to the accumulator pressure level; the higher the accumulator pressure the higher the power peak amplitude. However, peak power can be reduced by increasing the moment of inertia of the flywheel or decreasing geometrical displacement of the DHPMS pumping pistons, as shown in Fig. 5.8. The initial pressure of the accumulator is 18 MPa and a load mass of 200 kg is used. The studied trajectory is the same as in the previous tests in this section.

Graph (a) in Fig. 5.8 shows the simulated powers when the studied DHPMS is used but the moment of inertia of the flywheel is three times bigger; hence, geometrical displacement of the six-piston DHPMS is 30 cm^3, the rotational speed is set to 750 r/min, and the moment of inertia is 45 kgm^2. The maximum power taken from the electric motor reduces about 40% from the original. Decreasing geometrical displacement of a six-piston DHPMS to one third has a similar effect to the peak power, as shown in graph (b) in Fig. 5.8. However, the power of the electric motor alters at higher frequency because the rotational speed is set to 2250 r/min.

Increasing the number of pumping pistons reduces the peak power the most effectively, as shown in graph (c) in Fig. 5.8. The modeled DHPMS has 18 pistons and its geometrical displacement is 30 cm^3; hence, a rotational speed of 750 r/min is needed to achieve the same maximum flow that the six-piston machines have. The maximum power required from the electric motor is only about 0.7 kW in this case.

5.4 Proof of concept by measurements

The concept of the DHH is also tested by measurements. The position feedback is not used for the displacement controlled lift cylinder but the compressed fluid volume is estimated according to the measured cylinder pressures. In addition, the leakage through each on/off control valve is estimated in order to achieve accurate position tracking. The controller parameters used in the tests are shown in Table 5.3. One of the DHPMS outlets is connected to the rod side of the lift cylinder, while the piston side is connected to the pressurized tank. Thus, the area used in the volume control is 21 cm^2. The geometrical piston displacement is set to 5 cm^3 and the dead volume of each pumping cylinder is 40 cm^3. The oil bulk modulus is estimated to be 1300 MPa. The correction factors for the compression volumes are set such that the position tracking is good when the leakage coefficient utilized by the controller is $290 \cdot 10^{-15}$ $m^3/(s\ Pa)$. The oil temperature is about 30 °C throughout the measurements.

Table 5.3: Utilized controller parameters.

Parameter	Value	Parameter	Value
Actuator rod side area	21 cm^2	CF for pumping at BDC	1.2
DHPMS cylinder dead volume	40 cm^3	CF for motoring at BDC	1.4
DHPMS piston displacement	5 cm^3	CF for pumping at TDC	1.0
Oil bulk modulus	1300 MPa	CF for motoring at TDC	1.0

Figure 5.9 shows a measured response of the displacement controlled single-acting lift cylinder; thus, the accumulator is not used in the first case. The rotational speed of the electric motor is set to 750 r/min using a frequency converter and the load mass at the boom end is 200 kg. In addition, the nominal flow capacity of the damping orifice is set to 2 l/min at the pressure difference of 0.5 MPa. The reference trajectory is the same as is used in the previous simulations; the lift cylinder piston is first driven 0.2 m inward and then back to its initial position. The position tracking performance is shown in graph (a) in Fig. 5.9. The starting is slow for both the retracting and extending movements due to the large compression volume. However, the positioning error is under 1 mm. Graph (b) in Fig. 5.9 shows that the piston velocity is also smooth without oscillations but the slowness of the inertial load can be seen as a rounded shape in the curve.

Cylinder chamber A is connected to the pressurized tank. The pressure level rises about 0.6 MPa during the retracting movement and lowers about 0.4 MPa during the extending movement, as shown in Graph (c) in Fig. 5.9. Chamber B pressure is affected by the load force and the accumulator is kept unpressurized. Graph (d) in Fig. 5.9 shows that the rotational speed is steady during the boom lifting but races when the boom is lowered down. The output power of the cylinder is around 2.2 kW for the lifting, whereas the number is −1.7 kW for the lowering movement, as shown in graph (e) in Fig. 5.9. The average power of the electric motor for the lifting and lowering is 3.3 kW and −0.9 kW, respectively. Altogether, the trajectory requires 1.1 kJ of energy (W_{Cylinder}) but 5.9 kJ is consumed (W_{EMotor}), as shown in graph (f) in Fig. 5.9. An estimated 0.2 kJ is taken from the tank line. The utilization rate of the cylinder outlet is mostly 67% during the trajectory, which ends in 776 valve switchings in total (graph (g) in Fig. 5.9).

Figure 5.10 shows the measured characteristics of the DHH. The position and velocity curves are almost identical in comparison with the previous experiment, where the accumulator is not utilized (graphs (a) and (b) in Fig. 5.10). In this case, however, the accumulator is charged to the pressure of 12 MPa before starting the trajectory. The accumulator is thereafter only used for balancing the total hydraulic energy of the DHPMS outlets; thus, the charging back to the target pressure is disabled. Graph (c) in Fig. 5.10 shows that the accumulator pressure drops down to 5 MPa during the boom lifting and rises again to 8 MPa while the boom is lowered down to its original position. The lift cylinder pressures are identical compared with those in the reference measurement. The hybridization greatly affects the rotational speed; the curve is smooth throughout the experiment as the electric motor does not race during the lowering movement (graph (d) in Fig. 5.10). The output power of the lift cylinder is again around 2.2 kW during the boom lifting and -1.7 kW during the boom lowering, as shown in graph (e) in Fig. 5.10. However, the power consumed by the electric motor is flattened out significantly; the highest value occurs during the lifting movement and is about 2 kW. At the end of the trajectory, the energy outputted by the lift cylinder is around 1.2 kJ and the input power from the electric motor is about 3.3 kJ, as shown in graph (f) in Fig. 5.10. Additionally, around 3.6 kJ is taken from the accumulator, whereas an estimated 0.4 kJ is fed to the tank line during the trajectory. Graph (g) in Fig. 5.10 shows that the utilization rate of the accumulator outlet saturates to 100% during the boom lifting; thus, the power utilized by the actuator cannot be fully covered by the accumulator. It can be seen also that the power is taken from the accumulator when the leakage is compensated. The total number of valve switchings is 1394 for the measured trajectory.

The DHH is also tested using a higher initial pressure in the accumulator. Figure 5.11 shows an experiment where the accumulator is charged to 18 MPa before starting the trajectory. Again, the position and velocity curves resemble the curves measured from the reference system, as shown in graphs (a) and (b) in Fig. 5.11. The accumulator pressure shown in graph (c) in Fig. 5.11 starts to decrease before the lifting movement due to leakage. In addition, the accumulator is utilized when the leakage from the actuator outlet is compensated. After the boom is lifted up, the accumulator pressure is about 7.3 MPa. The regenerative boom lowering raises the accumulator pressure by about 4.2 MPa. The lift cylinder pressures again are similar compared with the pressures in the reference measurement. The rotational speed of the DHPMS stays smooth throughout the trajectory, as shown in graph (d) in Fig. 5.11. Rather high peaks can be seen in the power of the electric motor in the beginning of the lifting movement due to the unfavorable pressure ratio between the cylinder and the accumulator (graph (e) in Fig. 5.11). Otherwise, the input power taken from the electric motor is somewhat constant on average. The power curve of the cylinder is almost identical compared with the one in the reference measurement. The effect of the leakages can also be seen in the energy curve of the accumulator; the energy is constantly wasted to some extent, as shown in graph (f) in Fig. 5.11. The consumed accumulator energy is about 4 kJ at the end of the trajectory, while 3.3 kJ is taken from the electric motor. In addition, the estimated energy fed to the tank line is around 0.1 kJ. The energy of the lift cylinder is about 1.2 kJ for the trajectory. The utilization rate of the accumulator outlet depends on the pressure ratio as the DHPMS is transforming the energy, whereas the rate of the cylinder outlet is dependent on the trajectory (graph (g) in Fig. 5.11). In this case, the total number of valve switchings is 1192.

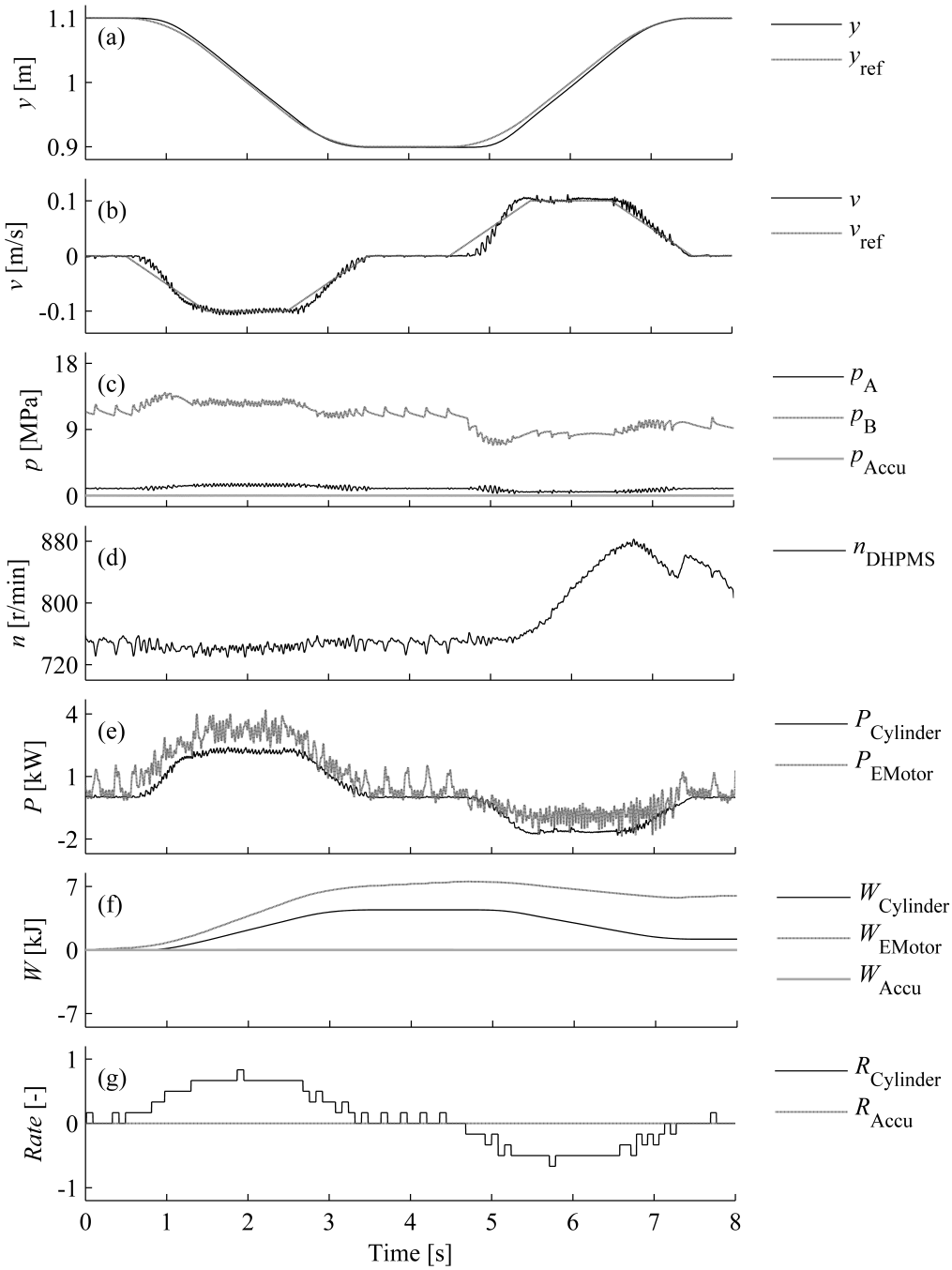

Figure 5.9: Measured characteristics of a reference system (accumulator not used) using a load mass of 200 kg: Piston position (a), piston velocity (b), pressures (c), rotational speed (d), powers (e), energies (f), and outlet utilization rates (g).

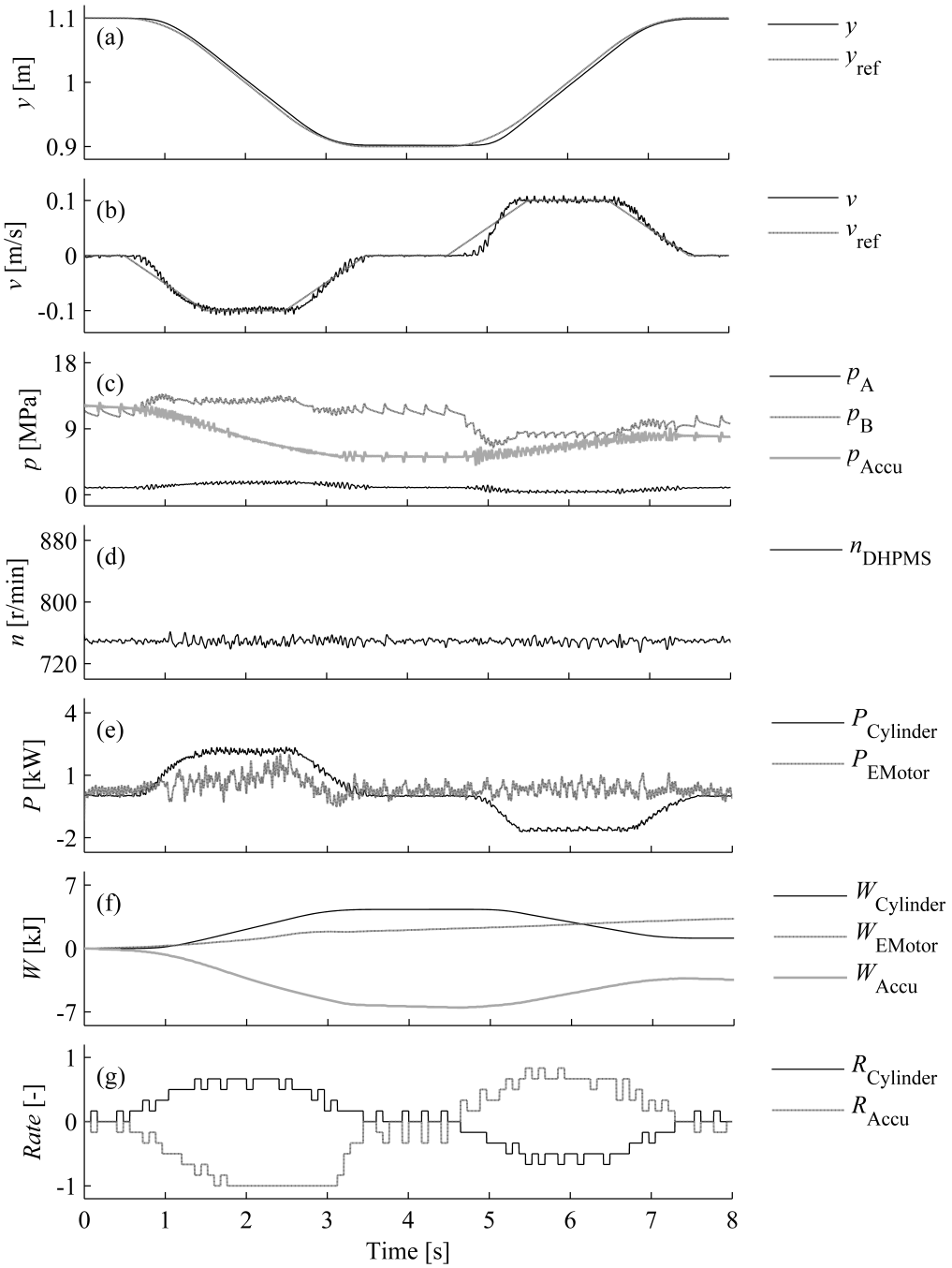

Figure 5.10: Measured characteristics of the DHH (initial pressure of the accumulator is 12 MPa) with a load mass of 200 kg: Piston position (a), piston velocity (b), pressures (c), rotational speed (d), powers (e), energies (f), and outlet utilization rates (g).

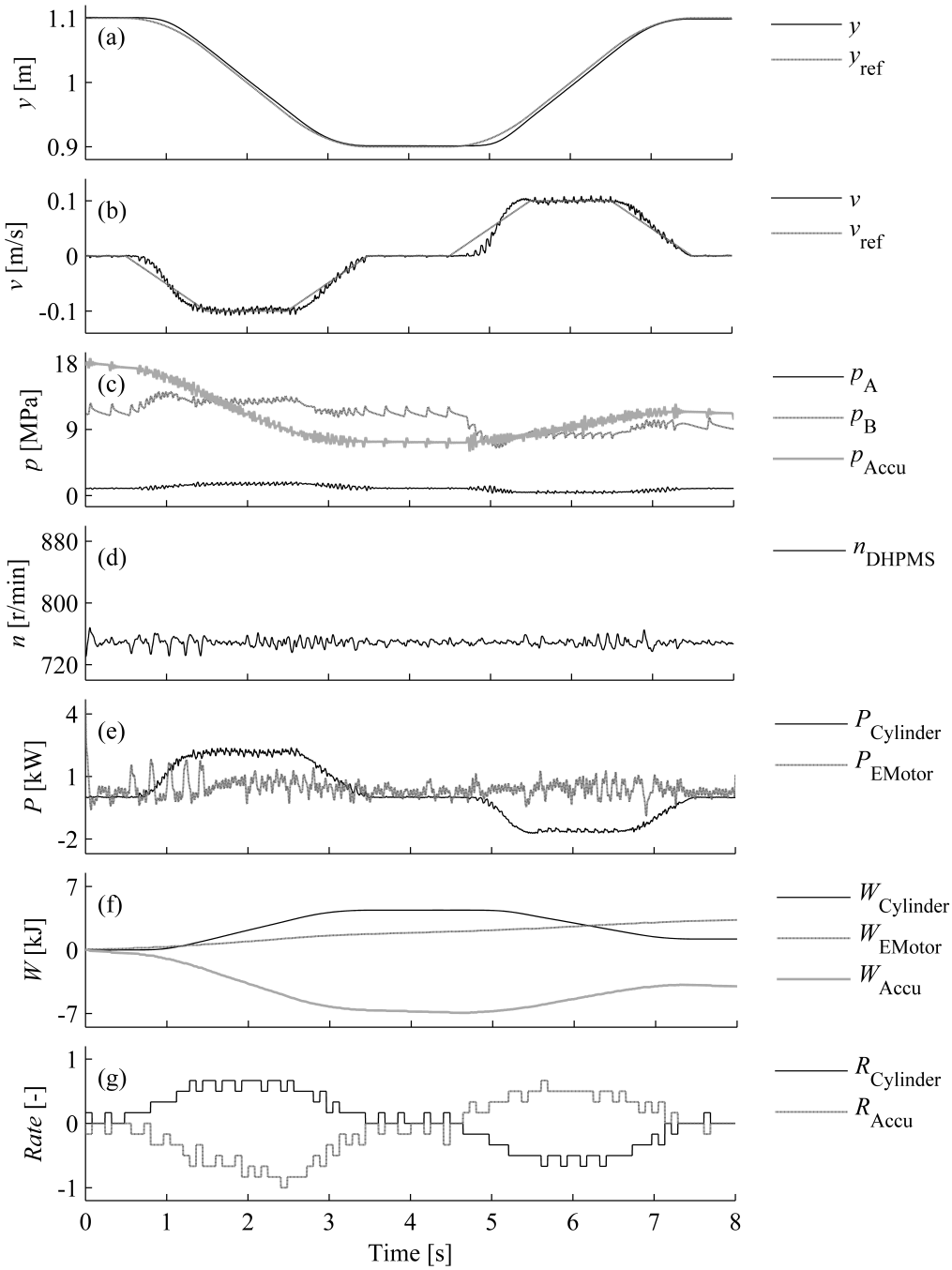

Figure 5.11: Measured characteristics of the DHH (initial pressure of the accumulator is 18 MPa) with a load mass of 200 kg: Piston position (a), piston velocity (b), pressures (c), rotational speed (d), powers (e), energies (f), and outlet utilization rates (g).

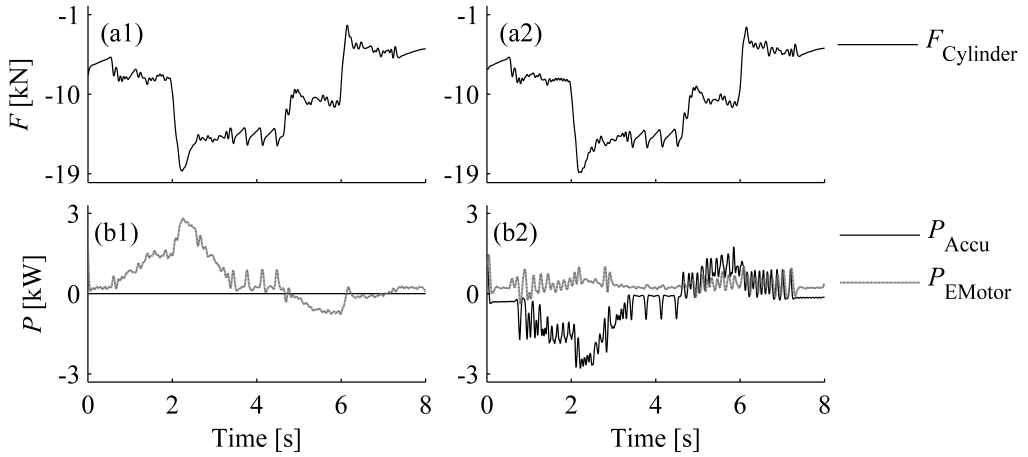

Figure 5.12: Measured response to a changing load mass without an accumulator (on the left) and with the hybridized system (on the right): Cylinder forces (a), and input powers (b).

The DHH is also tested for its response to the changing load force. In addition, a reference measurement without utilizing the accumulator is carried out. The same trajectory is used as in the previous experiments, but the load mass of 50 kg increases to 200 kg in the middle of the lifting movement. Correspondingly, the additional 150 kg disengages in the middle of the lowering movement. The accumulator is initially charged to a pressure of 15 MPa. The results with regard to the lift cylinder force and the input powers are shown in Fig. 5.12. For the presented signals, the cut-off frequency of 10 Hz is used in the low pass filter implementation. It can be seen that a rapid change in the load force from about -8 kN to -18 kN occurs during the retracting movement at the time of 2 s (graphs (a1) and (a2) in Fig. 5.12). During the extending movement, the load force changes from about -11 kN to -3 kN at the time of 6 s. The curves also show that the load force has strong dependency on the moving direction; the effect is caused by the difference in mechanical friction forces.

The required power for the boom trajectory is taken from the electric motor in its entirety when the accumulator is not used. While the boom is lifted up the power of the electric motor is around 1.5 kW before, and around 2.7 kW after, the additional load attaches, as shown in graph (b1) in Fig. 5.12. The power falls to negative when the boom starts to lower down, but it rises close to zero at the moment when the load force increases. In the hybridized system the required power is mainly taken from the accumulator, whereas the recuperated energy is stored into the accumulator. Graph (b2) in Fig. 5.12 shows that the accumulator power is around -1.5 kW on average before the load change during the boom lifting. After the load change the value is about -2.7 kW correspondingly. On the other hand, the accumulator is charged with average power of about 1 kW before the additional load mass is disengaged during the boom lowering. Thereafter, the regenerative power roughly halves. The power taken from the electric motor is relatively smooth despite of the rapid changes in the load force. The maximum power required during the movement is 1 kW. The highest peak that occurs in the very beginning of the measurement is caused by a pumping stroke to the accumulator.

5.5 Expandability to a multi-actuator system

5.5.1 Modeled system

In order to control both the lift and tilt cylinders of the studied excavator boom, four DHPMS outlets are needed. Additionally, an extra outlet needs to be reserved for an accumulator when a hybrid system is considered. Hence, a DHPMS with five independent outlets has to be implemented, as shown in Fig. 5.13. The modeled DHPMS has 18 pistons and its geometrical displacement is 30 cm^3. The moment of inertia of the flywheel is 0.3 kgm^2 and the rotational speed of the electric motor is set to 1500 r/min. Otherwise the modeled system has the same parameters as presented in Chapter 3; however, the supply lines and the cylinders are duplicated.

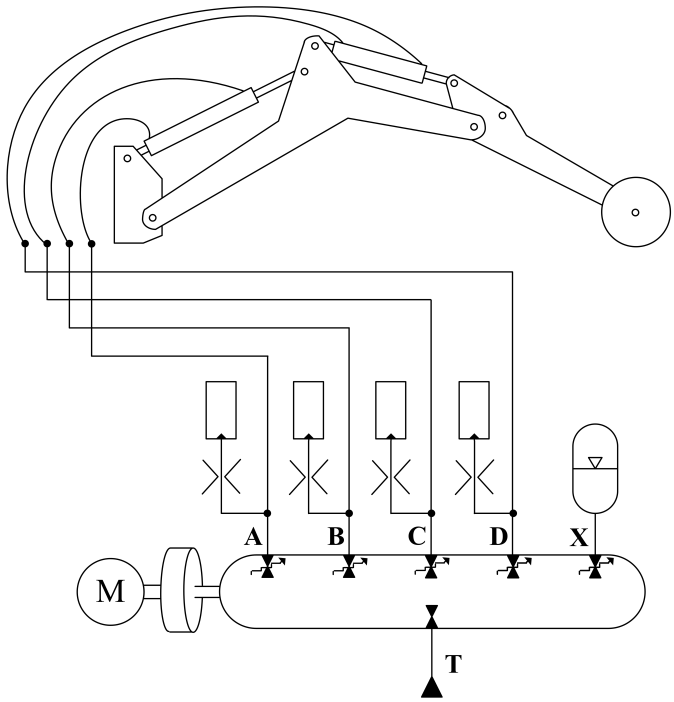

Figure 5.13: Displacement controlled excavator boom utilizing the DHH [73].

A control logic for the displacement controlled actuators is expanded from the rules presented in Section 4.2. In the case of two actuators, the pumping and motoring modes can be selected for outlets A, B, C, D, or tank T. Hence, the minimizing function has 21 elements because it is irrational to pump to and motor from the same outlet simultaneously. The controller considers the compressibility of the fluid utilizing the cylinder pressures, but position feedback is not used for the lift and tilt cylinders. The back-pressure control also has a similar principle as in the case of one actuator. In the case of two actuators, however, the cylinder which has the lowest back-pressure is prioritized. A mode value can be always changed to T, but it cannot be changed to A, B, C, or D unless the mode (pumping or motoring) is preselected for T.

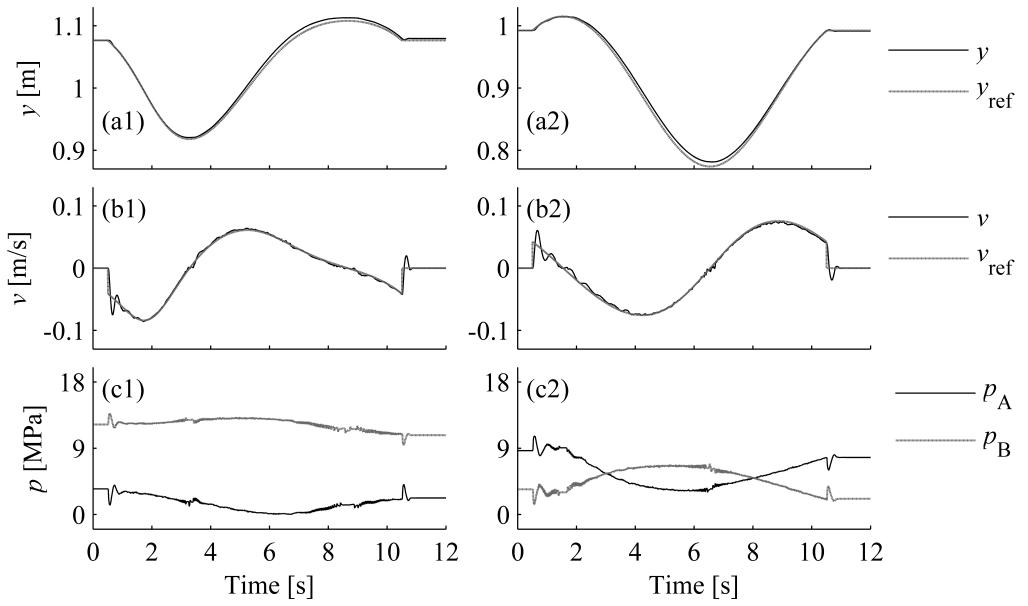

Figure 5.14: Simulated characteristics of the displacement controlled boom without cylinder back-pressure control (load mass is 400 kg): Lift cylinder piston position (a1), tilt cylinder piston position (a2), lift cylinder piston velocity (b1), tilt cylinder piston velocity (b2), lift cylinder pressures (c1), and tilt cylinder pressures (c2).

The principle for the accumulator energy control presented in Section 5.2 can also be adapted to the DHH with multiple actuator outlets. In this case, the accumulator energy is controlled in relation to the energy flow in the actuator outlets in order to keep the total hydraulic energy at the DHPMS outlets close to zero. In addition, the pressure level of the accumulator can be controlled between the work cycles using a separate logic. The target value for the accumulator pressure is either a user-defined constant or it can vary in relation to the maximum system pressure. In addition, the logic prevents the accumulator pressure from dropping too low or rising excessively high.

5.5.2 Simulation results

The simulated position and velocity tracking as well as the cylinder pressures of the displacement controlled boom without the cylinder back-pressure control are shown in Fig. 5.14. The load mass is 400 kg and the piston references for the tilt and lift cylinders are selected such that the boom tip draws a circle with a diameter of 1 m. The maximum position tracking error is 7.4 mm for the lift cylinder (graph (a1) in Fig. 5.14) and 8.1 mm for the tilt cylinder, correspondingly (graph (a2) in Fig. 5.14). The velocity curves are smooth for both actuators, as shown in graphs (b1) and (b2) in Fig. 5.14. The back-pressure of the cylinders, however, varies notably during the trajectory as the load forces change in relation to the boom orientation. Graph (c1) in Fig. 5.14 shows that the pressure in the lift cylinder even drops to zero. On the other hand, the back-pressure of the tilt cylinder increases significantly while the load force decreases.

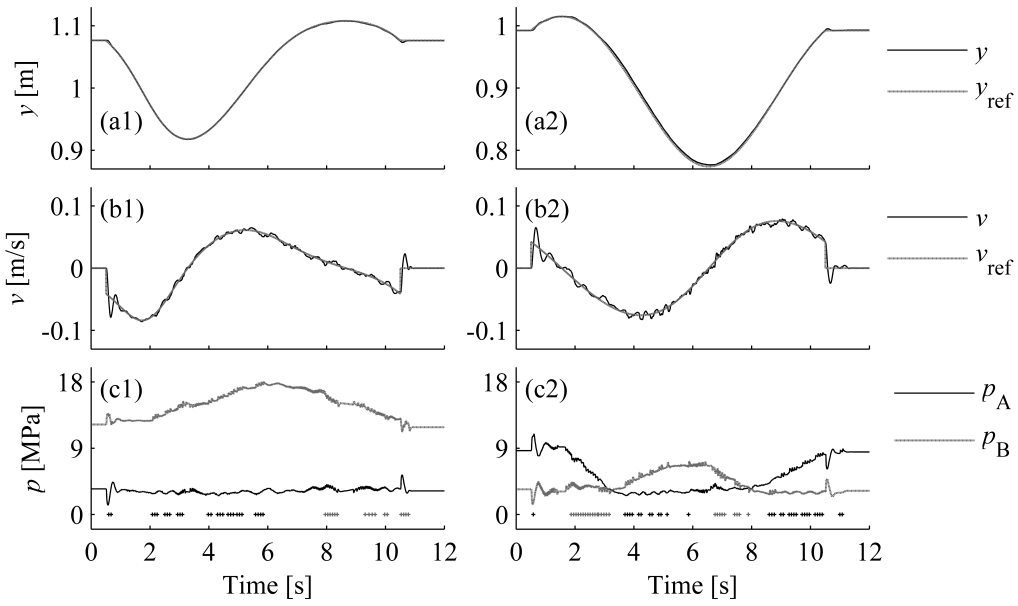

Figure 5.15: Simulated characteristics of the displacement controlled boom with cylinder back-pressure control (load mass is 400 kg): Lift cylinder piston position (a1), tilt cylinder piston position (a2), lift cylinder piston velocity (b1), tilt cylinder piston velocity (b2), lift cylinder pressures (c1), and tilt cylinder pressures (c2).

Figure 5.15 shows the effect of the cylinder back-pressure control. The position tracking accuracy improves as the maximum error is 3.2 mm for the lift cylinder (graph (a1) in Fig. 5.15) and 5.1 mm for the tilt cylinder (graph (a2) in Fig. 5.15). The velocity curves are not as smooth as in the previous case (graphs (b1) and (b2) in Fig. 5.15). A disturbance in the actuator flow excites the system to oscillate. The lift cylinder pressures are shown in graph (c1) in Fig. 5.15, whereas graph (c2) in Fig. 5.15 shows the tilt cylinder pressures. The range for the minimum pressures is set to $3 - 3.5$ MPa and the controller utilizes filtered pressure signals ($\gamma = 0.01$). In addition, the back-pressure controller can interfere only with every 37th mode decision. The preselected modes for the lift cylinder have been changed by the pressure controller 26 times due to low pressure (black plus sign) and 16 times due to high pressure (gray plus sign). The corresponding numbers are 32 and 26 for the tilt cylinder. It can be seen that the minimum pressure of the cylinders stays quite constant despite the changing load force. Moreover, cavitation of the cylinder chamber can be avoided by controlling the minimum pressure.

The trajectory is studied for energy consumption without utilizing the accumulator (Fig. 5.16) and the accumulator attached (Fig. 5.17). In both cases, the back-pressures are controlled and the same parameters are used. Hence, the position and velocity tracking performance are alike whether the accumulator is used or not. Graph (a) in Fig. 5.16 shows that the required power is taken from the electric motor as a whole when the accumulator is not used as a secondary power source. The input power is 3.5 kW at maximum but it also flows toward the electric motor during the trajectory. A constant power loss for the idling DHPMS is about 74 W.

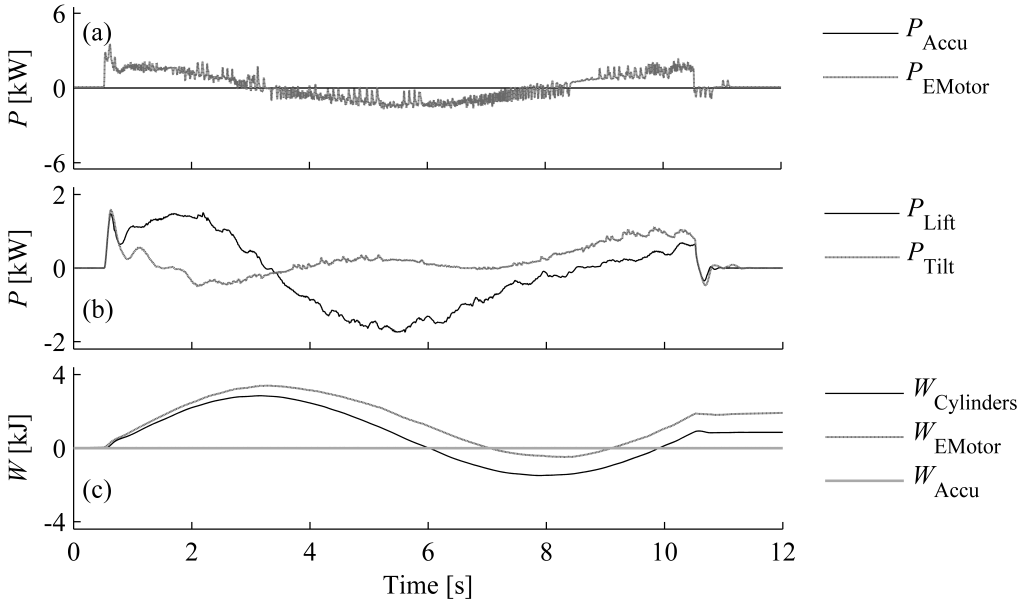

Figure 5.16: Simulated characteristics of the displacement controlled boom with cylinder back-pressure control (load mass is 400 kg): Input power (a), output power (b), and energies (c).

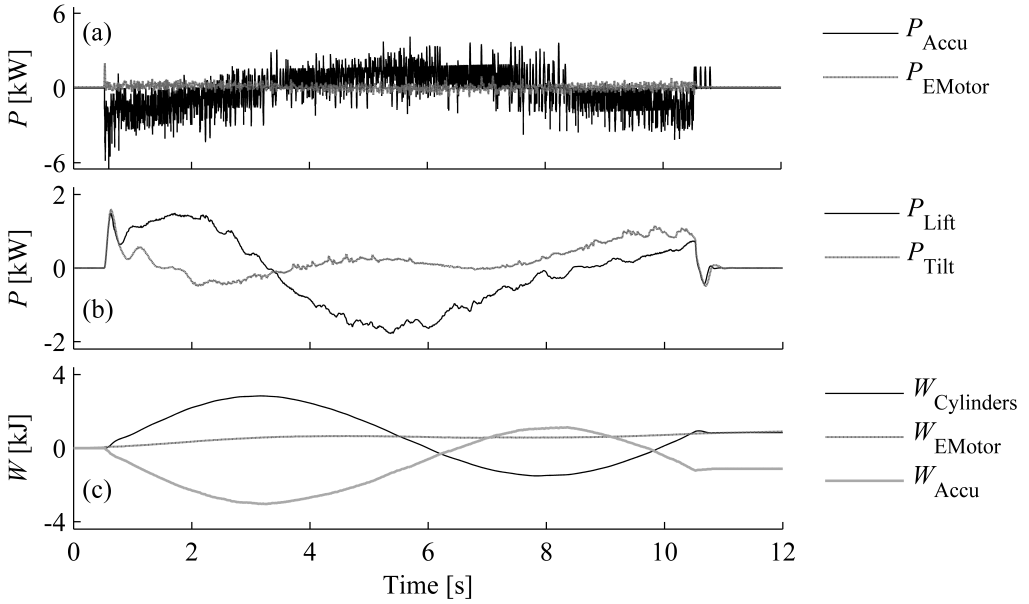

Figure 5.17: Simulated characteristics of the displacement controlled hybridized boom with cylinder back-pressure control (load mass is 400 kg): Input power (a), output power (b), and energies (c).

The lift and tilt cylinder powers are shown in graph (b) in Fig. 5.16. The actuator powers are either positive or negative depending on the direction of movement of the pistons and the boom orientation. The power of the lift cylinder varies between $-1.7 - 1.5$ kW and the range is $-0.5 - 1.6$ kW for the tilt cylinder, correspondingly. The total actuator energy is around 0.9 kJ at the end of the trajectory, whereas the energy taken from the electric motor is about 1.9 kJ, as shown in graph (c) in Fig. 5.16. The cumulative energy in the pressurized tank line is around zero at the end of the trajectory. Hence, the losses are 1.0 kJ.

In the hybridized system, the accumulator is used as a power source/sink in order to stabilize the power of the electric motor. The initial pressure of the accumulator is 14 MPa but at the end of the trajectory the pressure is 13.2 MPa, as the charging logic is not used. Graph (a) in Fig. 5.17 shows that the simulated power of the electric motor is close to zero on average during the movement, but has a slight ripple. The largest power peak (2 kW) occurs in the beginning of the trajectory where the velocity references of the cylinders change stepwise. The accumulator power has values between $-6.5 - 4.1$ kW. The cylinder powers shown in graph (b) in Fig. 5.17, are identical compared with the powers in the previous case. The energy taken from the accumulator, as well as the total cylinder energy, are around 0.9 kJ. Additionally, 1.1 kJ is taken from the accumulator, as shown in graph (c) in Fig. 5.17. About 0.1 kJ of hydraulic energy is fed to the pressurized tank during the trajectory. Hence, the losses are 1.0 kJ.

5.6 Analysis of the results

The DHH has been implemented by attaching a hydraulic accumulator to one outlet of the DHPMS and using it as a secondary power source. The control idea is to balance the hydraulic energy of the DHPMS outlets over time, which results in stabilized prime mover power. Moreover, displacement controlled actuation is used in order to enable the energy recuperation. The controller utilizes the measured outlet pressures and approximates the change in energies according to geometrical piston displacement; thus, the optimal mode for the accumulator outlet can be selected according to the decided actuator modes.

The simulations show that the capacity of the hydraulic accumulator can be fully utilized because the DHPMS can operate as a transformer; Thus, the energy can be effectively taken from and stored into the accumulator for its whole pressure range. However, the pressure ratio of the actuator and accumulator affects the produced power ripple. The fluctuation in prime mover power is at its minimum when the pressure ratio is close to one. On the other hand, the worst case occurs when the accumulator pressure is much higher than the actuator pressure. The means of reducing the negative effect of an unfavorable pressure ratio are increasing the moment of inertia of the flywheel or decreasing geometrical displacement of a single pumping piston of the DHPMS. If displacement is reduced, it is more beneficial to increase the number of pumping pistons than increase the rotational speed in order to maintain the flow properties; momentary forces caused by the pumping pistons are greater at higher speed. According to the simulations the amount of system losses is of the same size whether the accumulator is utilized or not, and whatever the pressure level of the accumulator is. The losses mainly originate from the DHPMS as the pressure losses are constantly present in control valves.

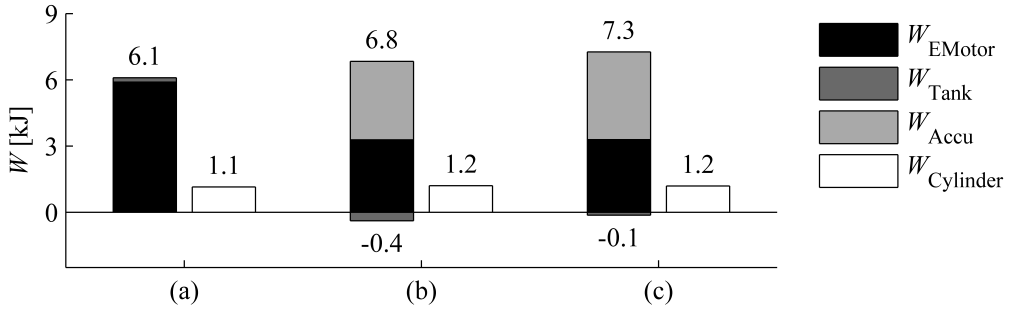

Figure 5.18: Measured energies for the trajectory (averages of three repetitions): Displacement controlled system without accumulator (a), displacement controlled system with accumulator at 12 MPa (b), and displacement controlled system with accumulator at 18 MPa (c).

The experimental tests also prove the feasibility of the DHH; the power of the electric motor can be effectively stabilized by using the accumulator as an energy source/sink. The system is even able to respond to a rapid change in the load force as long as fast pressure measurements are utilized. Figure 5.18 shows the measured energies for the trajectory with a constant load mass of 200 kg. The system losses are 5.0 kJ when the accumulator is not used (a), whereas the number is 5.2 kJ for the DHH with accumulator initial pressure of 12 MPa (b). Correspondingly, the total losses are 6.0 kJ for a system with accumulator initial pressure of 18 MPa (c). The losses are significantly bigger than the simulation results indicate due to the hydro-mechanical losses in the DHPMS and leaking control valves. What is notable is that using the accumulator does not significantly increase the losses. The differences in the results can be explained by increased leakage loss in the case of the pressurized accumulator: the higher the pressure the bigger the leakage flow. The energy is also fed to the pressurized tank line during the trajectory because more energy is required for the boom lifting than is possible to be recovered while the boom is lowered down. The lower the accumulator pressure compared with the actuator pressure the higher the utilization rate of the accumulator outlet, which can be seen as increased electrical energy consumption, as shown in Table 5.4

Table 5.4: Estimated energy consumption of DHPMS control valves for the studied trajectory (averages of three repetitions) according to the number of switchings.

Case	Number of switchings	Electrical energy
(a) Accumulator not used	779	0.8 kJ
(b) Initial pressure of 12 MPa	1399	1.4 kJ
(c) Initial pressure of 18 MPa	1195	1.2 kJ

The concept of the DHH can also be extended to systems with more than just one actuator. The studied simulation case shows that the DHPMS can successfully control both the lift and tilt cylinders using direct actuation. Moreover, the accumulator can be used as a secondary power source to balance the power of the electric motor; utilizing the accumulator does not increase the system losses, but for the most part they are caused by hydro-mechanical losses in the DHPMS.

6 Discussion

As the results indicate, displacement control by using the DHPMS is a feasible method for boom actuation. Good position tracking performance can be attained without using piston position feedback. However, geometrical displacement of the DHPMS pistons has to be small enough to achieve good controllability at small velocities as well. Smaller geometrical displacement further means higher rotational speed or larger number of pumping pistons in order to maintain the maximum flow rate of the DHPMS. The direct displacement control approach can also be highly efficient. Figure 6.1 shows the total losses of the studied systems in percentage terms. Trajectory with a load mass of 200 kg is investigated and the energy loss in a proportional controlled system (Case 5) is considered as a reference. For the displacement controlled double-acting cylinder (Case 1) the energy losses are 54% of the reference value, whereas the number is 48% for the displacement controlled single-acting cylinder (Case 2). Proportional control excessively wastes energy for the flow throttling. Additionally, energy is consumed also during the boom lowering. Displacement control minimizes the flow throttling losses and allows energy recuperation. The difference in losses of displacement controlled systems can be explained by the pressure losses in the supply lines and the amount of leakage flow; in the case of the double-acting cylinder both the DHPMS outlets are used and the losses become greater. Cases 3 and 4 represent the relative losses of the DHH, where the initial pressure of the hydraulic accumulator is 12 MPa and 18 MPa, respectively. The losses are bigger at higher pressure level due to the leaking control valves of the DHPMS.

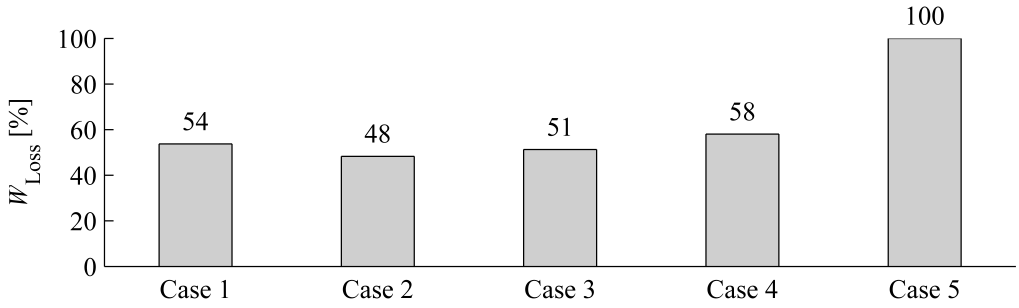

Figure 6.1: Measured losses of the studied systems when the load mass of 200 kg is used (calculated averages based on three repetitions of each measurement): Displacement controlled double-acting cylinder (Case 1), displacement controlled single-acting cylinder (Case 2), DHH with accumulator initial pressure of 12 MPa (Case 3), DHH with accumulator initial pressure of 18 MPa (Case 4), and proportional controlled cylinder (Case 5).

The experimental results show that the losses of the displacement controlled system and the DHH are comparable; the results indicate that using the accumulator as an energy source/sink does not reduce the system efficiency. The charging process of the accumulator, however, is left aside from the studied work cycle. The electric motor and the accumulator are considered as equal power sources and only the change in their energy balance is studied, as is the energy balance of the actuator (see Fig. 1.16). The sources of the losses are therefore between the power sources and the actuator. Thus, the system losses mainly consist of hydro-mechanical losses in the DHPMS if the leakage-free on/off control valves are used, as shown by the simulations. The losses during the accumulator charging depend on the charging power because the losses of the DHPMS are time-dependent. For the studied prototype, the accumulator will become useless in the long run due to the leakage losses of the DHPMS. However, the study proves that for a properly designed system the accumulator can be used efficiently in the DHH; the flow sharing between the accumulator and actuators does not increase the system losses.

For a DHPMS assembly, the control valves are a crucial factor; in addition to a leakage-free structure, high flow capacity is required, not forgetting fast dynamics. The electrical energy consumption of the valves has to be moderate as well, and the frequent switching cycles impose the high requirements for durability. The friction forces and the cylinder dead volumes also need to be taken into account when finding an optimal design for the machine. The studied prototype DHPMS was modified from a commercial water pump unit having the maximum pressure of 20 MPa; therefore, moderate pressure levels were used in the tests. In modern-day hydraulics, however, the pressure levels often exceed 40 MPa to make the systems lighter and higher in power density. From a component durability point of view, there are no limitations to build a digital machine suitable for higher pressure levels. In case of a smaller actuator, however, the DHPMS is required to have smaller piston displacement in order to maintain the good controllability of the direct actuation. In addition, the small displacement of individual pistons keeps the pressure and torque ripples low; thus, the negative effect of fast transients on the component durability can be minimized. Nevertheless, the proposed additional volumes with throttling orifices also dampen oscillations of the displacement controlled system effectively. For the measured trajectory, the passive damping method increases overall losses only of about 2%; hence, an impact on the system efficiency is marginal.

As the concept of the DHH can be extended to systems with several actuators, this novel approach could be a solution for more energy efficient hydraulics. The most beneficial targets of application could be mobile machines such as excavators and loaders, which have large boom systems with high inertial load. In these systems, the accumulator could be used effectively as a secondary power source and the potential energy could be recuperated. In the best possible scenario, the prime mover of the working machine could be sized significantly smaller. In the case of diesel engines, smaller size implies smaller fuel consumption and reduced emissions. The DHH approach might be applied for the drive train of mobile machines as well. Additionally, a merging of electric drives and the DHH should be considered; the superior power density of hydraulics combined with the green technology could provide a competitive alternative over traditional solutions. In summary, the simulations and the experimental results show the great potential of DHH technology, but still more research work is required before the systems are ready for commercialization.

7 Conclusion

This thesis investigates an energy efficient boom actuation by using a piston-type DHPMS with displacement controlled actuators. A method for displacement control has been proposed as well as a control method for stabilizing the power of a prime mover in the case of a hybridized system. The feasibility of the control methods has been validated by simulations and experimental tests. In addition, the energy saving potential of the studied approach has been validated by simulations and experimental tests. Thus, the individual objectives of the research have been fulfilled.

The results imply that it is possible to implement the direct control approach. This also gives an answer to the research question; good velocity tracking performance of a boom cylinder can be achieved even with a DHPMS having only six pumping pistons and low rotational speed. The controllability is poor only at small actuator velocities due to low displacement resolution. In addition, a model based control approach provides good position tracking without using position feedback of the cylinder piston. For the hybrid system an accumulator can be used as a secondary power source and for storing recoverable energy. The DHH clearly is able to stabilize the power of the prime mover by covering the demanded power using the accumulator.

With proper design of the DHPMS the approach could bring the efficiency of hydraulic systems to a whole new level - a nearly lossless system should not be an impossibility. Moreover, the hybrid design allows the prime mover to be sized significantly smaller. In the case of a diesel engine, for example, the reduction in size means smaller consumption and emissions. Hence, in addition to smaller production costs due to a simpler system, the benefits lie also in reduced operating costs and environmental load.

As a recommendation for future work, the optimal construction of the DHPMS should be researched; as the performance of the hybrid system mainly depends on the performance of the DHPMS, the losses produced by the machine need to be minimized. Additionally, an optimal configuration at the system level should be considered as well. In multi-actuator systems a benefit of displacement control may be debatable for actuators having low power demand and no ability to return energy, especially when low speed actuation is considered. Therefore, ELS supply pressure control with valve controlled actuators could be used together with displacement controlled actuators. The number of DHPMS outlets would also decrease if some of the actuators required only one outlet instead of two. The DHH could also be applied to power trains in the future. In conclusion, the concept of the DHH is promising from the energy efficiency point of view and should be considered as a worthy alternative to conventional systems.

Bibliography

[1] X. Liang and T. Virvalo, "What's wrong with energy utilization in hydraulic cranes," in *The Fifth International Conference on Fluid Power Transmission and Control, ICFP'2001*, Hangzhou, China, 2001.

[2] M. Luomaranta, "A stable electro hydraulic load sensing system based on a microcontroller," in *The 6th Scandinavian International Conference on Fluid Power, SICFP'99*, Tampere, Finland, 1999.

[3] M. Drujovic and S. Helduser, "New control strategies for electrohydraulic load sensing," in *Power Transmission and Motion Control, PTMC 2004*, Bath, UK, 2004.

[4] R. Finzel, S. Helduser, and D.-S. Jang, "Electro-hydraulic dual-circuit system to improve the energy efficiency of mobile machines," in *The 7th International Fluid Power Conference, 7. IFK*, Aachen, Germany, 2010.

[5] M. Erkkilä, T. Jalkanen, E. Lehto, and T. Virvalo, "Negative load sensing," in *The 7th International Fluid Power Conference, 7. IFK*, Aachen, Germany, 2010.

[6] B. Eriksson, J. Larsson, and J.-O. Palmberg, "Study on individual pressure control in energy efficient linder drives," in *The 4th FPNI Ph.D Symposium*, Sarasota, Florida USA, 2006.

[7] A. Hansen, H. Pedersen, T. Andersen, and L. Wachmann, "Investigation of energy saving separate meter-in separate meter-out control strategies," in *The 12th Scandinavian International Conference on Fluid Power, SICFP'11*, Tampere, Finland, 2011.

[8] J. Mattila and T. Virvalo, "Energy-efficient motion control of a hydraulic manipulator," in *The 2000 IEEE International Conference on Robotics & Automation*, San Francisco, California USA, 2000.

[9] R. Scheidl, H. Kogler, and B. Winkler, "Hydraulic switching control - objectives, concepts, challenges and potential applications," *Magazine of Hydraulics, Pneumatics, Tribology, Ecology, Sensorics, Mechatronics*, no. 1, pp. 7–18, 2013.

[10] A. Laamanen, M. Linjama, and M. Vilenius, "The effect of coding method on pressure peaks in digital hydraulic system," in *The 4th FPNI Ph.D Symposium*, Sarasota, Florida USA, 2006.

[11] M. Linjama, K. Koskinen, and M. Vilenius, "Accurate trajectory tracking control of water hydraulic cylinder with non-ideal on/off valves," *International Journal of Fluid Power*, vol. 4, no. 1, pp. 7–16, Apr. 2003.

[12] M. Linjama and M. Vilenius, "Improved digital hydraulic tracking control of water hydraulic cylinder drive," *International Journal of Fluid Power*, vol. 6, no. 1, pp. 7–16, Mar. 2005.

[13] M. Huova and M. Linjama, "Energy efficient digital hydraulic valve control utilizing pressurized tank line," in *The 8th International Fluid Power Conference, 8. IFK*, Dresden, Germany, 2012.

[14] L. Siivonen, M. Linjama, M. Huova, and M. Vilenius, "Fault detection and diagnosis of digital hydraulic valve system," in *The 10th Scandinavian International Conference on Fluid Power, SICFP'07*, Tampere, Finland, 2007.

[15] L. Siivonen, M. Linjama, M. Huova, and M. Vilenius, "Jammed on/off valve fault compensation with distributed digital valve system," *International Journal of Fluid Power*, vol. 10, no. 2, pp. 73–82, 2009.

[16] L. Siivonen, M. Huova, M. Linjama, H. Försterling, E. Stamm, and T. Deubel, "Fault tolerance of digital hydraulics in high dynamic hydraulic system," in *The 14th Scandinavian International Conference on Fluid Power, SICFP'15*, Tampere, Finland, 2015.

[17] H. Fischer, A. Laamanen, A. Iso-Heiko, O. Schäfer, M. Karvonen, O. Karhu, K.Huhtala, V.-P. Pulkkinen, and A. Huttunen, "Digital hydraulics on rails - pilot project of improving reliability on railway rolling stock by utilizing digital valve system," in *The 14th Scandinavian International Conference on Fluid Power, SICFP'15*, Tampere, Finland, 2015.

[18] M. Linjama, H.-P. Vihtanen, A. Sipola, and M. Vilenius, "Secondary controlled multi-chamber cylinder," in *The 11th Scandinavian International Conference on Fluid Power, SICFP'09*, Linköping, Sweden, 2009.

[19] A. Dell'Amico, M. Carlsson, E. Norlin, and M. Sethson, "Investigation of a digital hydraulic actuation system on an excavator arm," in *The 13th Scandinavian International Conference on Fluid Power, SICFP'13*, Linköping, Sweden, 2013.

[20] M. Huova, A. Laamanen, and M. Linjama, "Energy efficiency of three-chamber cylinder with digital valve system," *International Journal of Fluid Power*, vol. 11, no. 3, pp. 15–22, 2010.

[21] E. Bishop, "Digital hydraulic transformer - approaching theoretical perfection in hydraulic drive efficiency," in *The 11th Scandinavian International Conference on Fluid Power, SICFP'09*, Linköping, Sweden, 2009.

[22] E. Bishop, "Digital hydraulic transformer - for energy efficient hydraulic drives," in *The Second Workshop on Digital Fluid Power, DFP'09*, Linz, Austria, 2009.

[23] L. Wadsley, "Optimal system solutions enabled by digital pumps," in *The 52nd National Conference on Fluid Power, NCFP 2011*, Las Vegas, Nevada USA, 2011.

[24] J. Tammisto, M. Huova, M. Heikkilä, M. Linjama, and K. Huhtala, "Measured characteristics of an in-line pump with independently controlled pistons," in *The 7th International Fluid Power Conference, 7. IFK*, Aachen, Germany, 2010.

[25] M. Ehsan, W. Rampen, and S. Salter, "Modeling of digital-displacement pump-motors and their application as hydraulic drives for nonuniform loads," *Journal of Dynamic Systems Measurement and Control*, vol. 122, no. 1, pp. 210 – 115, Jun. 1997.

[26] M. Linjama and K. Huhtala, "Digital pump-motor with independent outlets," in *The 11th Scandinavian International Conference on Fluid Power, SICFP'09*, Linköping, Sweden, 2009.

[27] M. Linjama and J. Tammisto, "New alternative for digital pump-motor-transformer," in *The Second Workshop on Digital Fluid Power, DFP'09*, Linz, Austria, 2009.

[28] C. Williamson, J. Zimmerman, and M. Ivantysynova, "Efficiency study of an excavator hydraulic system based on displacement-controlled actuators," in *ASME/Bath Symposium on Fluid Power and Motion Control, FPMC 2014*, Bath, UK, 2008.

[29] C. Williamson and M. Ivantysynova, "Power optimization for multi-actuator pump-controlled systems," in *The 7th International Fluid Power Conference, 7. IFK*, Aachen, Germany, 2010.

[30] C. Williamson and M. Ivantysynova, "Stability and motion control of inertial loads with displacement controlled hydraulic actuators," in *Proceedings of the 6th FPNI Ph.D Symposium on Fluid Power, FPNI2010*, West Lafayette, Indiana USA, 2010.

[31] J. Zimmerman and M. Ivantysynova, "Reduction of engine and cooling power by displacement control," in *Proceedings of the 6th FPNI Ph.D Symposium on Fluid Power, FPNI2010*, West Lafayette, Indiana USA, 2010.

[32] E. Busquets and M. Ivantysynova, "A multi-actuator displacement-controlled system with pump switching - a study of the architecture and actuator-level control," *JFPS International Journal of Fluid Power System*, vol. 8, no. 2, pp. 29 – 39, Aug. 2015.

[33] R. Ivantysyn and J. Weber, "Novel open circuit displacement control architecture in heavy machinery," in *Proceedings of the 8th FPNI Ph.D Symposium on Fluid Power, FPNI2014*, Lappeenranta, Finland, 2014.

[34] T. Minav, C. Bonato, P. Sainio, and M. Pietola, "Direct driven hydraulic drive," in *The 9th International Fluid Power Conference, 9. IFK*, Aachen, Germany, 2014.

[35] T. Minav, P. Sainio, and M. Pietola, "Direct-driven hydraulic drive without conventional oil tank," in *ASME/Bath Symposium on Fluid Power and Motion Control, FPMC 2014*, Bath, UK, 2014.

[36] T. Minav, P. Sainio, and M. Pietola, "Efficiency of direct driven hydraulic setup in arctic conditions," in *The 14th Scandinavian International Conference on Fluid Power, SICFP'15*, Tampere, Finland, 2015.

[37] H. T. S. Heitzig, "Aspects of digital pumps in closed circuit," in *The Fourth Workshop on Digital Fluid Power, DFP'11*, Linz, Austria, 2011.

[38] C. C. Locateli, H. C. Belan, E. R. D. Pieri, P. Krus, and V. J. D. Negri, "Actuator speed control using digital hydraulics," in *ASME/Bath Symposium on Fluid Power and Motion Control, FPMC 2014*, Bath, UK, 2014.

[39] K.-E. Rydberg, "Energy efficient hydraulic hybrid drives," in *The 11th Scandinavian International Conference on Fluid Power, SICFP'09*, Linköping, Sweden, 2009.

[40] P. Puddu and M. Paderi, "Hydro-pneumatic accumulators for vehicles kinetic energy storage: Influence of gas compressibility and thermal losses on storage capability," *Energy*, vol. 57, pp. 326 – 335, Aug. 2013.

[41] J. Juhala, J. Kajaste, and M. Pietola, "Thermal insulation in enhancing performance characteristics of hydraulic accumulator," in *ASME/Bath Symposium on Fluid Power and Motion Control, FPMC 2012*, Bath, UK, 2012.

[42] A. Stroganov and L. Sheshin, "Accumulator efficiency improvement: Heat insulation or heat regeneration," in *The 11th Scandinavian International Conference on Fluid Power, SICFP'09*, Linköping, Sweden, 2009.

[43] W. Hufenbach, A. Ulbricht, D. Barfußß, M. Birke, B. Zhou, and K. Kunze, "Lightweight hydraulic components in novel multi-material-design for mobile applications," in *The 9th International Fluid Power Conference, 9. IFK*, Aachen, Germany, 2014.

[44] Z. Du, K. Cheong, P. Li, and T. Chase, "Fuel economy comparisons of series, parallel and HMT hydraulic hybrid architectures," in *The 1st American Control Conference, ACC 2013*, Washington, DC, United States, 2013.

[45] R. Kumar and M. Ivantysynova, "The hydraulic hybrid alternative for toyota prius - a power management strategy for improved fuel economy," in *The 7th International Fluid Power Conference, 7. IFK*, Aachen, Germany, 2010.

[46] F. Bender, T. Bosse, and O. Sawodny, "An investigation on the fuel savings potential of hybrid hydraulic refuse collection vehicles," *Waste Management*, vol. 34, pp. 1577 – 1583, Sept. 2014.

[47] M. Sprengel and M. Ivantysynova, "Investigation and energetic analysis of a novel hydraulic hybrid architecture for on-road vehicles," in *The 13th Scandinavian International Conference on Fluid Power, SICFP'13*, Linköping, Sweden, 2013.

[48] T. Verkoyen, J. Schmitz, N. Vatheuer, M. Inderelst, and H. Murrenhoff, "Retrofittable hydraulic hybrid system for road vehicles," in *The 7th International Fluid Power Conference, 7. IFK*, Aachen, Germany, 2010.

[49] P. Achten, G. Vael, M. Sokar, and T. Kohmäscher, "Design and fuel economy of a series hydraulic hybrid vehicle," in *The 7th JFPS International Symposium on Fluid Power*, Toyama, Japan, 2008.

[50] G. Vael and P. Achten, "Iht controlled serial hydraulic hybrid passenger cars," in *The 7th International Fluid Power Conference, 7. IFK*, Aachen, Germany, 2010.

[51] Y.-L. Chen, S.-A. Liu, J.-H. Jiang, T. Shang, Y.-K. Zhang, and W. Wei, "Dynamic analysis of energy storage unit of the hydraulic hybrid vehicle," *International Journal of Automotive Technology*, vol. 14, no. 1, pp. 101–112, Jan. 2013.

[52] W. Wu, J. Hu, C. Jing, Z. Jiang, and S. Yuan, "Investigation of energy efficient hydraulic hybrid propulsion system for automobiles," *Energy*, vol. 73, pp. 497–505, Aug. 2014.

[53] Y. Sun, J. Garcia, and M. Krishnamurthy, "A novel fixed displacement electric-hydraulic hybrid (EH2) drivetrain for city vehicles," in *Transportation Electrification Conference and Expo, ITEC'13*, Dearborn, Detroit, United States, 2013.

[54] F. Tavares, R. Johri, A. Salvi, S. Baseley, and Z. Filipi, "Hydraulic hybrid powertrain-in-the-loop integration for analyzing real-world fuel economy and emissions improvements," in *SAE 2011 Commercial Vehicle Engineering Congress and Exhibition*, Rosemont, Illinois USA, 2011.

[55] J. Taylor, W. Rampen, A. Robertson, and N. Caldwell, "Digital displacement hydraulic hybrids - parallel hybrid drives for commercial vehicles," in *2013 JSAE Annual Congress (Spring)*, Yokohama, 2013.

[56] J. Taylor, W. Rampen, D. Abrahams, and A. Latham, "Demonstration of a digital displacement hydraulic hybrid bus," in *2015 JSAE Annual Congress (Spring)*, Yokohama, 2015.

[57] M. Erkkilä, F. Bauer, and D. Feld, "Universal energy storage and recovery system - a novel approach for hydraulic hybrid," in *The 13th Scandinavian International Conference on Fluid Power, SICFP'13*, Linköping, Sweden, 2013.

[58] K. Einola, "Prestudy on power management of a cut-to-length forest harvester with a hydraulic hybrid system," in *The 13th Scandinavian International Conference on Fluid Power, SICFP'13*, Linköping, Sweden, 2013.

[59] K. Einola and M. Erkkilä, "Dimensioning and control of a hydraulic hybrid system of a cut-to-length forest harvester," in *The 9th International Fluid Power Conference, 9. IFK*, Aachen, Germany, 2014.

[60] S. Tikkanen, M. Kliffken, C. Erhet, and S. Baseley, "Hydraulic hybrid systems for working machines and commercial vehicles," in *The 51st National Conference on Fluid Power, NCFP 2008*, Las Vegas, Nevada USA, 2008.

[61] R. Hippalgaonkar, M. Ivantysynova, and J. Zimmerman, "Fuel savings of a mini-excavator through a hydraulic hybrid displacement controlled system," in *The 8th International Fluid Power Conference, 8. IFK*, Dresden, Germany, 2012.

[62] R. Hippalgaonkar and M. Ivantysynova, "A series-parallel hydraulic hybrid mini-excavator with displacement controlled actuators," in *The 13th Scandinavian International Conference on Fluid Power, SICFP'13*, Linköping, Sweden, 2013.

[63] K. Heybroek, G. Vael, and J.-O. Palmberg, "Towards resistance - free hydraulics in construction machinery," in *The 8th International Fluid Power Conference, 8. IFK*, Dresden, Germany, 2012.

[64] W. Shen, J. Jiang, X. Su, and H. Karimi, "Control strategy analysis of the hydraulic hybrid excavator," *Journal of the Franklin Institute*, Apr. 2014.

[65] S. Tikkanen and H. Tommila, "Hybrid pump drive," in *The 14th Scandinavian International Conference on Fluid Power, SICFP'15*, Tampere, Finland, 2015.

[66] M. Linjama, M. Huova, M. Pietola, J. Juhala, and K. Huhtala, "Hydraulic hybrid actuator: Theoretical aspects and solution alternatives," in *The 14th Scandinavian International Conference on Fluid Power, SICFP'15*, Tampere, Finland, 2015.

[67] M. Heikkilä, J. Tammisto, M. Huova, K. Huhtala, and M. Linjama, "Experimental evaluation of a piston-type digital pump-motor-transformer with two independent outlets," in *ASME/Bath Symposium on Fluid Power and Motion Control, FPMC 2010*, Bath, UK, 2010.

[68] M. Heikkilä and M. Linjama, "Direct connection of digital hydraulic power management system and double acting cylinder - a simulation study," in *The Fourth Workshop on Digital Fluid Power, DFP'11*, Linz, Austria, 2011.

[69] M. Heikkilä and M. Linjama, "Improving damping characteristics of displacement controlled digital hydraulic system," in *The Fifth Workshop on Digital Fluid Power, DFP'12*, Tampere, Finland, 2012.

[70] M. Heikkilä and M. Linjama, "Displacement control of a mobile crane using a digital hydraulic power management system," *Mechatronics - The Science of Intelligent Machines*, vol. 23, no. 4, pp. 452 – 461, June 2013.

[71] M. Heikkilä, M. Karvonen, M. Linjama, S. Tikkanen, and K. Huhtala, "Comparison of proportional control and displacement control using digital hydraulic power management system," in *ASME/Bath Symposium on Fluid Power and Motion Control, FPMC 2014*, Bath, UK, 2014.

[72] M. Heikkilä and M. Linjama, "Hydraulic energy recovery in displacement controlled digital hydraulic system," in *The 13th Scandinavian International Conference on Fluid Power, SICFP'13*, Linköping, Sweden, 2013.

[73] M. Heikkilä, M. Linjama, and K. Huhtala, "Digital hydraulic power management system with five independent outlets - simulation study of displacement controlled excavator crane," in *The 9th International Fluid Power Conference, 9. IFK*, Aachen, Germany, 2014.

[74] S. Roberts, "Control charts based on geometric moving averages," *Technometrics*, vol. 1, no. 3, pp. 239 – 250, 1959.

[75] M. Karvonen, M. Heikkilä, M. Huova, M. Linjama, and K. Huhtala, "Simulation study - improving efficiency in mobile boom using digital hydraulic power management system," in *The 12th Scandinavian International Conference on Fluid Power, SICFP'11*, Tampere, Finland, 2011.

[76] M. Karvonen, M. Heikkilä, M. Huova, and M. Linjama, "Analysis by simulation of different control algorithms of a digital hydraulic two-actuator system," *International Journal of Fluid Power*, vol. 15, no. 1, pp. 33 – 44, Mar. 2014.

[77] M. Karvonen, M. Heikkilä, S. Tikkanen, M. Linjama, and K. Huhtala, "Aspects of the energy consumption of a digital hydraulic power management system supplying a digital and proportional valve controlled multi actuator system," in *ASME/Bath Symposium on Fluid Power and Motion Control, FPMC 2014*, Bath, UK, 2014.

[78] M. Karvonen, M. Heikkilä, M. Linjama, and K. Huhtala, "Analysis of signals and power flow in a digital hydraulic multi actuator application," in *Proceedings of the 8th FPNI Ph.D Symposium on Fluid Power, FPNI2014*, Lappeenranta, Finland, 2014.

[79] M. Karvonen, M. Heikkilä, M. Huova, M. Linjama, and K. Huhtala, "Inspections on control performance of a digital hydraulic power management system supplying digital and proportional valve driven multi-actuator system," in *The 9th International Fluid Power Conference, 9. IFK*, Aachen, Germany, 2014.

[80] A. Ellman and R. Piché, "A two regime orifice flow formula for numerical simulation," *Journal of Dynamic Systems, Measurement, and Control*, vol. 121, no. 4, pp. 721–724, Dec. 1999.

[81] C. Canudas de Wit, H. Olsson, K. Åström, and P. Lischinsky, "A new model for control of systems with friction," *IEEE Transactions on Automatic Control*, vol. 40, no. 3, pp. 419–425, Mar. 1995.

[82] M. Heikkilä, J. Tammisto, M. Huova, K. Huhtala, and M. Linjama, "Experimental evaluation of a digital hydraulic power management system," in *The Third Workshop on Digital Fluid Power, DFP'10*, Tampere, Finland, 2010.

Appendix A: Measured quantities

Experiment	Measurement point	Low-pass filtration
Figs. 4.8 - 4.11	Piston position: y (XIV)	4^{th} Order
	Piston velocity: v (XIV)	$f_{\text{CutOff}} = 50$ Hz
	Pressure: p_{A} (IX)	$\zeta = 0.7$
	Pressure: p_{B} (VII)	
	Rotational speed: n_{DHPMS} (XII)	
	Power: P_{Cylinder} (IX, VII, XIV)	
	Power: P_{EMotor} (XII)	
	Energy: W_{Cylinder} (IX, VII, XIV)	
	Energy: W_{EMotor} (XII)	
	Energy: W_{DHPMS} (II, III, X, XI)	
Fig. 4.12	Piston velocity: v (XIV)	4^{th} Order
		$f_{\text{CutOff}} = 50$ Hz
		$\zeta = 0.7$
Figs. 4.16 - 4.17	Piston position: y (XIV)	4^{th} Order
	Piston velocity: v (XIV)	$f_{\text{CutOff}} = 50$ Hz
	Pressure: p_{A} (IX)	$\zeta = 0.7$
	Pressure: p_{B} (VII)	
	Pressure: p_{S} (V)	
	Rotational speed: n_{DHPMS} (XII)	
	Power: P_{Cylinder} (IX, VII, XIV)	

	Power: P_{EMotor} (XII)	
	Energy: W_{Cylinder} (IX, VII, XIV)	
	Energy: W_{EMotor} (XII)	
	Energy: W_{DHPMS} (II, III, X, XI)	
Fig. 4.18	Pressure: p_{S} (V)	4^{th} Order
		$f_{\mathrm{CutOff}} = 50$ Hz
		$\zeta = 0.7$
Figs. 5.9 - 5.11	Piston position: y (XIV)	4^{th} Order
	Piston velocity: v (XIV)	$f_{\mathrm{CutOff}} = 50$ Hz
	Pressure: p_{A} (IX)	$\zeta = 0.7$
	Pressure: p_{B} (VII)	
	Pressure: p_{accu} (II)	
	Rotational speed: n_{DHPMS} (XII)	
	Power: P_{Cylinder} (IX, VII, XIV)	
	Power: P_{EMotor} (XII)	
	Energy: W_{Cylinder} (IX, VII, XIV)	
	Energy: W_{EMotor} (XII)	
	Energy: W_{Accu} (II, X)	
Fig. 5.12	Cylinder force: F_{Cylinder} (IX, VII, XIV)	4^{th} Order
	P_{Accu} (II, X)	$f_{\mathrm{CutOff}} = 10$ Hz
	P_{EMotor} (XII)	$\zeta = 0.7$

Appendix B: Simulation parameters

Component	Parameter	Value	Unit
Boom	Mass of lift boom part A	50	kg
	Length of lift boom part A	1.0	m
	Mass of lift boom part B	40	kg
	Length of lift boom part B	0.69	m
	Mass of tilt boom	30	kg
	Length of tilt boom	0.9	m
Oil	Bulk modulus	1500	MPa
Lift Cylinder	Piston side area	31	cm^2
	Rod side area	21	cm^2
	Stroke length	0.5	m
	Dead volume A	50	cm^3
	Port orifice A nominal flow (@ 0.5 MPa)	100	l/min
	Port orifice A transition pressure	0.1	MPa
	Dead volume B	50	cm^3
	Port orifice B nominal flow (@ 0.5 MPa)	100	l/min
	Port orifice B transition pressure	0.1	MPa
Tilt Cylinder	Piston side area	31	cm^2
	Rod side area	21	cm^2
	Stroke length	0.35	m

	Dead volume A	50	cm^3
	Port orifice A nominal flow (@ 0.5 MPa)	100	l/min
	Port orifice A transition pressure	0.1	MPa
	Dead volume B	50	cm^3
	Port orifice B nominal flow (@ 0.5 MPa)	100	l/min
	Port orifice B transition pressure	0.1	MPa
Dynamic friction	Bristle stiffness	11.5	MN/m
	Damping coefficient	303	kNs/m
	Viscous friction coefficient	950	Ns/m
	Coulomb friction force	900	N
	Static friction force	1150	N
	Stribeck velocity	10	mm/s
Supply lines	Hose volume A	0.98	l
	Hose A bulk modulus	600	MPa
	Damping volume A	5	l
	Damping orifice A nominal flow (@ 0.5 MPa)	1.3	l/min
	Port orifice A transition pressure	0.01	MPa
	Hose volume B	0.98	l
	Hose B bulk modulus	600	MPa
	Damping volume B	5	l
	Damping orifice B nominal flow (@ 0.5 MPa)	1.3	l/min
	Port orifice B transition pressure	0.01	MPa
Accumulator	Nominal volume	4	l
	Inflation pressure	3	MPa
	Hose volume	1	l
	Hose bulk modulus	500	MPa
	Port orifice nominal flow (@ 0.5 MPa)	224	l/min
	Port orifice transition pressure	0.1	MPa

Electric motor	Nominal slip	50	r/min
	Nominal torque	122	Nm
Flywheel	Moment of inertia	0.15	kgm^2
Six-piston DHPMS	Piston diameter	20	mm
	Piston stroke	16	mm
	Chamber dead volume	37	cm^3
	Valve delay	1	ms
	Valve rate	2000	1/s
	Valve nominal flow (@ 0.5 MPa)	23	l/min
	Inlet pressure	1	MPa

Tampereen teknillinen yliopisto
PL 527
33101 Tampere

Tampere University of Technology
P.O.B. 527
FI-33101 Tampere, Finland

ISBN 978-952-15-3758-5
ISSN 1459-2045